SIR telomere silencing depends on nuclear envelope lipids and modulates sensitivity to a lysolipid drug

Condensed title: LysoPC alters NE shape and telomere silencing

Maria Laura Sosa Ponce[1], Mayrene Horta Remedios[1], Sarah Moradi-Fard[2], Jennifer A Cobb[2,3†], Vanina Zaremberg[1†]*

[1] Department of Biological Sciences, University of Calgary, Calgary, AB, Canada.

[2] Departments of Biochemistry & Molecular Biology and Oncology, Robson DNA Science Centre, Arnie Charbonneau Cancer Institute, Cumming School of Medicine, Calgary, AB, Canada.

[3] Department of Biochemistry and Microbiology, University of Victoria, Victoria, BC, Canada.

[†] Labs contributed equally to this work.

* Lead Contact: email: vzarembe@ucalgary.ca

Highlights:

Keywords: Nuclear morphology, lysophosphatidylcholine, edelfosine, SIR complex, Rap1, transcription, nuclear envelope, Spt23/Mga2, Opi1, lipid metabolism, lipid droplets, yeast

Author contributions

M.L.S.P., J.A.C. and V.Z. designed the research.

M.L.S.P., M.H.R. and S.M.F. performed experiments.

M.L.S.P., M.H.R., S.M.F., J.A.C. and V.Z. analyzed the data.

M.L.S.P., J.A.C. and V.Z. wrote the manuscript.

Summary

The nuclear envelope (NE) is important for nuclear organization. This study shows that changes in NE lipid composition from lysolipid treatment decreases Sir4 association with telomeres, their clustering at NE, and triggers lipid-specific transcriptional circuits regulated by membrane-sensing factors.

Abstract

The nuclear envelope (NE) is important in maintaining genome organization. The role of lipids in the communication between the NE and telomere silencing was investigated, including how changes in lipid composition impact gene expression and overall nuclear architecture. For this purpose, yeast cells were treated with the non-metabolizable lysophosphatidylcholine analog edelfosine, known to accumulate at the perinuclear endoplasmic reticulum. Edelfosine treatment induced NE deformation and disrupted telomere clustering but not anchoring. In addition, the association of Sir4 at telomeres measured by ChIP decreased. RNA-seq analysis showed altered expression of Sir-dependent genes located at sub-telomeric (0-10 kb) regions, which was consistent with Sir4 dispersion. Transcriptomic analysis revealed that two lipid metabolic circuits were activated in response to edelfosine, one mediated by the membrane sensing transcription factors, Spt23/Mga2, and the other by a transcriptional repressor, Opi1. Activation of these combined transcriptional programs resulted in higher levels of unsaturated fatty acids and the formation of nuclear lipid droplets. Interestingly, cells lacking Sir proteins displayed resistance to unsaturated fatty acids and edelfosine, and this phenotype was connected to Rap1.

GRAPHICAL ABSTRACT

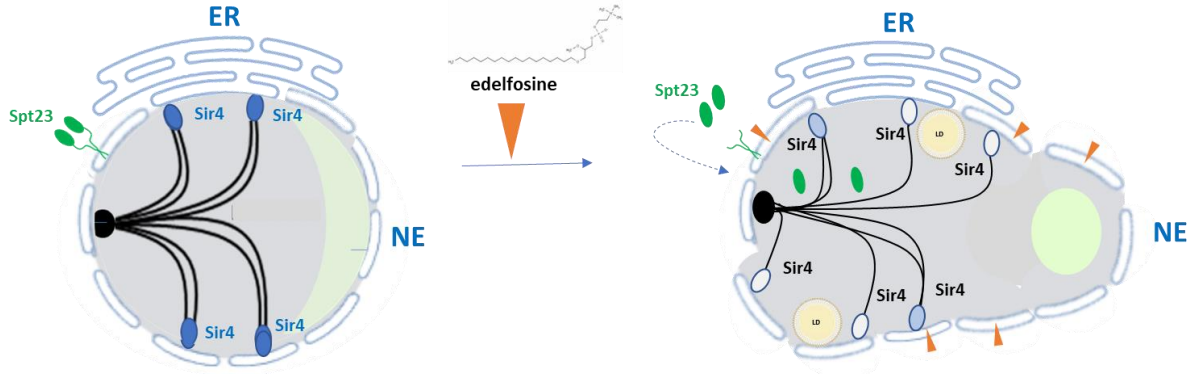

Introduction

The nuclear envelope (NE) is a double membrane layer contiguous with the endoplasmic reticulum (ER) that protects genomic material from the rest of the cell. The envelope is strategically positioned for sensing stress and transducing signals about lipid homeostasis into the nucleus, and is structurally critical for organizing the genome (Bahmanyar and Schlieker, 2020).

As with all eukaryotes, the nucleus of budding yeast is highly organized. The yeast nucleus is arranged in a Rabl configuration, where centromere clustering at the NE causes chromosomes to occupy spatially constrained territories, promoting clustering between telomeres anchored at the NE (Bystricky et al., 2005; Hozé et al., 2013; Jin et al., 1998). The nucleolus, which is the site of rDNA transcription and ribosome biogenesis, is also tethered to the NE and forms a crescent-shaped subnuclear compartment (Oakes et al., 1993; Taddei and Gasser, 2012; Yang et al., 1989). Therefore, the NE is a key player in the organization of the nucleus.

Interaction with the NE promotes the local accumulation of transcription factors (TFs) and transcription regulators (TRs) at telomeres and rDNA, facilitating silencing (Taddei and Gasser, 2012). The most thoroughly characterized example of proteins that interact with NE-bound anchors involves the formation of heterochromatin by the Silent Information Regulator (SIR) protein complex, which includes Sir2, Sir3, and Sir4 for deacetylation of lysine 16 of histone H4 (Grunstein and Gasser, 2013). In budding yeast, heterochromatin forms at telomeres and the mating type loci *HML* and *HMR* on chromosome 3. Another silencing factor, Sir1, contributes to transcriptional repression at the silent *HM* mating-type loci, but not at telomeres (Aparicio et al., 1991; Pillus and Rine, 1989). Telomere positioning at the NE occurs through two redundant pathways, where telomere-associated Sir4 binds with the inner nuclear membrane (INM) proteins Esc1 and Mps3, or alternatively where yKu70/80 binds with Mps3 (Hediger et al., 2002; Bupp et

al., 2007). Sir4 and Sir3 bind telomeres through interactions with Rap1 (Luo et al., 2002; Moretti et al., 1994), which itself is bound to the double-stranded TG_{1-3} moiety (Buchman et al., 1988a), and together with Sir2, a highly conserved NAD-dependent histone deacetylase (Imai et al., 2000), they form the SIR repressive complex. This complex associates with nucleosomes containing Rap1 bound DNA and self-propagates along sub-telomeric sequences (Grunstein and Gasser, 2013). Telomere anchoring at the periphery increases the relative concentration of SIR proteins, which can also interact in *trans* with SIR proteins bound to other telomeres to form clusters (Gotta et al., 1996; Taddei et al., 2009). The 32 telomeres of a yeast haploid cell typically cluster in ~3-5 foci during log phase (Laroche et al., 1998; Moradi-Fard et al., 2016). Although anchoring facilitates the formation of repressive compartments at the periphery, which silences sub-telomeric genes, anchoring can occur in the absence of SIR proteins, and association with the nuclear periphery is not a prerequisite for transcriptional silencing (Taddei and Gasser, 2012; Taddei et al., 2009). Importantly, a reduction in SIR protein association with sub-telomeric regions has been observed in response to DNA damage and stress, indicating that regulation of silencing may be a way to control gene expression at specific silent chromatin domains (Mills et al., 1999; Martin et al., 1999; Ai et al., 2002).

As described above, the pathways that regulate NE anchoring and clustering of telomeres depend on reversible interactions between proteins bound to chromosomes and NE membrane proteins. The impact of NE lipids on these pathways and gene expression is currently unknown. However, some links between lipid metabolism and chromatin organization have been previously identified. For example, decreased fatty acid synthesis due to mutations in acetyl-CoA carboxylase coincided with elevated histone acetylation and contribute to the increased expression of factors regulated by histone deacetylases, similar to cells where *SIR2* has been deleted (Galdieri and

Vancura, 2012; Papsdorf and Brunet, 2019). Acetyl-CoA derived from the breakdown of fatty acids accounts for a significant portion of the carbon source used in histone acetylation, indicating that transcriptional regulation is impacted by changes in the lipid landscape (McDonnell et al., 2016). Changes in lipid metabolic pathways have also been shown to affect NE size and shape, most notably with the accumulation of phosphatidic acid (PA), a key metabolic intermediate in membrane lipid synthesis, causing a large expansion of the NE, particularly at the nucleolus (Campbell et al., 2006; Witkin et al., 2012; Carman and Han, 2019; Wolinski et al., 2015). The nucleolus-associated NE also defines a membrane subdomain that becomes actively involved in triacylglycerol (TAG) metabolism in response to cell cycle and nutrient signals (Barbosa et al., 2019).

Beyond the nucleolus, not much is known about how other nuclear territories respond to lipid changes at the nuclear envelope. However, there are studies suggesting lipid homeostasis may affect telomere regulation. For example, Sir3 binding and silencing at sub-telomeres is compromised in response to chlorpromazine, an amphiphilic drug that perturbs internal membrane structures by interacting with the polar headgroups of phospholipids (De Filippi et al., 2007; Ai et al., 2002). Additionally, the telomerase antagonist Rif1, a protein that competes with Sir3 and Sir4 for binding to Rap1, is recruited to the NE through palmitoylation (Park et al., 2011; Fontana et al., 2019; Wotton and Shore, 1997). Previous work has also implicated sterols and sphingolipids in the regulation of telomere clustering. Cells lacking Arv1, a factor required for normal intracellular sterol distribution in yeast and mammalian cells (Tinkelenberg et al., 2000), displayed abnormal nuclear morphology and compromised telomere clustering (Ikeda et al., 2015; Papagiannidis et al., 2021). Similar effects were observed when sphingolipid levels decreased in response to pharmacological tools or mutations that inhibited enzymes of the ceramide

biosynthetic pathway (Kajiwara et al., 2012; Ikeda et al., 2015). Sterols and sphingolipids are known to form domains in biological membranes based on their preferential interaction, and yeast cells respond to changes in sterol composition of their membranes by adjusting sphingolipids levels (Guan et al., 2009). Lysophosphatidylcholine (lysoPC) lipid analogues disrupt sterol-sphingolipid domains in yeast (Zaremberg et al., 2005). Cells with mutations in ergosterol (*erg3*Δ mutant) or sphingolipid biosynthesis (*lcb1-100* mutant) were hypersensitive to lysoPC related drugs (Zaremberg et al., 2005), while cells lacking chromatin modifiers like Sir4 displayed resistance to these lysoPC analogues (Cuesta-Marbán et al., 2013), pointing to a possible link between membrane lipid alterations and nuclear organization and gene silencing.

We investigated how alterations in membrane lipid composition imposed by a lysoPC burden impact nuclear architecture and gene expression. With this intention, yeast cells were treated with edelfosine, a non-metabolizable lysoPC analogue that accumulates at the NE. Edelfosine belongs to a group of antineoplastics and antiprotozoals known to target membranes. We previously validated budding yeast as a model organism to study this family of non-metabolizable lysoPC lipid analogues using edelfosine as the prototype (Zaremberg et al., 2005). This antitumor therapeutic was shown to function through a novel mechanism involving selective disruption of lipid rafts at the plasma membrane, which in yeast was characterized by sterol internalization and degradation of the lipid raft-associated proton pump Pma1 (Zaremberg et al., 2005; Czyz et al., 2013). Once internalized, edelfosine accumulated at the perinuclear ER (pER) in both yeast (Cuesta-Marbán et al., 2013) and mammalian cells (Bonilla et al., 2015; Gajate et al., 2012). Intriguingly, cells lacking components of the SIR complex like Sir4 displayed resistance to edelfosine (Cuesta-Marbán et al., 2013), opening the possibility that lipid composition in the ER/NE impacts nuclear architecture.

Here we report that edelfosine led to severe changes in the structure of the NE and nuclear associated compartments. We quantified significant changes in nucleolar morphology and telomere clustering, but not telomere anchoring. Using an unbiased RNA-sequencing approach we showed that edelfosine treatment led to a partial loss of silencing in sub-telomeric regions and increased transcription of genes controlled by Spt23 and Mga2 membrane-sensing transcription factors. The inactive membrane-bound forms of Spt23/Mga2 were cleaved in response to edelfosine, resulting in their translocation from the ER membrane into the nucleus. In addition, a dispersion of the SIR complex from telomeres accompanied the transcriptional changes initiated at the NE in the presence of edelfosine. Our work supports a model where disruption of the NE architecture by a lysoPC drug analogue were sufficient to trigger changes in membrane-associated transcription factors and chromatin regulators, connecting nuclear membrane lipid composition to genome organization and transcriptional regulation.

Results

Nuclear envelope deformation results in disruption of nuclear architecture

Due to its large phosphocholine head group and a single long saturated acyl tail (18:0), edelfosine has an “inverted cone shape” geometry, inducing membrane bending and disrupting lipid packing (Bierbaum et al., 1979). In addition, the presence of ether linkages to the *sn-1* and *sn-2* positions of the glycerol backbone render this lysoPC analogue metabolically stable, as it cannot be remodelled (Kny, 1969). Given that edelfosine accumulates at the NE (Cuesta-Marbán et al., 2013), we treated yeast cells with edelfosine to alter NE lipid composition in a controlled manner, so that we could investigate its impact on nuclear architecture and transcriptional activity.

Using live imaging in cells expressing the ER marker Sec63^{GFP}, we observed a 3-fold increase in non-spherical nuclei after treatment with 20µM edelfosine for 90 minutes (Figure 1A). These deformations in the NE resulted in diverse nuclear shapes deviating from sphericity, with some resembling those seen in yeast with altered PA homeostasis (Campbell et al., 2006; Witkin et al., 2012; Carman and Han, 2019; Wolinski et al., 2015). Asymmetric NE expansion from high PA levels is known to occur in a region of the NE adjacent to the nucleolus, dubbed a nuclear flare (Witkin et al., 2012). Thus, we next examined if deformation of the NE by edelfosine affected nucleolar morphology. Using the nucleolar marker Nop1^{CFP} in combination with the NE marker Nup49^{GFP}, we observed condensation and a significant shrinkage of the nucleoli in edelfosine treated cells (Figure 1B). Interestingly, condensed nucleoli were positioned within a flare-like region of the NE induced by edelfosine.

Unlike other chemotherapeutic drugs, edelfosine does not target DNA, despite accumulating in the NE. However, edelfosine has been shown to induce DNA fragmentation by production of reactive oxygen species after extended treatment (Renis et al., 2000; Zhang et al., 2007). To determine whether DNA damage was being induced in the timescale of our experiments, the phosphorylation of Rad53 and histone H2A^{Ser129} were analyzed by western blot after edelfosine treatment (Figure S1). No checkpoint signaling response to DNA damage was observed with either of these markers.

To gather further insight about the overall impact of NE deformation, we next investigated other territories and compartments with links to the periphery. Since telomeres show perinuclear anchoring and clustering (Figure 2A), we next determined whether these properties were altered by edelfosine. First, anchoring was assessed by visualizing individual telomeres using the system where lacI-GFP conjugates to lacO arrays integrated in either Tel06R or Tel08L (Figure 2B)

(Meister et al., 2010). No significant change in telomere association with the periphery was detected after edelfosine treatment, indicating anchoring continued even with extensive alterations in NE shape, delineated by Nup49^{GFP} (Figure 2C and Figure S2A). We next determined telomere clustering by performing live cell imaging of Rap1^{GFP} foci. In line with previous reports, we observed that 32 telomeres in haploid cells clustered in ~ 3-5 foci (Figure 2D) (Laroche et al., 1998; Moradi-Fard et al., 2016). Upon edelfosine treatment, this increased to ~6-7 foci, suggestive of a defect in clustering, where Rap1-bound telomeres are not spatially bundled as effectively (Figure 2D). Consistent with this interpretation, Rap1 recovery by ChIP at three different telomeres, Tel01L, Tel06R, and Tel15L, was statistically similar in the presence and absence of edelfosine (Figure 2E), indicating that the increased number of foci did not result from massive changes in the association of Rap1 with telomeres. Moreover, Rap1 protein levels (Figure 2F) and the fraction of Rap1 associated with the membrane fraction (Figure S2B) did not change, indicating that Rap1 bound telomeres remained anchored at the periphery when the NE was distorted by edelfosine treatment. Importantly, cell cycle analysis by flow cytometry found that cells accumulated in G1 and depleted from S/G2 in response to edelfosine, which indicates that the increase in Rap1 foci is not due to an increase in the number of cells with double DNA content (Figure S2C).

Altogether, these findings support the notion that NE deformations induced by edelfosine resulted in the loss of NE sphericity affecting all regions of the nuclear membrane, from flares associated with the nucleolus to regions interacting with the bulk of the DNA. These NE deformations, in turn, impacted nuclear architecture, inducing nucleolar compaction and altering telomere clustering, but not anchoring.

The SIR complex is susceptible to lipid alterations at the NE

We next investigated the SIR complex in edelfosine, as defects in telomere clustering, which can occur independently of anchoring, are associated with dispersion of the SIR complex normally bound at telomeres (Ruault et al., 2011). Moreover, as mentioned above, a chemogenomic screen previously identified *sir4*Δ mutant cells as edelfosine resistant (Czyz et al., 2013; Cuesta-Marbán et al., 2013). Since the screen was performed in the BY4741 background, we first manually verified these results in W303, the background used in the current study. As with *sir4*Δ, deletion of *SIR2* or *SIR3* led to edelfosine resistance compared to wild type (Figure 3A). Expression of *SIR4* from a centromeric plasmid reverted edelfosine resistance in *sir4*Δ (Figure S3A).

To explore how edelfosine impacted SIR interactions with telomeres, we next performed ChIP with $Sir4^{Myc}$. There was a marked decrease in $Sir4^{Myc}$ recovery at the three telomeres we monitored (Figure 3B). To complement ChIP, we also performed live cell imaging with $Sir4^{GFP}$ after edelfosine treatment, and observed a reduction in punctate foci formation, which is suggestive of a defect in telomere clustering (Figure 3C) (Moradi-Fard et al., 2016; Palladino et al., 1993). Taken together, these results suggest that deformation of the NE by edelfosine destabilize protein-protein interactions mediated by the SIR complex at telomeres, resulting in Sir4 dispersion and a reduction in telomere clustering. Of note, sensitivity to edelfosine was not affected by C-terminal tagging Sir4 with GFP (Figure S3B).

Transcriptional changes induced by NE deformation

So far, we have shown that edelfosine induced NE membrane deformations with consequential changes in nuclear architecture, impacting Sir4 association with telomeres and their clustering, as well as nucleolar compaction. These results suggest a loss of Sir-dependent transcriptional regulation at telomeres and decreased transcription in the nucleolus. Yeast cells

exposed to various stressors have shown rDNA compaction (reviewed in Matos-Perdomo & Machín, 2019). This phenotype is linked with epigenetic changes as a consequence of altered protein interactions with the NE, as exemplified by rDNA tethering to the NE through the chromosome linkage INM proteins (CLIP) complex (Golam Mostofa et al., 2018; Mekhail et al., 2008; Chan et al., 2011) in combination with the Sir2 histone deacetylase (Gottlieb and Esposito, 1989; Bryk et al., 1997; Fritze et al., 1997; Smith and Boeke, 1997). Similarly, telomere clustering at the NE serves as a platform where protein-protein interactions are strengthened, reinforcing transcriptional silencing (Taddei et al., 2009). Many different NE scaffolding proteins and DNA interacting factors could collaborate to modulate the NE changes imposed by edelfosine into transcriptional changes at telomeres and in the nucleolus. In order to assess the overall transcriptional response, we therefore performed RNA-sequencing (RNA-seq) in the presence of edelfosine. We reasoned that information acquired by this unbiased approach would not only be a resource for understanding the full physiological impact of edelfosine at the molecular level, but also had the potential to reveal unique edelfosine-induced transcriptional changes associated with abnormal NE morphology distinct from the 'general response' accompanying most stressors.

A total of 224 genes were found to be differentially expressed in edelfosine when a stringent cut-off of > ln(2)-fold change was used together with a false discovery rate of $p < 0.01$. Of these, 119 genes were upregulated and 105 were downregulated (complete list in Table S1). We found that 12.6% of the targets upregulated > 2-fold resided in sub-telomeric regions. By contrast, only 4.2% of all genes in the yeast genome are encoded within this same region (p-value 0.0001 by Fisher's exact test) (Taddei et al., 2009).

To harmonize the observed Sir4 dispersion detected by microscopy and ChIP with sub-telomeric changes in transcription, we queried known SIR targets before moving on to a more

expanded analysis of the RNA-seq data. We reasoned that the dispersion of SIRs from telomeres could contribute to the transcriptional changes we detected. Sir2-dependent silencing is prevalent in a zone 0-10 kb from the chromosome ends (Hughes et al., 2000; Bernstein et al., 2000; Ellahi et al., 2015), whereas Hda1 deacetylase acts preferentially within ~10-25 kb from telomeres (Robyr et al., 2002), and Rpd3 deacetylase impacts transcription and functions at boundary sites in sub-telomeric regions to prevent the spreading of heterochromatin in opposition to Sir2 (Zhou et al., 2009; Bernstein et al., 2000; Rundlett et al., 1996; Ehrentraut et al., 2010). Of the 120 genes present in the 0-10 kb zone, 29 were upregulated in response to edelfosine when using a cut-off of > ln(0.5)-FC (Table S2).

Two gene families known to be silenced by SIR were represented among this set, including the seri**pau**perin (*PAU*) family (Ai et al., 2002) and the **co**nserved **s**equence (*COS*) gene family (MacDonald et al., 2015; Bedalov et al., 2001). Given that the coding sequence is nearly identical within each family, we designed both specific (*PAU20*, *COS5*, *COS10*) and general (*PAUG'*, *COSG'*) primers to perform qPCR experiments (Figure S3D, E). As these are known SIR targets, *COS* expression was indeed higher in *sir4*Δ mutants compared to wild type in the absence of edelfosine (Figure S3F). Consistent with the RNA-seq, edelfosine induced a 2.5 ± 0.49 and 1.5 ± 0.82 ln-fold increase in transcription of *PAU* and *COS* genes respectively (Figure S3G). In the cells where *SIR4* was deleted, edelfosine-induced transcription was significantly lower for both gene families compared to wild type, although there was a mild increase in *PAU* expression (1.5 ± 0.23) in *sir4*Δ mutants (Figure S3G).

Furthermore, as expected for Sir4 dispersion considering the protein level of Sir4 remained constant after edelfosine treatment (Figure S3C), known internal (non-sub-telomeric) Sir4 targets represented 22.9% of the downregulated genes in edelfosine (p-value 2.56E-8 by Fisher's exact

test; complete list in Table S3) (Taddei et al., 2009). Taken together, these data support our model that changes in transcription upon edelfosine treatment occur in part through Sir4 disruption and reduced localization to telomeres.

Ribosomal protein genes emerged as the most significantly enriched category of downregulated genes (Figure S4B), consistent with the accompanied rDNA compaction and an expected overall decrease of ribosomal biogenesis. Moreover, in alignment with a recent study demonstrating stress inhibits rRNA processing first rather than rDNA transcription (Szaflarski et al., 2022), we found no significant difference in transcription of the rDNA by qPCR of the 35S fragment (Figure S4C, D).

Transcription factors mediating changes induced by NE deformation

Next, we looked for over-represented transcription factors (TFs) and transcription regulators (TRs) that could bind to the promoter regions of the two sets of up-and down-regulated genes after edelfosine treatment. Gene promoter analysis with TFs and TRs based on DNA binding was next performed using Yeastract (Monteiro et al., 2020). This analysis identified 6 and 7 TFs/TRs for the up- and down- regulated gene clusters, respectively (p-value <1E-05; Tables 1 and 2). In the cluster of upregulated genes, there was an enrichment of binding sites for TRs involved in the response to oxidative stress and metals. For the cluster of down-regulated genes, we identified Rap1 and its co-regulators of ribosomal protein genes Ifh1 and Fhl1 (Cherel and Thuriaux, 1995; Wade et al., 2004; Rudra et al., 2007), as well as TFs Fkh1 and Fkh2. Interestingly, 36.2% of the down-regulated genes overlapped with known Rap1 targets (Figure 4A, B) (Lieb et al., 2001). Of these, 89.5% were ribosomal protein genes (Figure 4B and Table S4). Representative Rap1 target genes selected for validation by qPCR substantiated the RNA-seq findings (Figure

4C). Taken together with the nucleolar condensation we observed by microscopy (Figure 1B), our data point to a decrease in ribosome biogenesis after edelfosine treatment.

RAP1 is an essential gene, however a truncated allele missing 165 amino acids at the C-terminus, *rap1-17*, attenuates the repression of ribosomal protein genes in response to secretory pathway defects and disrupts silencing of sub-telomeric regions (Mizuta et al., 1998; Kyrion et al., 1992; Buck and Shore, 1995). By contrast, another characterized allele carrying two missense mutations at amino acids 726 and 727, *rap1-12*, results in loss of silencing at the homothallic mating (*HM*) loci, but does not alter transcription from ribosomal protein genes (Mizuta et al., 1998; Sussel and Shore, 1991; Buck and Shore, 1995). Cell growth on plates containing edelfosine showed that *rap1-17*, but not *rap1-12*, increased edelfosine resistance (Figure 4D). Interestingly, the *rap1-17* C-terminal truncation mutant described above also lacks the domain responsible for interacting with and recruiting Sir4 to telomeres (Cockell et al., 1995; Moretti and Shore, 2001; Luo et al., 2002). In sum, these results support and expand our findings with the SIR complex and suggest the C-terminus of Rap1 facilitates interactions with Sir4 that mediate edelfosine sensitivity.

Spt23 and Mga2 are activated in response to edelfosine

To understand the mechanism by which changes in the lipid composition at the NE are sensed and communicated to the nucleus, we directed our RNA-seq analysis to differentially expressed genes related to lipid metabolism and transport in response to edelfosine. For these combined categories, an estimated ~ 9% (109 genes) and ~ 4.5% (60 genes) of the total transcripts differentially expressed [> 0.5 (ln)-fold change cut-off and $p < 0.01$] were upregulated and downregulated, respectively, in edelfosine. Distinct metabolic branches affecting all lipid classes, including glycerolipids, sphingolipids and sterols, were mapped for each of the up and down

datasets (Figure 5A and Table S5). Two critical transcriptional circuits that regulate lipid metabolic pathways clearly emerged from this analysis: Opi1/Ino2/4-mediated repression and Spt23/Mga2 activation. Furthermore, Spt23 was identified as a transcription factor enriched from the RNA-seq analysis (Table 1) and its targets were among the group of transcripts displaying the most dramatic changes in response to edelfosine with >2(ln)-fold change (Figure 5B and Table S5). Spt23, together with its paralog Mga2, maintain NE integrity by way of an ER to nucleus signaling pathway (Zhang et al., 1999). Spt23/Mga2 regulates lipid remodelling by activating expression of *OLE1*, the gene encoding the only fatty acid desaturase present in budding yeast (Zhang et al., 1999; Chellappa et al., 2001; Auld et al., 2006; Martin et al., 2007; Fang et al., 2017; Romero et al., 2018). To confirm activation of the Spt23/Mga2 circuit, we measured transcription of *OLE1* and other targets of Mga2 and Spt23 by qPCR upon edelfosine treatment. Consistent with the RNA-seq results, *OLE1, ICT1, IZH1, IZH2, IZH4* and *MGA2* itself were upregulated while no changes were observed for *SPT23 or IZH3* (Figure 5B, inset). In addition, we also confirmed by qPCR the repression of *INO1*, a representative target of Opi1, and *OPI1* self-repression (Jesch et al., 2005; Nikawa and Kamiuto, 2004) upon edelfosine treatment (Figure 5B, inset).

It is worth noting that Spt23 and Mga2 have been previously proposed to be antagonists of silencing (Dula and Holmes, 2000). In fact, 40% of the sub-telomeric genes differentially expressed by treatment with edelfosine can be mapped to the Spt23 regulated network (Table S5). Therefore, Spt23/Mga2 emerged as strong candidates to sense the lipid changes imposed by edelfosine at the NE.

Spt23 and Mga2 form homodimers that insert into the ER membrane by a single transmembrane helix, which is sensitive to the lipid environment (Ballweg et al., 2020). High lipid saturation triggers ubiquitylation, which then signals for the subsequent proteolytic release of a

transcriptionally active N-terminal fragment that translocates into the nucleus, inducing *OLE1* expression (Figure 6A) (Hoppe et al., 2000). Based on the enrichment of Spt23 targets in the transcriptomic analysis, we next tested whether edelfosine treatment triggered the processing and subsequent translocation of Spt23 and Mga2 into the nucleus. To this end, we performed live cell imaging of cells expressing either ^{GFP}Spt23 or ^{GFP}Mga2 from a constitutive promoter wherein proteins were GFP tagged at their N-terminus. Cells harboring either construct showed ER localization (Figure S5), but after a short 30-minute treatment with edelfosine, 98% and 63% of the GFP signal from cells expressing ^{GFP}Spt23 and ^{GFP}Mga2 respectively were found in the nucleus, indicative of protein processing and translocation (Figure 6B, C). Importantly, the nuclear localization of ^{GFP}Spt23 or ^{GFP}Mga2 was not a general stress response, as no changes were observed when cells were treated with high levels of methyl methane sulfonate (MMS), an alkylating agent that causes DNA damage. ^{GFP}Spt23 and ^{GFP}Mga2 processing was further corroborated by western blot. Cleavage of ^{GFP}Spt23 could be seen as early as 10 minutes after treatment with edelfosine, with the protein being almost undetectable after 30-minute due to its short half-life (Hoppe et al., 2000) (Figure 6D). ^{GFP}Mga2 processing appeared slower (Figure 6E), as both the membrane bound precursor and the soluble active forms were detected after 60 minutes. These results support a role for Spt23 and Mga2 as sensors for changes in the lipid environment imposed by edelfosine accumulation in the NE, and as mediators of the transcriptional response aimed at triggering lipid remodeling in a landscape where the *de novo* synthesis of glycerolipids was repressed.

Membrane alterations by edelfosine precede changes in nuclear architecture

As mentioned above, Spt23 and Mga2 are believed to function as silencing antagonists (Dula and Holmes, 2000). Edelfosine triggers Spt23/Mga2 processing and subsequent

translocation into the nucleus and, as demonstrated above, edelfosine also triggered SIR complex delocalization within the nucleus (Figure 3). The lipid changes associated with NE deformation and Spt23/Mga2 activation could subsequently induce alterations in nuclear organization, including telomere clustering and Sir4 dispersion. Alternatively, a loss of the SIR complex from telomeres in response to edelfosine treatment could result in altered transcription, sensitizing the membrane and resulting in NE conformational changes. To bring insight to these possibilities, we wanted to determine which occurs first: membrane deformation or SIR dispersion. Spt23 and Mga2 are functionally redundant, but the loss of both is lethal (Zhang et al., 1997, 1999), precluding us from determining Sir4 recovery and localization in cells where both were deleted. However, we reasoned that if morphological alterations of the NE and lipid sensing by Spt23 and Mga2 occurred upstream, then changes in nuclear shape and Spt23/Mga2 processing would still occur in the absence of Sir4. Indeed, edelfosine induced NE deformations in *sir4*Δ mutants similarly to *SIR4*$^{+}$cells (Figure 7A). Moreover, ^{GFP}Spt23 and ^{GFP}Mga2 translocation was similar in *sir4*Δ and wild-type cells upon edelfosine treatment (Figures 7B, C). Interestingly, in *sir4*Δ mutant cells the level of upregulation in some Spt23/Mga2 targets reproducibly decreased after edelfosine treatment, including the transcription of *OLE1* (Figure 7D).

We next sought to assess if fatty acid unsaturation was augmented in response to edelfosine and if this increase was dependent on Sir4. In line with the upregulation of *OLE1* transcription, neutral lipid analysis of cells treated with edelfosine exhibited higher levels of unsaturated free fatty acids (FFA). Interestingly, this increase was significantly less in *sir4*Δ mutants (Figure 8A). These results support a model whereby edelfosine-induced alterations in lipid composition at the NE are sensed by Spt23/Mga2, resulting in the activation of *OLE1* and a concomitant accumulation of unsaturated FFAs.

A build-up of edelfosine together with unsaturated FFAs could result in a synergistic lipotoxic effect, suggesting that the presence of the SIR complex decreases the lipid detoxifying capacity of yeast. To challenge this idea, we tested the fitness of *sir* mutants on two unsaturated fatty acids commonly found in the yeast lipidome, oleate (18:1) and palmitoleic acid (16:1). Similar to plating on edelfosine, all of the *sir* mutants grew better on these unsaturated FAs compared to wild type (Figure 8B and 8C). The *gpt2*Δ mutant was included as a control as it does not grow on oleate but grows on palmitate (Lockshon et al., 2007; Marr et al., 2012). This suggests that the SIR complex compromises the lipid detoxifying capacity of yeast.

One cellular strategy behind lipid detoxification at the NE is to direct excess fatty acids towards TAG synthesis and lipid droplet (LD) biogenesis (Barbosa et al., 2019; Romanauska and Köhler, 2021). Depending on the status of lipid-related transcriptional circuits, these LDs could accumulate inside the nucleus (nLDs) or face the cytosol (cLDs). When the Opi1/Ino2-4 circuit is repressed by deletion of *INO4*, ~30% of cells display nLDs in addition to cLDs. By contrast, when *OLE1* is overexpressed, either directly or through constitutive activation of Mga2, only cLDs are produced (Romanauska and Köhler, 2021). Furthermore, when Mga2 is constitutively activated in *ino4*Δ cells, nLDs are still produced. The latter scenario resembles the transcriptional status of cells treated with edelfosine. Since our transcriptomic analysis showed simultaneous Spt23/Mga2 activation and Opi1/Ino2/4 repression, we reasoned the inner nuclear membrane could induce production of nLDs in response to a lysoPC burden. To this end, the number of LDs and their localization was assessed by staining cells expressing the ER marker ^{DsRed}HDEL with BODIPY 493/503 (Szymanski et al., 2007) (Figure 8D). In wild type cells, the number of LDs increased from 10.04 ± 3.33 LDs/cell to 12.29 ± 3.61 LDs/cell after edelfosine treatment (Figure 8E). A strong contributor to the increase in LDs was the formation of nLDs inside the nucleus, as ~25%

of wild type cells treated with edelfosine had at least one nLD (Figure 8F). Although cells lacking Sir4 displayed fewer LDs in control (7.92 ± 3.06 LDs/cell), there was a similar overall increase to 11.07 ± 4.54 LDs/cell upon edelfosine treatment (Figure 8E).

LD bulging from the nuclear membrane towards the nucleoplasm could be a significant contributor to NE deformation, disrupting telomere clustering and overall nuclear architecture independently of transcriptional silencing. Although deacetylation by the SIR complex appears to decrease the lipid detoxifying capacity of yeast since edelfosine and oleate tolerance increases in sir mutant cells, deletion of *SIR4* did not reverse LD formation after edelfosine. In all, these results indicate nLD formation is part of the cellular response to edelfosine, and that it occurs independently of Sir4.

Discussion

The nucleus, the defining feature of eukaryotic cells, is delimited by a double membrane structure that contains associated integral and peripheral proteins and is vital for the processes regulating nuclear compartmentalization. The architecture of the nucleus is highly regulated, and disruption of its structure has been linked to functional defects such as aberrant gene silencing, loss of chromatin anchoring, incomplete chromosome segregation and faulty cellular differentiation (Golden et al., 2009; Schreiner et al., 2015; Smith et al., 2017; Teixeira et al., 2002). Important, but seemingly often overlooked players in nuclear architecture and regulation, are the lipids that comprise the NE, although perturbations directed at glycerolipid metabolism have been shown to affect NE shape, impacting mainly the NE membrane closely associated with the nucleolus (Santos-Rosa et al., 2005; Siniossoglou et al., 1998; Campbell et al., 2006; Barbosa et al., 2019).

In this study, our work revealed that changing the lipid composition of the NE through a lysolipid burden impacted nuclear architecture and gene expression. Lysolipids are known to introduce membrane deformations and are usually present in small amounts in biological membranes, as they are rapidly re-acylated or metabolized (Fuller and Rand, 2001). Therefore, we manipulated the NE lipid composition by treating cells with edelfosine, a lysoPC analogue that cannot be altered or metabolized. Our data support a model wherein edelfosine-induced changes within the membrane triggered a distinct transcriptional response, indicating contacts between chromatin-associated factors and the nuclear membrane are functionally sensitive to variations in the lipid environment. Deformation of the NE from edelfosine treatment led to changes in genome organization, supporting transcriptional programs aimed at correcting membrane defects and lipid detoxification. Two subnuclear compartments, the nucleolus and telomeres, switched their transcriptional status in response to edelfosine. Telomere clustering decreased and in general transcription of genes in sub-telomeric regions increased, whereas the nucleolus became more compact and there was an overall repression of genes regulating ribosome biogenesis.

The SIR complex is susceptible to a lysolipid burden

Components of the SIR complex are known to shuttle between telomeres and the nucleolus, the two subnuclear compartments that showed pronounced changes in their transcriptional status during edelfosine treatment (Gotta et al., 1997; Kennedy et al., 1997; Radman-Livaja et al., 2011). SIRs promote telomere clustering, and Sir3 directly promotes long-range contacts between distant chromatin regions, and acts as a molecular bridge between the rDNA and telomeres (Ruault et al., 2021; Hoppe et al., 2002; Radman-Livaja et al., 2011).

SIR association with chromatin at telomeres was highly reactive to an increased burden of lysolipids, like the one imposed by edelfosine. Edelfosine-treated cells led to a reduction in

telomere clustering with partial release of Sir4 from telomeres (Figures 2D & 3C) and a reduction in silencing of sub-telomeric regions (Table S2). It is estimated that ~6% of sub-telomeric genes are silenced by SIRs (Ellahi et al., 2015). While our RNA-seq data showed a loss of silencing at many known SIR targets like *COS7*, *COS4*, *THI5*, *COS8*, *COS1*, *PAU22* and *FDH1* in response to edelfosine (Table S2) (Ellahi et al., 2015; Ai et al., 2002) our data did not perfectly align with all previously reported SIR targets (Ellahi et al., 2015). For example, *IMD2* expression was downregulated 2.8 ln-fold change in response to edelfosine (Table S2), while the opposite effect was seen in sir deletion mutants (Ellahi et al., 2015) suggesting this gene may also be the target of tighter repression by another HDAC or transcription repressor activated by edelfosine. Understanding the overall impact of edelfosine on SIR targets and SIR-independent targets will indeed require additional investigations.

In contrast to Sir4, Rap1 remained bound to telomeres and the telomeres themselves remained anchored after edelfosine treatment. One model to explain these data, which would be in line with how edelfosine functions in lipid bilayers, is that the fluid nature of the membrane decreases where telomeres anchor, impacting the natural dynamics of how they normally cluster (Schober et al., 2008; Hozé et al., 2013). That is to say, while telomere anchoring to the membrane relies on the interaction of chromatin factors with peripheral and integral membrane proteins like Esc1 and Mps3, respectively, clustering relies more on membrane fluidity, allowing the lateral movement of these proteins to bundle and be further stabilized by Sir-mediated *trans* interactions. Edelfosine is known to disturb membrane domain organization at the PM (Ausili et al., 2008; Zaremberg et al., 2005; Cuesta-Marbán et al., 2013; Czyz et al., 2013), and it is reasonable to propose that edelfosine is acting similarly once reaching the ER/NE. An additional contribution to NE deformation and obstruction for telomere clustering may come from the bulging of nuclear

LDs in an attempt of cells to recalibrate the fatty acyl composition of the membrane to ease the lysoPC burden.

Edelfosine-induced repression of ribosomal protein genes

Although Rap1 recovery at telomeres was minimally altered after edelfosine treatment, our study did find that edelfosine induced repression of ribosomal protein genes, which are known to be regulated by Rap1. While a reduction in ribosome biogenesis is part of a general stress response, the signaling pathways leading to a coordinated Rap1-dependent repression of ribosomal protein expression differs depending on the stress. For example, it was previously demonstrated that the *rap1-17* allele prevents ribosomal repression during the secretory stress response, but not the heat shock (Mizuta et al., 1998) or nitrogen starvation responses (Miyoshi et al., 2001). As with the secretory pathway, edelfosine resistance of *rap1-17*, but not *rap1-12*, suggests that repression of ribosomal proteins induced by the lipid drug requires Rap1 C-terminus interaction with Sir4. Altogether, the observed resistance of cells lacking SIR complex components or the C-terminal end of Rap1 supports a model whereby Sir4 binding to Rap1 contributes to edelfosine toxicity (Figures 3A & 4D).

Sensing lipid changes by Spt23/Mga2 and Opi1, what is being sensed?

Our unbiased RNA-seq approach identified Spt23 and Mga2 transcription factors as membrane sensors that are sensitive to the lipid changes induced by edelfosine. The inactive forms of Spt23/Mga2 reside in the ER/NE membranes and have been previously shown to sense membrane fluidity (Covino et al., 2016), although this concept has been recently challenged by uncovering a particular sensitivity of Mga2 to the degree of lipid saturation instead of viscosity (Ballweg et al., 2020).

What Spt23 and Mga2 are sensing in edelfosine treated cells remains an open question. Activation of these transcription factors was an early event noticed in live cells as early as 30 minutes, thus they might be capable of sensing the saturated C18:0 tail or the change in membrane curvature directly introduced by this lysoPC analogue. Indeed, it is the combination of membrane curvature and composition that modulates lipid packing and protein recruitment (Vanni et al., 2014), opening the possibility that Spt23/Mga2 are sensitive to one or both of these membrane properties.

It is known that edelfosine reduces the stored membrane curvature elastic stress, which is a membrane property that plays a role in the recruitment of several proteins to membranes (Dymond et al., 2008). One such protein is the CTP:phosphocholine cytidylylphosphotransferase (CCT) which localizes to the nucleus and senses curvature through an amphipathic helix (Haider et al., 2018; Taneva et al., 2012; Attard et al., 2000). CCT represents the rate limiting and committed step for the synthesis of PC through the Kennedy pathway, and edelfosine alters its recruitment to membranes while inhibiting the pathway in both yeast and mammalian cells (Boggs et al., 1995; Zaremberg and McMaster, 2002). Of note, it has been shown that in hepatocytes nLDs recruit CCTα (Fujimoto, 2022; Sołtysik et al., 2019). Since we show herein that edelfosine induces nLD biogenesis (Fig 8E), this mechanism could also contribute to the effects previously associated with edelfosine treatment and its impact on CCT activity and the Kennedy pathway.

Opi1 is a transcriptional repressor and the downregulation of Opi1 targets by our RNA-seq analysis suggests that Opi1 is released from the ER and translocated to the nucleus. This occurs in conditions of low PA or in conditions where cytosolic acidification leads to protonation of the phosphate group in PA (Loewen et al., 2004; Young et al., 2010). Edelfosine induces rapid cytosolic acidification (Czyz et al., 2013; Zaremberg et al., 2005). The combined activation of

Spt23/Mga2 and Opi1 circuits by edelfosine would result in the upregulation of FA unsaturation and glycerolipid remodelling pathways and a shutdown of de novo glycerolipid synthesis.

Lipid changes and nuclear territories: insights from edelfosine transcriptomics

The combined analysis of previous lipidomic (Tambellini et al., 2017) and current transcriptomic and neutral lipid profile analysis point to major changes in neutral lipid metabolism leading to unsaturated FA and DAG accumulation (Figure 8A). Importantly, a membrane subdomain linked to lipid droplet biogenesis has been defined at the nuclear envelope tightly connected to the nucleolus (Romanauska and Köhler, 2018). Interestingly, the trans-acylase Lro1 was recently shown to be enriched in this subdomain in response to cell cycle and nutrient signals (Barbosa et al., 2019). Lro1 consumes DAG while generating TAG and LysoPC, which is re-acylated by a PC remodelling pathway (Oelkers et al., 2000). The accumulation of a non-metabolizable LysoPC analogue like edelfosine at the NE would frustrate cellular attempts for re-acylation, resulting in membrane deformation and possible inhibition of TAG synthesis, inducing local DAG accumulation. The lipid metabolic landscape emerging from edelfosine transcriptomic results certainly supports accumulation of DAG through the repression of biosynthetic pathways that consume DAG and the upregulation of several catabolic branches directly producing DAG through TAG lipolysis, phospholipase C, and PA phosphatase Pah1 activities (Figure 5A).

In summary, our work suggests that disruption of the nuclear membrane is sufficient to induce changes in membrane-associated transcription factors and chromatin remodellers. Edelfosine has been studied as a chemotherapeutic, particularly in leukemic bone marrow purging (Vogler and Berdel, 2009; Mollinedo et al., 2004). The current work suggests that the NE could represent a novel target for chemotherapeutics, since lipid drugs like edelfosine are not mutagenic and appear to regulate the activity of sirtuins, which are known to be relevant in the development

of multiple chronic diseases (Wang et al., 2012; Bindu et al., 2016; Winnik et al., 2015; Kurylowicz, 2016).

Materials and Methods

Reagents. Unless otherwise indicated, all reagents were purchased from Fisher or Sigma. Yeast extract, peptone, and yeast nitrogen base were from MP Biomedicals (Santa Ana, CA). BODIPY™ 493/503 was ordered from Fisher Invitrogen (D3922). All lipids were ordered from Sigma [1-2-dioleyl-*sn*-glycerol (800811C), oleic acid (O1008-1G), 1,2,3,-trioleylglycerol (870110O) and cholesteryl oleate (C9253)], except for ergosterol (Fluka Analytical, 45480). Edelfosine was the kind gift of Medmark Pharma GmbH.

Yeast strains, plasmids and primers. Detailed information on yeast strains, plasmids and primers used in this study is provided in Tables 3, 4 and 5 respectively.

Strains expressing DsRed-HDEL were transformed with the integrating plasmid pAM41 using the standard transformation protocol (Guthrie and Fink, 1991). Strain JC4881 was created by mating and tetrad dissection, as described previously (Morin et al., 2009). Briefly, parental strains of opposite mating types were streaked on YPD with one intersecting area to allow mating and produce diploids. Diploids were selected and sporulation was then induced by streaking on 2% potassium acetate plates Tetrads were identified by light microscopy and their cell walls were digested with 5 ug/mL Zymolyase (amsbio, 120491-1) in 1M sorbitol for 5 minutes at 30°C. Tetrads were then dissected using a Zeiss Axioskop 40 dissecting microscope and progeny expressing only the markers of interest were saved as the indicated strains. Genotypes were confirmed by colony PCR and sequencing.

SIR4, *MGA2* and *SPT23* coding sequences were PCR amplified from yeast genomic DNA (lab strain W303) using gateway compatible primers (Table 5). The amplified product was then cloned into Gateway™ pDONR™221 donor vector (ThermoFisher) to generate the corresponding entry clones. Entry clones for each indicated gene were confirmed by standard DNA sequencing (DNA sequencing facility, University of Calgary). *SIR4* was then subcloned into the *S. cerevisiae* Advanced Gateway™ Destination Vector pAG415GPD-ccdB, while *MGA2* and *SPT23* were subcloned into *S. cerevisiae* Advanced Gateway™ Destination Vector pAG415GPD-EGFP-ccdB (Alberti et al., 2007). The *S. cerevisiae* Advanced Gateway™ Destination Vectors were a gift from Susan Lindquist (Addgene kit #1000000011).

Table 3- Yeast strains used in this study

Strain	**Genotype**	**Source**
W303	*Mat a ura3-1 his3-11,15 leu2-3,112 trp1-1 ade2-1 can1-100*	R. Rothstein
JC470	*Mat a* W303 with *RAD5*$^{+}$	J Cobb
JC471	*Mat alpha* W303 with *RAD5*$^{+}$	J Cobb
JC1822	JC471 with *RAP1-GFP::LEU2*	Moradi-Fard et al., 2016

JC2494	JC471 with *8HIS-Smt3::TRP1 RAP1-13MYC:HIS*	This study
JC3737	JC470 with *sir4Δ::HIS3*	Moradi-Fard et al., 2016
JC3786	JC470 with *sir2Δ::TRP1*	This study
JC4311	JC470 with *sir3Δ::HIS3*	This study
JC4263	JC471 with *nup49::NUP49-GFP*	Moradi-Fard et al., 2021
JC4438	JC471 with *SIR4-GFP::KanMX6 TelVII::URA3*	Gasser lab (GA2140)
JC4881	JC470 with *RAP1-13MYC::HIS3* Cross of JC2494 x JC470	This study
JC5046	JC470 with *SIR4-GFP::KanMX6* Cross of JC4438 x JC470	This study
JC5047	JC470 with *SIR4-GFP::KanMX6 HDEL-DsRed::LEU2*	This study
GA1275	W303 with *SIR4-13MYC::KanMX6*	Perrod et al., 2001
GA1459	*MATa ade2-1 can1-100 his3-11,15::GFP-LacI-HIS3 trp1-1 ura3-1 leu2-3,112 nup49::NUP49-GFP-URA3 TELVI-R::lacO-lexA-TRP1* Kind gift of Dr. Susan Gasser	Hediger et al., 2002
GA1986	*MATa ade2-1 can1-100 his3-11,15::GFP-LacI-HIS3 trp1-1 ura3-1 leu2-3,112 nup49::NUP49-GFP-URA3 TELVIII-L::lacO-lexA-TRP1* Kind gift of Dr. Susan Gasser	Hediger et al., 2002
CMY204	W303 with *gpt2Δ::TRP1*	Zaremberg and McMaster, 2002
VZY452	JC470 with *DsRed-HDEL::LEU2*	This study
KM014	W303 with *rap1::LEU2 [pRS313-RAP1]*	Yeast Genome Resource Centre*
KM015	W303 with *rap1::LEU2 [pRS313-rap1-12]*	Yeast Genome Resource Centre*
KM016	W303 with *rap1::LEU2 [pRS313-rap1-17]*	Yeast Genome Resource Centre*
BY4741	*MATa his3Δ leu2Δ met15Δ ura3Δ*	Euroscarf
mga2Δ	BY4741 with *mga2Δ::KanMX4*	Euroscarf
spt23Δ	BY4741 with *spt23Δ::KanMX4*	Euroscarf
VZY397	BY4741 with *DsRed-HDEL::LEU2*	This study

VZY453	BY4741 with *sir4Δ::KanMX4 DsRed-HDEL::LEU2*	This study

*Strain provided by the NBRP, Japan.

Table 4 – Plasmids used in this study

Plasmid	**Description**	**Source**
Ycplac111-Sec63-GFP	SEC63 promoter, Sec63-GFP (CEN, *LEU2*)	Santos-Rosa et al., 2005
pAG415-ccdB	GPD promoter (CEN, *LEU2*)	Alberti et al., 2007
pAG415-Sir4	GPD promoter, Sir4 (CEN, *LEU2*)	This study
pAG415-EGFP-ccdB	GPD promoter, EGFP (CEN, *LEU2*)	Alberti et al., 2007
pAG415-EGFP-Mga2	GPD promoter, EGFP-Mga2 (CEN, *LEU2*)	This study
pAG415-EGFP-Spt23	GPD promoter, EGFP-Spt23 (CEN, *LEU2*)	This study
pAM41	pRS305-DsRED-HDEL Kind gift of Dr. Scott D. Emr	Manford et al., 2012
pFN4	NOP1 promoter, Nop1-CFP (CEN, *URA3*)	Bystricky et al., 2005

Table 5 – Primers used in this study

Primer	**Sequence**
SIR4-Gateway-F	GGGG ACA AGT TTG TAC AAA AAA GCA GGC TCT ATG CCA AAT GAC AAT AAG
SIR4-Gateway-R	GGGG AC CAC TTT GTA CAA GAA AGC TGG GTC ATA CGG TTT TAT CTC CTT
MGA2-Gateway-F	GGGG ACA AGT TTG TAC AAA AAA GCA GGC TCT ATG CAG CAG AAC AGT GAG TTC
MGA2-Gateway-R	GGGG AC CAC TTT GTA CAA GAA AGC TGG GTC CTA ACT GAC AAT TAA ATC GTT
SPT23-Gateway-F	GGGG ACA AGT TTG TAC AAA AAA GCA GGC TCT ATG ATG AGT GGC ACA GGA AAC
SPT23-Gateway-R	GGGG AC CAC TTT GTA CAA GAA AGC TGG GTC TTA ATT GAC TCG CAT GTC GTT
PAU20-qPCR-F	GAC GAA AGA GTC AAC TTG GTG
PAU20-qPCR-R	TGG TGA CTT GGT CTG GGG A
PAUGen-qPCR-F	GCTACTGCTTCCGCAACCA
PAUGen-qPCR-R	TCAACATGGTGGTGAAGTCAC
COS5-qPCR-F	CCA AGA AGC GTT CAG AAC AAC
COS5-qPCR-R	GAA GCT GAA CGT CTT CCA GG

COS10-qPCR-F	CCA GTA GTT CAA ATA CAG TAC AG
COS10-qPCR-F	GCT TCT TGG CAG TCA GTA CC
COSGen-qPCR-F	AAGATGCAGTTCTTGTCGACTAT
COSGen-qPCR-R	TCTTTGCAGAGAGAACGCGG
P2-qPCR-F	ACGATGAGAGACTGTTCAGGTTAAA
P2-qPCR-R	GGGTTGATGCGTATTGAGAGATA
P3-qPCR-F	CCAATTGTTCCTCGTTAAGGTATTT
P3-qPCR-R	ATTCAGGGAGGTAGTGACAATAAA
P4-qPCR-F	GTTTGAGAATAGGTCAAGGTCATTTC
P4-qPCR-R	GTTTCCCTCAGGATAGCAGAAG
IGS2-qPCR-F	CCACCACACTCCTACCAATAAC
IGS2-qPCR-R	AGGTAGTCAGATGAAAGATGAATAGAC
RPL9A-qPCR-F	GTCACCAAGGGTTACAAGTACA
RPL9A-qPCR-R	CAATTTCGTCCTTAACGTTGGTG
RPS26B-qPCR-F	TACCCAGAATACGCCTTGCC
RPS26B-qPCR-R	CAAAGCTTTCTTTGCGGCAG
SSB1-qPCR-F	TTCAAGGTGCTATCTTGACC
SSB1-qPCR-R	GGTTGTCAGCACATGTAGTA
RPP1B-qPCR-F	GTCTGGGCTGATGTTTACGC
RPP1B-qPCR-R	GAAACCCATGTCGTCGTCAG
RPS12-qPCR-F	AGTTGGTTGAAGGTTTGGCT
RPS12-qPCR-R	AGTTTCAGCACCCCAGTTCT
RPL8B-qPCR-F	AGCAAGACGCTTCTCCAAAG
RPL8B-qPCR-R	TCTTACACAAAGCTGGTAGGAA
RPS22A-qPCR-F	AGCACGGTTACATTGGTGAA
RPS22A-qPCR-R	CAGAGGTGGTCAAGATGACG
OPI1-qPCR-F	CCAGCGAGCAGTCTATTGTG
OPI1-qPCR-R	CAGTGATGTACTGTGGACGC
INO1-qPCR-F	GATGTAACGCCCACTGTTCA
INO1-qPCR-R	AGTCATGGAGCCGAAGTAGT
IZH1-qPCR-F	TCGGTATCCAAGGGGTTCTT

IZH1-qPCR-R	TGGCTTTCAAGTGGCATACA
IZH2-qPCR-F	CCGGAATGGCAAAGAGACAA
IZH2-qPCR-R	AGTGAAGAACCCGAGAGCAG
IZH3-qPCR-F	GCTGGGTGTATTTGGTGTGT
IZH3-qPCR-R	GATTTGTATGTGACGGGGCT
IZH4-qPCR-F	TCGAACGAGAATGCAGAGAC
IZH4-qPCR-R	GTGGTGGGGAACAAAGGTATC
OLE1-qPCR-F	ACCGCTTTCGTCATTCCAAC
OLE1-qPCR-R	TTGTCACGAGGGGTTCTTCT
SPT23-qPCR-F	CTAGCATAGAGCCTGACGGA
SPT23-qPCR-R	ATCATCCACGGTCATTTGGG
ICT1-qPCR-F	ATGGCGGAAGGATAACAAGC
ICT1-qPCR-R	AGTGGATAGGTGGTGTTGGG
MGA2-qPCR-F	CGAGAACAAAGAAGAGCCGC
MGA2-qPCR-R	TGCCTTATGGTGCCTGCAAT
ACT1-qPCR-F	TGTCCTTGTACTCTTCCGGT
ACT1-qPCR-R	CCGGCCAAATCGATTCTCAA
TEL01L-ChIP-F ChrI 82-102	CAGCCCTAATCTAACCCTGG
TEL01L-ChIP-R ChrI 300-282	GTATGGTGAGTAGGTCATG
TEL06R-ChIP-F ChrVI 269990-270012	GTGTGTAGTGATCCGAACTCAGT
TEL06R-ChIP-R ChrVI 270109-270080	CTAGCATATTGATATGGCGTACGCACACGT
TEL15L-ChIP-F ChrXV 121-148	CCCTAATCTAACCCTGTCCAACCTGTCT
TEL15L-ChIP-R ChrXV 506-481	TGGTATATACTATAGCATCCGTGGGC
Lrr-ChIP-F ChrV 469104–469125	GCACTTAATTGGCGTAAGCTG
Lrr-ChIP-R ChrV 469157–469177	TCGCAGGAGCATATTTCGTA

Growth conditions. Yeast strains were grown in synthetic defined minimal medium (SD) containing 0.67% yeast nitrogen base without amino acids, 2% filtered sterilized glucose and 0.1%

tryptophan, 0.1% methionine, 0.1% leucine, 0.1% lysine, 0.1% arginine, 0.1% histidine, 0.02% adenine, and 0.02% uracil to fulfill strain auxotrophies. Additional adenine (0.004%, SD+Ade) was added to prevent vacuolar fluorescence in *ade2* strains used for live microscopy. Yeast cultures were routinely grown at 30 °C with shaking (200 rpm). Standard transformation protocol was used and cells carrying plasmids of interest were selected on selective media (Guthrie and Fink, 1991).

All experiments were conducted in exponential growth phase. Cells were routinely grown overnight in SD+Ade unless otherwise indicated. The absorbance at 600-nm (A_{600}) of the cultures was monitored with a ThermoScientific™ GENESYS™ 30 Visible Spectrophotometer. Cultures were diluted the following day in fresh media and cells were grown into log phase for ~4 hours. For experiments with edelfosine, the lyophilized drug was dissolved in ethanol as a 20 mM fresh stock. Log phase cells were standardized to A_{600} ~0.4, then incubated with the vehicle (0.095% ethanol) or 20 μM edelfosine at 30 °C with shaking for the indicated time in each experiment.

For experiments determining sensitivity to free fatty acids, defined minimal media was prepared, with glucose replaced by 4 mM oleic acid or 1.18 mM palmitoleic acid in the treatment plates. Fresh oleic or palmitoleic acid from a -20°C stock was dissolved in 500 μL DMSO (Sigma, D-8418) then added into autoclaved warm medium to reach the final concentration. For control plates containing 2% glucose, DMSO was added to a 1% final concentration.

Fluorescence Microscopy. Cells expressing the indicated fluorescent protein conjugates were grown into log phase as described above, then diluted to A_{600} ~0.4 and treated with 20 μM edelfosine or ethanol for the indicated time periods. Cells were pelleted at the indicated timepoints, resuspended in ~10 μL of cleared media and mounted on agarose pads prepared from the same media in which the cells were cultured. Images were acquired with a Zeiss AxioImager Z2 upright epifluorescence microscope. ZEISS Zen blue imaging software and Zeiss plan Apochromat 100x/1.4 oil immersion objective lens were used for image acquisition. Z-stacks were taken in seventeen 0.24 μm steps and deconvolved using the constrained iterative algorithm available in the Zen 2.3 Pro software. Colibri 7 LED light and 90 High Efficiency filter sets were used for excitation of CFP, GFP, and DsRed. For CFP signal, samples were excited at 423/44 nm and emission was captured at 475 nm, while for GFP signal, samples were excited at 469/38 nm and emission was captured at 509 nm, and for DsRed signal, samples were excited at 555/30 nm and emission was captured at 610 nm. For images using both CFP and GFP linear unmixing was performed using the built-in settings from Zen 2.3 Pro software. Image analysis was performed manually using FIJI (Schindelin et al., 2012).

For microscopy using BODIPY™ 493/503, 1 mL aliquots of cells that had been treated with edelfosine or the vehicle for 90 minutes were incubated with 1 μL of 5 mM BODIPY in DMSO for 5 minutes at 30 °C. Cells were then washed with 500 μL PBS and BODIPY signal was captured in the GFP channel. All quantitation of phenotypes was done by manual analysis of Z-stacks in FIJI, with the exception of nucleolar volume. For nucleolar volume quantification, three dimensional (X, Y, Z) stacks of yeast cells carrying $Nop1^{CFP}$ were acquired using the CFP channel. After image deconvolution, the 3D Object Counter Volume plug-in of FIJI (Bolte and Cordelières, 2006) was used to measure the volume of the nucleolus (CFP signal) in μm^3.

Chromatin Immunoprecipitation. Cells expressing Sir4^{MYC} or Rap1^{MYC} were grown into log phase as described above, then diluted to A_{600} ~ 0.4 in 50 mL liquid media and treated with 20 μM edelfosine or ethanol for 60 minutes before crosslinking with 1.1% Formaldehyde Solution (Sigma) for 15 minutes followed by quenching with 0.125 M glycine for 5 minutes at room temperature. ChIP of yeast cells was performed as described in Lee and Keung, 2018. Briefly, cells were digested with 0.5 mg/mL zymolyase at 30 °C until spheroblasts were detected using a light microscope. Spheroblasts were lysed in NP-S buffer [0.5 mM spermidine, 0.075 % NP-40, 10 mM Tris-HCl pH 7.4, 50 mM NaCl, 5 mM MgCl2, 1 mM CaCl2, 1 mM 2-mercaptoethanol, supplemented with protease inhibitor cocktail (Roche), 0.5% (w/v) Sodium Deoxycholate and 1mM PMSF] for 10 minutes on ice. DNA was sheared using a Bioruptor sonicator for four sets of 15 × 30s at amplitude of 50% with 30s shut off intervals and immunoprecipitated using sheep anti-mouse conjugated Dynabeads (Invitrogen) coupled with 1:10 mouse anti MYC antibody (Abcam, 9E10 ab32) for 2 hrs at 4°C. Immunoprecipitates were washed once with NP-S buffer and twice with wash buffer [100 mM Tris pH 8, 0.5% NP-40, 1 mM EDTA, 500 mM NaCl, 500 mM LiCl, supplemented with 0.5% (w/v) Sodium Deoxycholate, 1mM PMSF and protease inhibitor pellet (Roche)] at 4°C, each for 5 minutes with shaking at 2,200 g. Real-time qPCR reactions were carried out in technical triplicates using SYBR Green with a QuantStudio™ 6 Flex Real-Time PCR System (Applied Biosystems, Life Technologies Inc.). Ct (cycle threshold) values of Ab-coupled beads and uncoupled beads were used to calculate the fold enrichment of protein at three native sub-telomeres (Tel01L, Tel06R and Tel15L) compared to a control late replicating region on Chromosome V (469104–469177).

Flow Cytometry. Wild-type (JC470) cells were grown into log phase as described above, then diluted to A_{600} ~0.4 in 10 mL liquid media. The 0-minute timepoint was taken at this time, by fixing 300 μL of culture in 1 mL 95% EtOH. Cells were then treated with either 0.095 % ethanol or 20 μM edelfosine and aliquots were fixed at 30, 60 and 90 min. Cells were stored at 4°C for at least one overnight. Samples were prepared for flow cytometry by pelleting and washing with 1 mL 50 mM sodium citrate pH 7.0 solution. Cells were resuspended in 500 μL sodium citrate solution with 50 μg/mL RNAse A (ThermoFisher, EN0531) and incubated for one hour at 50 °C. Samples were subsequently incubated for an additional hour at 50 °C with 20 μL of 10mg/mL proteinase K (Invitrogen, AM2542). Samples were then pelleted and resuspended in 500 μL sodium citrate solution with 10 μg/mL propidium iodide (Sigma, 537059-50MG). Cell clumps were broken up by brief (3 s) sonication at 10% amplitude using a probe sonicator. Cells were then analyzed for DNA content by propidium iodide staining using a ThermoFisher AttuneNxt Flow Cytometer. PI was excited at 488 nm. The flow cytometry results were analyzed using FlowJo™ v10.8 Software (BD Life Sciences) and figures were prepared by plotting PI signal vs cell count (Becton, 2021).

RNA-sequencing. Wild-type cells (two W303 replicates, one BY4741 replicate) were grown into log phase as described above, then diluted to A_{600} ~0.4 in 20 mL liquid media and treated with 20 μM edelfosine or ethanol for 60 minutes before flash-freezing**.** RNA was then extracted using the hot acid phenol protocol as previously described (Green and Sambrook, 2021). Briefly, yeast pellets were resuspended in 0.5 mL cold AE buffer (50mM NaOAc pH 5.2, 10mM EDTA) and

lysed at 65 °C by vortexing in 1.5% SDS and acid phenol. RNA and proteins were then separated with chloroform and RNA was precipitated from the supernatant using glycogen and ethanol.

RNA-sequencing and subsequent statistical analysis was performed by the Cumming School of Medicine's Centre for Health Genomics and Informatics, University of Calgary. All samples were found to have a RIN >8 as assessed via Agilent TapeStation assay. Fluorometric assays were used to obtain the concentration in ng/µl. One µg of total RNA input was used for all libraries. NEBNext® Poly(A) mRNA Magnetic Isolation Module (E7490) and NEBNext® Ultra™ II RNA Library Prep Kit for Illumina® (E7770, E7775) were used to prepare the libraries according to the manufacturer's instructions. Final libraries were again assessed via Agilent TapeStation assay, Qubit to obtain the concentration and Kapa qPCR to obtain the exact molarity of Illumina adapter ligated fragments according to the manufacturer's instructions. Sequencing was then performed on an Illumina NextSeq500 system using 150 cycle mid-output 2x75 bp paired end sequencing.

Gene Ontology analysis was performed using the ClueGo plug-in for Cytoscape (Shannon et al., 2003; Bindea et al., 2009) selecting for significantly overrepresented pathways with medium network specificity and GO term fusion enabled. Transcription factor enrichment was analyzed using Yeastract (Monteiro et al., 2020), selecting for transcription factors whose targets were significantly enriched by DNA binding evidence only. Additional analysis of the RNA-sequencing data was performed with the R/Rstudio computational platform (R Core Team, 2021). Volcano plots were made with the ggplot2 package (Wickham, 2016) as a scatter plot of ln(FC) vs -$\log_{10}$(FDR). Venn diagrams were made with the venndir package (jmw86069, 2020). Telomere enrichment was calculated using the hypergeometric distribution function in base R. Principal component analysis, which concluded that genetic background minimally contributed to differences in gene expression, and it was therefore sound to average W303 and BY4741 (Figure S4A), was performed using base R functions and scores were plotted with the ggplot2 package.

qPCR. Wild-type or *sir4*Δ cells (W303 background) were grown into log phase as described above, then diluted to A_{600} ~ 0.4 in 50 mL liquid media and treated with 20 µM edelfosine or ethanol for 60 minutes before flash-freezing. RNA was then extracted using the RNeasy Mini Kit (Qiagen) as per manufacturer directions from three biological replicates. Complementary DNA (cDNA) was prepared using QuantiTect Reverse Transcription Kit (Qiagen) as indicated by the manufacturer. RNA abundance was quantified using real-time qPCR reactions, which were carried out using SYBR Green (Applied Biosystems) with a QuantStudio™ 6 Flex Real-Time PCR System (Applied Biosystems, Life Technologies Inc.). Ct (cycle threshold) values of target genes were used to calculate the fold enrichment of mRNA abundance using the ΔCt method (Livak and Schmittgen, 2001) in treated cells compared to untreated cells. Primers used are listed in Table 3.

Spot-plating. For growth assays on solid media, cells were grown into log phase as described above and serially diluted 1:10 beginning with A_{600} ~0.5 unless otherwise noted in the figure caption. For experiments determining sensitivity to edelfosine, cells were spotted on SD+Ade plates with 2% glucose and either 0.095% ethanol or 20 µM edelfosine using a bolt replicator and incubated at 30°C for the indicated number of days.

For experiments determining sensitivity to free fatty acids, cells were spotted on control SD + 1% DMSO plates with 2% glucose or SD + 1% DMSO containing either 4 mM oleic acid or 1.18 mM palmitoleic acid.

Images were obtained using a GelDoc imager (BioRad) and are representative plates from a minimum of three independent experiments with two technical replicates per experiment.

Subcellular Fractionation. Membrane fractions were prepared as described previously (Marr et al., 2012). Briefly, cells were lysed using glass beads in 0.7 mL of GTE buffer [20% glycerol, 50 mM Tris-HCl, pH 7.4, 1 mM EDTA, Complete EDTA-free protease inhibitor mixture (Roche), 1 mM PMSF, 3 μg/mL pepstatin, and 1 mM phosphatase inhibitor mix (Sigma)]. Lysis was done by vortexing samples with glass beads five times for 30 s with 30 s intervals on ice in-between. Beads were washed with 0.5 mL of GTE buffer and the combined lysate was centrifuged at 16,000 × g for 15 min at 4 °C. The supernatant was then centrifuged at 450,000 × g for 15 min at 4 °C in a Beckman fixed angle rotor ultracentrifuge. Membranes were homogenized in GTE buffer using a Dounce homogenizer. Protein concentration was determined using the BCA assay (Thermo Scientific) with bovine serum albumin as a standard. Lysates and fractions (40 μg) were then analyzed by Western blot.

Western Blot. Ten A_{600} units of cells were grown under the indicated conditions, harvested, washed once with water, and flash-frozen before being resuspended in 1 mL cold 20% trichloroacetic acid (TCA) solution. Acid-washed glass beads were added to each sample and cells were disrupted using a Mini BeadBeater (BioSpec Products) twice for 1 min each at 4 °C. The liquid was collected and combined with cold 400 uL of 5% TCA to finalize protein precipitation. Samples were then centrifuged at 3,000 rpm in a pre-cooled microcentrifuge (Eppendorf 5415R) for 10 min at 4 °C. Pellets were resuspended in 150 μL of 1x Laemmli buffer [0.2 M Tris–HCl (pH 6.8), 8% SDS, 0.4% bromophenol blue, and 40% glycerol], neutralized with 50 μL of 2M TRIS and then boiled for 5 minutes. Samples were centrifuged again for 10 min at 3,000 rpm, 40 μL of sample was analyzed by SDS-PAGE.

To capture ^{GFP}Spt23, ten A_{600} units of W303 cells transformed with pAG415-EGFP-Spt23 were collected as above, but rather than being frozen, cells were immediately lysed using glass beads (1:1 volume) in 0.3 mL of GTE buffer [20% glycerol, 50 mM Tris-HCl, pH 7.4, 1 mM EDTA], supplemented with Complete EDTA-free Protease Inhibitor mixture (Roche), 1 mM PMSF and 3 μg/mL pepstatin. Lysis was done as described above using glass beads. Samples were centrifuged at 4000 rpm × 5 min at 4°C in a pre-cooled microcentrifuge (Eppendorf 5415R) and the supernatant was collected. After lysis, 10 μl of 4X SDS was added to 30 μl of samples, which were incubated for 2 minutes at room temperature before loading into the gel.

For western blot analysis, proteins were separated by 8% resolving gel containing trichloroethanol (TCE; Sigma) to visualize proteins (Ladner et al., 2004). Proteins were transferred to a polyvinylidene fluoride (PVDF) membrane (Millipore) using a Bio-Rad transfer system at 100 V for 1 h or 25 V for 16 hrs, and then stained with Red Ponceau (Sigma) to confirm transfer. The following primary antibodies were used: 1:5,000 mouse αMYC (Abcam, 9E10 ab32), 1:1,000 mouse αRap1 (Santa Cruz, sc374297), 1:1,000 mouse αGFP (Roche, 11814460001), 1:500 mouse

αPgk1 (Molecular Probes), 1:1,000 rabbit αH2A (Active Motif, 39235), 1:1,000 rabbit αH2A^{S129ph} (Active Motif, 39271) and 1:2,000 mouse αRad53 (Abcam, ab104232). Horseradish peroxidase conjugated secondary antibodies (Invitrogen, Thermo Fisher) and enhanced chemiluminescence (Amersham, GE Healthcare) were used for detection using an Invitrogen iBright FL1500 Imaging System.

Lipid extraction and neutral lipids analysis. Lipid extracts were prepared as described previously (Zaremberg and McMaster, 2002). Briefly, cells were concentrated by centrifugation, washed twice with water, and resuspended in 1 mL of $CHCl_3/CH_3OH$ (1/1, v/v), then stored overnight at -20 °C. Cells were disrupted for 1 minute at 4 °C in a Mini BeadBeater (BioSpec Products) with acid-washed glass beads. Beads were washed with 1.5 mL of $CHCl_3/CH_3OH$ (2/1, v/v), then 0.5 mL of $CHCl_3$ were added to the combined supernatant followed by 1.5 mL of water to facilitate phase separation. Lipids were dried under nitrogen, resuspended in 30 µL chloroform and 15 µL of this resuspension was loaded for separation on silica gel on TLC aluminum foils (Sigma-Aldrich, 60805-25EA) using a solvent system containing 80:20:1 petroleum ether/diethyl ether/acetic acid for separation of neutral lipids. Standard mix (10 µg/ each lipid) was loaded onto the plate. Standard mix consisted of a mix of 2 mg/mL solution of DAG, ergosterol, oleic acid, TAG, and cholesteryl oleate. Plates were developed with iodine vapors and imaged using a BioRad GelDoc. Images shown are representative of two independent experiments with two technical replicates per experiment.

Free fatty acid levels were calculated using densitometry, by measuring the pixel intensity of sample bands and comparing to a standard curve of 0.25, 0.5, 1 and 2 µg of pure oleic acid. Samples were normalized by determining total phosphate released from phospholipids. Phosphate was determined using the AMES assay (Ames, 1966). Briefly, lipid extracts were resuspended in chloroform and dried in glass test tubes. A standard curve of 0, 0.5, 1, 2, 4 and 6 mM NaH_2PO_4 solution was prepared alongside the samples and 30 µL of 10% w/v magnesium nitrate in ethanol was added to all tubes and ashed using a flame. The ash was then resuspended in 300 µL 0.5M HCl and boiled for 15 minutes. The free inorganic phosphate from this reaction was then visualized by adding 700 µL 1:6 10% w/v ascorbic acid in water : 0.42% w/v ammonium molybdate in 0.5M H_2SO_4 and developed for one hour at 37°C. All samples were prepared in duplicate. Absorbance was measured at 820 nm using a Biotek Synergy H1 Microplate Reader.

Statistical analysis. All statistical analysis was performed in GraphPad Prism 9.3.1. The following analyses were conducted depending on the experiment as indicated in each figure legend. A minimum of three independent experiments were analyzed in each case.

For categorical quantification analyzing the difference between only two variables, two-tailed unpaired t-tests were performed. For analyzing the difference between more than two variables, standard one-way ANOVA with Tukey's multiple comparisons post-test was used. For multiple comparisons, multiple unpaired t-tests were performed and corrected for multiple comparisons using the Holm-Šídák post-test (Holm, 1979). Additionally the Welch’s correction for unequal variance (Welch, 1947) was used when appropriate. For analysis of differences between wildtype and mutants in treated and untreated conditions, 2-way ANOVA with Šídák's multiple comparisons test was applied (Sidak, 1967).

For numerical quantification analyzing the difference between only two variables, two-tailed nested t-tests were performed. For analysis of differences between wildtype and mutants in treated and untreated conditions, nested one-way ANOVA with Šídák's multiple comparisons pos-test were performed.

Supplementary Data

Figure S1 is related to Figure 1, checking for DNA damage response in edelfosine.

Figure S2 is related to Figure 2, providing additional microscopy images and telomere interactions with the nuclear membrane, as well as cell cycle effects of edelfosine.

Figure S3 is related to Figure 3, with protein and sensitivity controls for Sir4 as well as qPCR gene expression of sub-telomeric genes.

Figure S4 is related to Figure 4, including principal component analysis and gene ontology of the RNA-seq, as well as qPCR of rDNA.

Figure S5 is related to Figure 6, providing additional microscopy images of the ER.

Supplementary Tables

Table S1 lists all genes differentially expressed in edelfosine.

Table S2 lists all sub-telomeric genes found to be significantly differentially expressed in edelfosine with chromosome coordinates.

Table S3 lists known internal gene targets of the SIR complex downregulated in edelfosine.

Table S4 lists known ribosomal protein genes bound by Rap1 downregulated in edelfosine.

Table S5 lists all lipid metabolism related genes differentially regulated in edelfosine.

Table 1- Transcription factors with DNA binding sites over-represented in upregulated genes Analysis of genes with >2-fold increase in response to edelfosine (119 genes) as determined by Yeastract (Monteiro et al., 2020) using DNA binding evidence only. P-values calculated using the hypergeometric test.

TF	Description	# of genes & (p-value)	References
Sko1	Basic leucine zipper transcription factor of the ATF/CREB family; forms a complex with Tup1p and Cyc8p to both activate and repress transcription; cytosolic and nuclear protein involved in osmotic and oxidative stress responses	44 (4.7E-12)	(Reimand et al., 2010; Niu et al., 2008; Ni et al., 2009)
Hot1	Transcription factor for glycerol biosynthetic genes; required for the transient induction of glycerol biosynthetic genes GPD1 and GPP2 in response to high osmolarity; targets Hog1p to osmostress responsive promoters; has similarity to Msn1p and Gcr1p	13 (1.2E-09)	
Spt23	ER membrane protein involved in regulation of OLE1 transcription; inactive ER form dimerizes and one subunit is then activated by ubiquitin/proteasome-dependent processing followed by nuclear targeting; SPT23 has a paralog, MGA2, that arose from the whole genome duplication	58 (1.3E-08)	(Auld et al., 2006; Reimand et al., 2010)
Yap6	Basic leucine zipper (bZIP) transcription factor; physically interacts with the Tup1-Cyc8 complex and recruits Tup1p to its targets; overexpression increases sodium and lithium tolerance; computational analysis suggests a role in regulation of expression of genes involved in carbohydrate metabolism; YAP6 has a paralog, CIN5, that arose from the whole genome duplication	38 (6.22E-08)	(Lee et al., 2002; Harbison et al., 2004; Ni et al., 2009; Reimand et al., 2010)
Cad1	AP-1-like basic leucine zipper (bZIP) transcriptional activator; involved in stress responses, iron metabolism, and pleiotropic drug resistance; controls a set of genes involved in stabilizing proteins; binds consensus sequence TTACTAA; CAD1 has a	27 (1.01E-07)	(Mazzola et al., 2015; Reimand et al., 2010; Haugen et al., 2004; Lee et al., 2002; Azevedo et al., 2007)

	paralog, YAP1, that arose from the whole genome duplication		
Adr1	Carbon source-responsive zinc-finger transcription factor; required for transcription of the glucose-repressed gene ADH2, of peroxisomal protein genes, and of genes required for ethanol, glycerol, and fatty acid utilization	31 (8.55E-07)	(Chua et al., 2006; Reimand et al., 2010; Karpichev et al., 2008)

Table 2- Transcription factors with DNA binding sites over-represented in downregulated genes. Analysis of genes with >2-fold decrease in response to edelfosine (115 genes) as determined by Yeastract (Monteiro et al., 2020) using DNA binding evidence only. P-values calculated using the hypergeometric test.

TF	Description	# of genes & (p-value)	Reference
Fkh1	Forkhead family transcription factor with a minor role in the expression of G2/M phase genes; negatively regulates transcriptional elongation; positive role in chromatin silencing at HML and HMR; regulates donor preference during switching	80 (0)	(Pondugula et al., 2009; Knott et al., 2012; Ostrow et al., 2014; Reimand et al., 2010; Workman et al., 2006; Harbison et al., 2004; Lee et al., 2002)
Ifh1	Coactivator that regulates transcription of ribosomal protein (RP) genes; recruited to RP gene promoters during optimal growth conditions via Fhl1p; subunit of CURI, a complex that coordinates RP production and pre-rRNA processing	42 (0)	(Rudra et al., 2005; Schawalder et al., 2004; Lavoie et al., 2010; Cai et al., 2013; Venters and Pugh, 2009; Wade et al., 2004; Reja et al., 2015)
Spt23	ER membrane protein involved in regulation of OLE1 transcription; inactive ER form dimerizes and one subunit is then activated by ubiquitin/proteasome-dependent processing followed by nuclear targeting; SPT23 has a paralog, MGA2, that arose from the whole genome duplication	62 (6.6E-14)	(Auld et al., 2006; Reimand et al., 2010)
Fhl1	Regulator of ribosomal protein transcription; has forkhead associated domain that binds phosphorylated proteins; also has forkhead DNA-binding domain but does not bind DNA in vitro; suppresses RNA pol III and splicing factor prp4 mutants	53 (1.11E-07)	(Rudra et al., 2005; Lee et al., 2002; Tai et al., 2017; Harbison et al., 2004; Kasahara et al., 2007; Lavoie et al., 2010)

Yap6	Basic leucine zipper (bZIP) transcription factor; physically interacts with the Tup1-Cyc8 complex and recruits Tup1p to its targets; overexpression increases sodium and lithium tolerance; computational analysis suggests a role in regulation of expression of genes involved in carbohydrate metabolism; YAP6 has a paralog, CIN5, that arose from the whole genome duplication	33 (6.0E-07)	(Lee et al., 2002; Harbison et al., 2004; Ni et al., 2009; Reimand et al., 2010)
Fkh2	Forkhead family transcription factor with a major role in the expression of G2/M phase genes; positively regulates transcriptional elongation; negative role in chromatin silencing at HML and HMR; substrate of the Cdc28p/Clb5p kinase	53 (7.82E-07)	(Pondugula et al., 2009; Harbison et al., 2004; Ostrow et al., 2014; Reimand et al., 2010; Linke et al., 2017; Ghavidel et al., 2018; Gefeng et al., 2000; Simon et al., 2001; Shapira et al., 2004; Workman et al., 2006)
Rap1	DNA-binding protein involved in either activation or repression of transcription, depending on binding site context; also binds telomere sequences and plays a role in telomeric position effect (silencing) and telomere structure	59 (9.6E-05)	(Chua et al., 2006; Reimand et al., 2010; Lavoie et al., 2010; Workman et al., 2006; Kasahara et al., 2007; Venters and Pugh, 2009; Lieb et al., 2001; De Sanctis et al., 2002; Buchman et al., 1988b; Yarragudi et al., 2007; Lee et al., 2002; Harbison et al., 2004; Hall et al., 2006; Reja et al., 2015)
Ndt80	Meiosis-specific transcription factor required for exit from pachytene and for full meiotic recombination; activates middle sporulation genes; competes with Sum1p for binding to promoters containing middle sporulation elements (MSE)	49 (1.4E-04)	(Nocedal et al., 2017; Reimand et al., 2010; Chu and Herskowitz, 1998)

Figure legends:

Figure 1 – The metabolically stable lysophosphatidylcholine analogue edelfosine alters nuclear envelope morphology and nuclear architecture. (**A**) Representative images of wild-type (W303) cells expressing the ER marker Sec63^{GFP} from a centromeric plasmid. Cells were imaged using live fluorescence microscopy after growth in SD-Leu+Ade and 90 minutes in the presence of edelfosine or the vehicle. Quantification of cells displaying abnormal nuclear membrane morphology is shown beside the microscopy images. Circles represent the percentage of cells displaying abnormal nuclear morphology in each experiment [two-sided Fisher's exact test gave a p-value < 0.0001 for each experiment (n=100 cells per treatment)]. Bars represent the mean of the three independent experiments ± SD. ** indicates a p-value < 0.01 as determined by two-tailed unpaired t-test (N=3). (**B**) Representative images of wild-type (W303) cells expressing the Nop1^{CFP} nucleolar marker expressed from a centromeric plasmid in cells with Nup49^{GFP} (nuclear envelope marker) endogenously tagged. Cells were imaged using live fluorescence microscopy after growth in SD-Ura+Ade and 90 minutes in the presence of edelfosine or the vehicle. The distribution of values from the quantification of nucleolar volume of cells (described in Materials and Methods) is shown beside the microscopy images. Values cumulative from three independent experiments (n = 163 Ctrl, 190 EDLF) are shown as small circles, with the means of each experiment shown as large circles. Bars represent the mean with 95% confidence interval from the pooled values. **** indicates a p-value < 0.0001 as determined by two-tailed nested t-test (N=3).

For all panels: Ctrl = vehicle; EDLF = edelfosine; scale bars represent 2 µm.

Figure 2 – Altered nuclear envelope shape disrupts telomere clustering but not tethering. (**A**) Schematic showing the Rabl conformation of yeast nuclei, where centromeres, telomeres and the nucleolus are tethered to the NE, and telomeres are clustered into 3-5 foci per cell that can be visualized by Rap1. (**B**) Schematic explaining the GFP constructs allowing for analysis of telomere tethering (created with BioRender.com). LacO repeats (6-10 kb) are incorporated into either Tel06R or Tel08L which are then bound by lacI^{GFP} conjugates. The large amount of lacO sites produces a bright focal point at the location of the tagged telomere, which stands out against the nuclear membrane delineated by Nup49^{GFP}. (**C**) Representative images of cells expressing the Tel08L constructs described in (B) that were imaged using live fluorescence microscopy after 90 minutes in edelfosine or the vehicle. Quantification of cells showing the telomere at the periphery for both Tel06R and Tel08L is shown beside the microscopy images. Circles represent the percentage of cells displaying telomere localization at the NE in each experiment [two-sided Fisher's exact test gave the p-values 0.2545, 0.8884 and 0.5461 for each Tel06R experiment (n $\geq$ 80 cells per treatment), and the p-values 0.0710, 0.1873, 0.3210, 0.6050, and 0.7854 for each Tel08L experiment (n $\geq$ 45 cells per treatment)]. The bar represents the mean of the experiments ± SD. Differences between control and edelfosine treatments were found to be non-significant by unpaired t-tests with Holm-Šídák correction for multiple comparisons (N=3 for Tel06R, N=5 for Tel08L). (**D**) Representative images of wild-type (W303) cells expressing Rap1^{GFP} imaged by live fluorescence microscopy after 90 minutes in edelfosine or the vehicle. The distribution of values from the quantification of the number of Rap1 foci per cell is shown beside the microscopy images. Values cumulative from three independent experiments (n=180 per treatment) are shown as small circles, with the means of each experiment shown as large circles. Bars represent the mean with 95% confidence interval from the pooled values. * indicates a p-value < 0.05 as determined by two-tailed nested t-test (N=3). (**E**) ChIP-qPCR of Rap1^{MYC} after 60 minutes in edelfosine or control. The fold enrichment at three native sub-telomeres (Tel01L, Tel06R and Tel15L) is shown,

normalized to a late replicating region on Chromosome V (469104–469177). Bars represent mean ± SD for four independent experiments while circles represent individual experiments. Differences between control and edelfosine treatments were found to be non-significant by unpaired t-tests with Holm-Šídák correction for multiple comparisons and Welch's correction for unequal variance (N=4). (**F**) Western blot of endogenous Rap1 in cells expressing 8HIS-Smt3 after 60 minutes with edelfosine or control. Bottom panel shows protein loading by red ponceau.

For all panels: Ctrl = vehicle; EDLF = edelfosine; scale bars represent 2 µm.

Figure 3 – The SIR complex is susceptible to lipid alterations at the NE. (**A**) Wild type (W303) cells or the indicated SIR complex mutants were serial diluted onto synthetic solid media containing 25 µM edelfosine or vehicle and incubated at 30°C for two days. (**B**) ChIP-qPCR of $Sir4^{MYC}$ after 60 minutes in edelfosine or the vehicle. The fold enrichment at three native sub-telomeres (Tel01L, Tel06R and Tel15L) is shown, normalized to a late replicating region on Chromosome V (469104–469177). Bars represent mean ± SD for four independent experiments while circles represent individual experiments. * indicates p-value <0.05; ** indicates p-value <0.01 as determined by unpaired t-tests with Holm-Šídák correction for multiple comparisons. (**C**) Representative images of cells expressing $Sir4^{GFP}$ and the ER marker ^{DsRed}HDEL (both endogenously tagged) visualized by live fluorescence microscopy after 90 minutes with edelfosine or vehicle. Scale bar represents 2 µm. The distribution of values from the quantification of the number of Sir4 foci per cell is shown beside the microscopy images. Values cumulative from three independent experiments (n=180 cells per treatment) are shown as small circles, with the means of each experiment shown as large circles. Bars represent the mean with 95% confidence interval from the pooled values. * indicates a p-value < 0.05 as determined by two-tailed nested t test (N=3).

For all panels: Ctrl = vehicle; EDLF = edelfosine.

Figure 4 – Ribosomal protein targets of Rap1 are repressed in edelfosine. (**A**) Volcano plot of genes downregulated in response to edelfosine as identified by RNA-Seq transcriptome analysis. Targets of Rap1 are coloured red. Genes confirmed by qPCR are labeled. (**B**) Venn diagram showing the overlap between genes strongly downregulated in edelfosine (< -2 ln(FC)) and genes known to be bound by Rap1 (Lieb et al., 2001), including ribosomal protein genes. (**C**) qPCR of genes identified in (A) compared to their RNA-seq values. Bars represent mean ± SD for three independent experiments while circles represent individual experiments. (**D**) The isogenic wild type (KM014) or the indicated Rap1 mutants were serial diluted onto defined solid medium containing 20 µM edelfosine (EDLF) or vehicle (Ctrl) and incubated at 30°C for two days. The first dilution of *rap1-17* cells was $A_{600} \sim 1$, while the other two strains were $A_{600} \sim 0.1$, which was experimentally determined to normalize strain growth on control plates.

Figure 5 – Lipid circuits activated in response to edelfosine. (**A**) Lipid transport and metabolic pathway map highlighting upregulated (green dots) and downregulated (red dots) genes detected by RNA-seq. Color code reflects the fold change as indicated in the figure. (**B**) Volcano plot of transcripts changed in response to edelfosine as identified by the RNA-Seq transcriptome analysis. Targets of Opi1/Ino2/4 are coloured red. Targets of Spt23 are coloured green. Genes confirmed by qPCR (inset) are labeled. For the inset, bars represent mean ± SD for three independent experiments while circles represent individual experiments.

Figure 6 – Spt23 and Mga2 sense changes in the membrane lipid environment induced by edelfosine. (**A**) Schematic illustrating the off-on states of the membrane packing sensors Mga2 and Spt23 and the release of the transcription factor N-end in response to changes in membrane environment (created with BioRender.com, adapted from Ballweg et al., 2020). (**B**) Representative images of ^{GFP}Spt23 expressed from a centromeric plasmid under the constitutive GPD promoter in *spt23*Δ cells or (**C**) ^{GFP}Mga2 expressed from a centromeric plasmid under the constitutive GPD promoter in *mga2*Δ cells were imaged after growth in SD-Leu+Ade and 30 minutes in the presence of edelfosine, the vehicle, or 0.1% methyl methane sulfonate (MMS). Quantification of cells displaying nucleoplasmic signal is shown beside the microscopy images. Nuclear localization was confirmed using the ER marker ^{DsRed}HDEL (Supplementary Figure 5). Circles represent the percentage of cells displaying nucleoplasmic signal in each experiment [Chi-square test gave a p-value < 0.0001 for each experiment ($n \geq 65$ cells per treatment)]. The bar represents the mean of the three experiments ± SD. ** indicates a p-value < 0.01 and **** indicates a p-value < 0.0001 as determined by standard one-way ANOVA with Tukey's multiple comparisons test (N=3). Schematics illustrate what was classified as nucleoplasmic signal for B and C. (**D**) Western blot of lysates from cells (W303) expressing ^{GFP}Spt23 or (**E**) ^{GFP}Mga2 from centromeric plasmids under the constitutive GPD promoter treated with edelfosine for the indicated times (D) or for 60-minutes (E) Bottom panels show protein loading visualized by TCE. P indicates precursor species (148.2kDa for Spt23, 153.9kDa for Mga2), while N indicates nucleoplasmic species (~90kDa + EGFP).

For all panels: Ctrl = vehicle; EDLF = edelfosine; scale bars represent 2 µm.

Figure 7 – NE deformation and Spt23/Mga2 activation are independent of Sir4. (**A**) Representative images of wild-type and *sir4*Δ cells expressing the ER marker Sec63^{GFP} from a centromeric plasmid. Cells were imaged using live fluorescence microscopy after growth in SD-Leu+Ade and 90 minutes in the presence of edelfosine or control. Quantification of non-round nuclei is shown beside the microscopy images. (**B**) Representative images of ^{GFP}Spt23 or (**C**) ^{GFP}Mga2 expressed from a centromeric plasmid under the constitutive GPD promoter in wild-type or *sir4*Δ cells imaged after growth in SD-Leu+Ade and 30 minutes in the presence of edelfosine or the vehicle. Quantification of nucleoplasmic signal is shown beside microscopy images. For all microscopy quantifications (**A, B, C**), circles represent the percentage of cells displaying the indicated phenotype in each experiment (n=100 cells per treatment), while the bar represents the mean of all independent experiments ± SD. Differences between wild-type and *sir4*Δ were found to be non-significant in both control and edelfosine treatments as determined by 2-way ANOVA with Šídák's multiple comparisons test (N=4 for NE, N=3 for Spt23 and Mga2). (**D**) qPCR of Spt23 and Opi1 targets in wild-type and *sir4*Δ cells treated for 60 minutes with edelfosine or vehicle expressed as ln(EDLF/Ctrl). Bars represent mean ± SD for three independent experiments while circles represent individual experiments. * indicates p-value <0.05 as determined by unpaired t tests with Holm-Šídák correction for multiple comparisons.

For all panels: Ctrl = vehicle; EDLF = edelfosine; scale bars represent 2 µm.

Figure 8 – Lipotoxicity response in SIR mutants. (**A**) Wild type or *sir4*Δ cells were treated with edelfosine or the vehicle for 60 minutes, and lipid extractions were performed as described in Materials and Methods. Neutral lipids were separated using thin layer chromatography with a solvent system composed of 80:20:1 petroleum ether/diethyl ether/acetic acid. Diacylglycerol (DAG); ergosterol (Erg); free fatty acids (FFA); triacylglycerol (TAG) and sterol esters (SE). FFA

were quantified as described in Methods. The fold-change of total FFA in edelfosine vs control is reported. Circles represent the fold-change for each experiment, while the bar represents the mean of the three experiments ± SD. * indicates a p-value < 0.05 as determined by two-tailed unpaired t-test (N=3). (**B**) Wild type (W303) cells or the indicated mutants were serial diluted onto synthetic solid media containing 4 mM oleic acid or (**C**) 1.18 mM palmitoleic acid or control plates containing glucose and vehicle (1% DMSO). Plates were incubated at 30 °C and imaged after three days of growth. (**D**) Representative images of wildtype (BY4741) or *sir4*Δ cells expressing ^{DsRed}HDEL treated with edelfosine or the vehicle for 90 minutes and stained with BODIPY™ to visualize lipid droplets (LDs) as described in Materials and Methods. Scale bar represents 2 µm. (**E**) The distribution of values from the quantification of the average number of LDs per cell. Values cumulative from three independent experiments (n ≥ 145 cells per treatment) are shown as small circles, with the means of each experiment shown as large circles. Bars represent the mean with 95% confidence interval from the pooled values. * indicates a p-value < 0.05 and ** indicates a p-values < 0.01 as determined by nested one-way ANOVA with Šídák's multiple comparisons test (N=3). (**F**) Quantification of cells displaying nuclear lipid droplets (nLDs). Circles represent the percentage of cells displaying nLDs in each experiment (n ≥ 45 cells per treatment)). The bar represents the mean of the three experiments ± SD. * indicates a p-value < 0.05 as determined by 2-way ANOVA with Šídák's multiple comparisons test (N=3).

For all panels: Ctrl = vehicle; EDLF = edelfosine.

Supplementary Figure 1- Edelfosine does not elicit a DNA damage response. (**A**) Anti-Rad53 western blot of whole cell lysates from cells (W303) treated with edelfosine, vehicle or 0.01% MMS for 60 minutes. Bottom panel shows protein loading by Red Ponceau. (**B**) Anti-phospho-Ser^{129}-H2A and anti-total H2A blot of whole cell lysate from cells expressing Sir4-13MYC or Heh1-13MYC treated with edelfosine, the vehicle or 0.01% MMS for 60 minutes.

Supplementary Figure 2 – Telomere interactions with the nuclear membrane are preserved in edelfosine. (**A**) Representative cells expressing the Tel06R constructs quantified in Figure 2B were imaged using live fluorescence microscopy after 90 minutes in edelfosine or the vehicle. Scale bar represents 2 µm. (**B**) Membrane and soluble fractions were collected from BY4741 cells expressing Spt23-TAP treated with 20 µM edelfosine or vehicle for 60 minutes as described in Materials and Methods, then blotted for detection of endogenous Rap1 and Pgk1. (**C**) Cell cycle analysis of wild type cells (W303) treated with edelfosine or vehicle for the indicated times.

For all panels: Ctrl = vehicle; EDLF = edelfosine.

Supplementary Figure 3 – Treatment with edelfosine induces expression of the SIR-dependent COS and PAU sub-telomeric gene families. (**A)** Growth of wild-type (W303) or *sir4*Δ cells expressing *SIR4* from a centromeric plasmid or the empty vector (EV) on SD-Leu+Ade plates containing 20 µM edelfosine or vehicle. Plates were incubated at 30°C and imaged after three days of growth. (**B**) Growth of wild-type (W303) or endogenously tagged *SIR4*-GFP cells on synthetic solid medium containing 20 µM edelfosine or vehicle. Plates were incubated at 30°C and

imaged after two days of growth. (**C**) Western blot of Sir4^{MYC} after 60 minutes with edelfosine or control. Bottom panel shows protein loading by TCE. (**D, E**) Sequence alignment of the highly similar COS (**D**) and PAU (**E**) family genes at the regions amplified by qPCR. Bold letters indicate binding sites for the general primers. (**F**) qPCR of the indicated genes in *sir4*Δ cells relative to wild type, expressed as ln(mutant/WT) or (**G**) in wild-type and *sir4*Δ cells treated for 60 minutes with edelfosine or vehicle expressed as ln(EDLF/Ctrl). Bars represent mean ± SD for three independent experiments while circles represent individual experiments. * indicates p-value <0.05 as determined by unpaired t tests with Holm-Šídák correction for multiple comparisons.

For all panels: Ctrl = vehicle; EDLF = edelfosine.

Supplementary Figure 4 – Genetic background and gene ontology analysis of RNA-sequencing hits. (**A**) Scatter plots of the first three principal component analysis scores for the transcriptional landscape of each sample submitted for RNA-sequencing. W303 samples are represented as circles while BY4741 samples are represented as triangles. Large circles indicate the mean PC score for each treatment. Red is Ctrl and blue is EDLF. (**B**) Molecular function GO terms enriched in genes downregulated (left) and upregulated (right) in edelfosine more than ln(1.5-fold). Legend demonstrating correlation of size and colour with the number of genes per term and the significance score, respectively, is in the middle. (**C**) Schematic of rDNA repeats showing regions amplified by qPCR primers. (**D**) qPCR of 35S rDNA targets (P2-4) in WT cells treated for 60 minutes with edelfosine or vehicle expressed as ln(EDLF/Ctrl) and normalized to *IGS2*. Bars represent mean ± SD for three independent experiments while circles represent individual experiments.

For all panels: Ctrl = vehicle; EDLF = edelfosine.

Supplementary Figure 5 – Spt23 translocates to the nucleus in response to edelfosine. Representative images of wild-type (W303) cells expressing ^{GFP}Spt23 from a centromeric plasmid under the constitutive GPD promoter and ^{DsRed}HDEL that were imaged after growth in SD-Leu+Ade and 60 minutes in the presence of edelfosine (EDLF), the vehicle (Ctrl), or 0.1% methyl methane sulfonate (MMS).

Acknowledgments

The authors would like to thank CM Unger and G Bertolesi for their helpful discussions, S. Gasser for sharing microarray data of internal SIR targets and S Gasser and S Emr for the kind gift of strains and plasmids. This work was supported by a Discovery Grant and a Discovery Accelerator Supplement from the Natural Sciences and Engineering Research Council (NSERC) to VZ and by operating grants from CIHR MOP-82736; MOP-137062 and NSERC 418122 awarded to JAC. MLSP is funded by a doctoral fellowship from NSERC and Alberta Innovates.

References

Ai, W., P.G. Bertram, C.K. Tsang, T.F. Chan, and X.F.S. Zheng. 2002. Regulation of subtelomeric silencing during stress response. *Mol. Cell*. 10:1295–1305. doi:10.1016/S1097-2765(02)00695-0.

Alberti, S., A.D. Gitler, and S. Lindquist. 2007. A suite of Gateway cloning vectors for high-throughput genetic analysis in Saccharomyces cerevisiae. *Yeast*. 24:913–919. doi:10.1002/YEA.1502.

Ames, B.N. 1966. Assay of inorganic phosphate, total phosphate and phosphatases. *Methods Enzymol.* 8:115–118. doi:10.1016/0076-6879(66)08014-5.

Aparicio, O.M., B.L. Billington, and D.E. Gottschling. 1991. Modifiers of position effect are shared between telomeric and silent mating-type loci in S. cerevisiae. *Cell*. 66:1279–1287. doi:10.1016/0092-8674(91)90049-5.

Attard, G.S., R.H. Templer, W.S. Smith, A.N. Hunt, and S. Jackowski. 2000. Modulation of CTP:phosphocholine cytidylyltransferase by membrane curvature elastic stress. *Proc. Natl. Acad. Sci. U. S. A.* 97:9032–9036. doi:10.1073/PNAS.160260697.

Auld, K.L., C.R. Brown, J.M. Casolari, S. Komili, and P.A. Silver. 2006. Genomic association of the proteasome demonstrates overlapping gene regulatory activity with transcription factor substrates. *Mol. Cell*. 21:861–871. doi:10.1016/J.MOLCEL.2006.02.020.

Ausili, A., A. Torrecillas, F.J. Aranda, F. Mollinedo, C. Gajate, S. Corbalán-García, A. De Godos, and J.C. Gómez-Fernández. 2008. Edelfosine is incorporated into rafts and alters their organization. *J. Phys. Chem. B*. 112:11643–11654. doi:10.1021/jp802165n.

Azevedo, D., L. Nascimento, J. Labarre, M.B. Toledano, and C. Rodrigues-Pousada. 2007. The S. cerevisiae Yap1 and Yap2 transcription factors share a common cadmium-sensing domain. *FEBS Lett.* 581:187–195. doi:10.1016/J.FEBSLET.2006.11.083.

Bahmanyar, S., and C. Schlieker. 2020. Lipid and protein dynamics that shape nuclear envelope identity. *Mol. Biol. Cell*. 31:1315. doi:10.1091/MBC.E18-10-0636.

Ballweg, S., E. Sezgin, M. Doktorova, R. Covino, J. Reinhard, D. Wunnicke, I. Hänelt, I. Levental, G. Hummer, and R. Ernst. 2020. Regulation of lipid saturation without sensing membrane fluidity. *Nat. Commun.* 11:1–13. doi:10.1038/s41467-020-14528-1.

Barbosa, A.D., K. Lim, M. Mari, J.R. Edgar, L. Gal, P. Sterk, B.J. Jenkins, A. Koulman, D.B. Savage, M. Schuldiner, F. Reggiori, P.A. Wigge, and S. Siniossoglou. 2019. Compartmentalized Synthesis of Triacylglycerol at the Inner Nuclear Membrane Regulates Nuclear Organization. *Dev. Cell*. 50:755-766.e6. doi:10.1016/J.DEVCEL.2019.07.009.

Becton, D. and C. 2021. FlowJo™ Software.

Bedalov, A., T. Gatbonton, W.P. Irvine, D.E. Gottschling, and J.A. Simon. 2001. Identification of a small molecule inhibitor of Sir2p. *Proc. Natl. Acad. Sci. U. S. A.* 98:15113–15118. doi:10.1073/PNAS.261574398.

Bernstein, B.E., J.K. Tong, and S.L. Schreiber. 2000. Genomewide studies of histone deacetylase function in yeast. *Proc. Natl. Acad. Sci. U. S. A.* 97:13708–13713. doi:10.1073/pnas.250477697.

Bierbaum, T.J., S.R. Bouma, and W.H. Huestis. 1979. A mechanism of erythrocyte lysis by lysophosphatidylcholine. *Biochim. Biophys. Acta - Biomembr.* 555:102–110. doi:10.1016/0005-2736(79)90075-0.

Bindea, G., B. Mlecnik, H. Hackl, P. Charoentong, M. Tosolini, A. Kirilovsky, W.H. Fridman, F. Pagès, Z. Trajanoski, and J. Galon. 2009. ClueGO: a Cytoscape plug-in to decipher functionally grouped gene ontology and pathway annotation networks. *Bioinformatics*. 25:1091–1093. doi:10.1093/BIOINFORMATICS/BTP101.

Bindu, S., V.B. Pillai, and M.P. Gupta. 2016. Role of Sirtuins in Regulating Pathophysiology of the Heart. *Trends Endocrinol. Metab.* 27:563–573. doi:10.1016/J.TEM.2016.04.015.

Boggs, K.P., C.O. Rock, and S. Jackowski. 1995. Lysophosphatidylcholine and 1-O-octadecyl-2-O-methyl-rac-glycero-3-phosphocholine inhibit the CDP-choline pathway of phosphatidylcholine synthesis at the CTP:phosphocholine cytidylyltransferase step. *J. Biol. Chem.* 270:7757–7764. doi:10.1074/JBC.270.13.7757.

Bolte, S., and F.P. Cordelières. 2006. A guided tour into subcellular colocalization analysis in light microscopy. *J. Microsc.* 224:213–232. doi:10.1111/J.1365-2818.2006.01706.X.

Bonilla, X., E.H. Dakir, F. Mollinedo, and C. Gajate. 2015. Endoplasmic reticulum targeting in Ewing's sarcoma by the alkylphospholipid analog edelfosine. *Oncotarget*. 6:14596. doi:10.18632/ONCOTARGET.4053.

Bryk, M., M. Banerjee, M. Murphy, K.E. Knudsen, D.J. Garfinkel, and M.J. Curcio. 1997. Transcriptional silencing of Ty1 elements in the RDN1 locus of yeast. *Genes Dev.* 11:255–269. doi:10.1101/GAD.11.2.255.

Buchman, A.R., W.J. Kimmerly, J. Rine, and R.D. Kornberg. 1988a. Two DNA-binding factors recognize specific sequences at silencers, upstream activating sequences, autonomously replicating sequences, and telomeres in Saccharomyces cerevisiae. *Mol. Cell. Biol.* 8:210–225. doi:10.1128/MCB.8.1.210.

Buchman, A.R., N.F. Lue, and R.D. Kornberg. 1988b. Connections between transcriptional activators, silencers, and telomeres as revealed by functional analysis of a yeast DNA-binding protein. *Mol. Cell. Biol.* 8:5086–5099. doi:10.1128/MCB.8.12.5086-5099.1988.

Buck, S.W., and D. Shore. 1995. Action of a RAP1 carboxy-terminal silencing domain reveals an underlying competition between HMR and telomeres in yeast. *Genes Dev.* 9:370–384. doi:10.1101/gad.9.3.370.

Bupp, J.M., A.E. Martin, E.S. Stensrud, and S.L. Jaspersen. 2007. Telomere anchoring at the nuclear periphery requires the budding yeast Sad1-UNC-84 domain protein Mps3. *J. Cell Biol.* 179:845–54. doi:10.1083/jcb.200706040.

Bystricky, K., T. Laroche, G. Van Houwe, M. Blaszczyk, and S.M. Gasser. 2005. Chromosome looping in yeast: telomere pairing and coordinated movement reflect anchoring efficiency and territorial organization. *J. Cell Biol.* 168:375–387. doi:10.1083/JCB.200409091.

Cai, L., M.A. McCormick, B.K. Kennedy, and B.P. Tu. 2013. Integration of multiple nutrient cues and regulation of lifespan by ribosomal transcription factor Ifh1. *Cell Rep.* 4:1063–1071. doi:10.1016/J.CELREP.2013.08.016.

Campbell, J.L., A. Lorenz, K.L. Witkin, T. Hays, J. Loidl, and O. Cohen-Fix. 2006. Yeast nuclear envelope subdomains with distinct abilities to resist membrane expansion. *Mol. Biol. Cell*. 17:1768–78. doi:10.1091/mbc.E05-09-0839.

Carman, G.M., and G.-S. Han. 2019. Fat-regulating phosphatidic acid phosphatase: a review of its roles and regulation in lipid homeostasis. *J. Lipid Res.* 60:2–6. doi:10.1194/jlr.S087452.

Chan, J.N.Y., B.P.K. Poon, J. Salvi, J.B. Olsen, A. Emili, and K. Mekhail. 2011. Perinuclear cohibin complexes maintain replicative life span via roles at distinct silent chromatin domains. *Dev. Cell*. 20:867–879. doi:10.1016/J.DEVCEL.2011.05.014.

Chellappa, R., P. Kandasamy, C.S. Oh, Y. Jiang, M. Vemula, and C.E. Martin. 2001. The membrane proteins, Spt23p and Mga2p, play distinct roles in the activation of Saccharomyces cerevisiae OLE1 gene expression. Fatty acid-mediated regulation of Mga2p activity is independent of its proteolytic processing into a soluble transcription activator. *J. Biol. Chem.* 276:43548–43556. doi:10.1074/JBC.M107845200.

Cherel, I., and P. Thuriaux. 1995. The IFH1 gene product interacts with a fork head protein in Saccharomyces cerevisiae. *Yeast*. 11:261–270. doi:10.1002/YEA.320110308.

Chu, S., and I. Herskowitz. 1998. Gametogenesis in yeast is regulated by a transcriptional cascade dependent on Ndt80. *Mol. Cell*. 1:685–696. doi:10.1016/S1097-2765(00)80068-4.

Chua, G., Q.D. Morris, R. Sopko, M.D. Robinson, O. Ryan, E.T. Chan, B.J. Frey, B.J. Andrews, C. Boone, and T.R. Hughes. 2006. Identifying transcription factor functions and targets by phenotypic activation. *Proc. Natl. Acad. Sci. U. S. A.* 103:12045–12050. doi:10.1073/PNAS.0605140103.

Cockell, M., F. Palladino, T. Laroche, G. Kyrion, C. Liu, A.J. Lustig, and S.M. Gasser. 1995. The carboxy termini of Sir4 and RAP1 affect Sir3 localization: Evidence for a multicomponent complex required for yeast telomeric silencing. *J. Cell Biol.* 129:909–924. doi:10.1083/jcb.129.4.909.

Covino, R., S. Ballweg, C. Stordeur, J.B. Michaelis, K. Puth, F. Wernig, A. Bahrami, A.M. Ernst, G. Hummer, and R. Ernst. 2016. A Eukaryotic Sensor for Membrane Lipid Saturation. *Mol. Cell*. 63:49–59. doi:10.1016/J.MOLCEL.2016.05.015.

Cuesta-Marbán, Á., J. Botet, O. Czyz, L.M. Cacharro, C. Gajate, V. Hornillos, J. Delgado, H. Zhang, F. Amat-Guerri, A.U. Acuña, C.R. McMaster, J.L. Revuelta, V. Zaremberg, and F. Mollinedo. 2013. Drug uptake, lipid rafts, and vesicle trafficking modulate resistance to an anticancer lysophosphatidylcholine analogue in yeast. *J. Biol. Chem.* 288:8405–18. doi:10.1074/jbc.M112.425769.

Czyz, O., T. Bitew, A. Cuesta-Marbán, C.R. McMaster, F. Mollinedo, and V. Zaremberg. 2013. Alteration of plasma membrane organization by an anticancer lysophosphatidylcholine analogue induces intracellular acidification and internalization of plasma membrane transporters in yeast. *J. Biol. Chem.* 288:8419–32. doi:10.1074/jbc.M112.425744.

Dula, M.L., and S.G. Holmes. 2000. MGA2 and SPT23 Are Modifiers of Transcriptional Silencing in Yeast. *Genetics*. 156:933–941. doi:10.1093/GENETICS/156.3.933.

Dymond, M., G. Attard, and A.D. Postle. 2008. Testing the hypothesis that amphiphilic antineoplastic lipid analogues act through reduction of membrane curvature elastic stress. *J. R. Soc. Interface*. 5:1371–1386. doi:10.1098/RSIF.2008.0041.

Ehrentraut, S., J.M. Weber, J.N. Dybowski, D. Hoffmann, and A.E. Ehrenhofer-Murray. 2010. Rpd3-dependent boundary formation at telomeres by removal of Sir2 substrate. *Proc. Natl. Acad. Sci. U. S. A.* 107:5522–5527. doi:10.1073/PNAS.0909169107.

Ellahi, A., D.M. Thurtle, and J. Rine. 2015. The chromatin and transcriptional landscape of native saccharomyces cerevisiae telomeres and subtelomeric domains. *Genetics*. doi:10.1534/genetics.115.175711.

Fang, Z., Z. Chen, S. Wang, P. Shi, Y. Shen, Y. Zhang, J. Xiao, and Z. Huang. 2017. Overexpression of OLE1 Enhances Cytoplasmic Membrane Stability and Confers Resistance to Cadmium in

Saccharomyces cerevisiae. *Appl. Environ. Microbiol.* 83:e02319-16. doi:10.1128/AEM.02319-16.

De Filippi, L., M. Fournier, E. Cameroni, P. Linder, C. De Virgilio, M. Foti, and O. Deloche. 2007. Membrane stress is coupled to a rapid translational control of gene expression in chlorpromazine-treated cells. *Curr. Genet.* 52:171–185. doi:10.1007/S00294-007-0151-0.

Fontana, G.A., D. Hess, J.K. Reinert, S. Mattarocci, B. Falquet, D. Klein, D. Shore, N.H. Thomä, and U. Rass. 2019. Rif1 S-acylation mediates DNA double-strand break repair at the inner nuclear membrane. *Nat. Commun.* 10:2535. doi:10.1038/s41467-019-10349-z.

Fritze, C.E., K. Verschueren, R. Strich, and R.E. Esposito. 1997. Direct evidence for SIR2 modulation of chromatin structure in yeast rDNA. *EMBO J.* 16:6495–6509.

Fujimoto, T. 2022. Nuclear lipid droplets - how are they different from their cytoplasmic siblings? *J. Cell Sci.* 135. doi:10.1242/JCS.259253/274537.

Fuller, N., and R.P. Rand. 2001. The Influence of Lysolipids on the Spontaneous Curvature and Bending Elasticity of Phospholipid Membranes. *Biophys. J.* 81:243–254. doi:10.1016/S0006-3495(01)75695-0.

Gajate, C., M. Matos-Da-Silva, E.L.-H. Dakir, R.I. Fonteriz, J. Alvarez, and F. Mollinedo. 2012. Antitumor alkyl-lysophospholipid analog edelfosine induces apoptosis in pancreatic cancer by targeting endoplasmic reticulum. *Oncogene*. 31:2627–2639. doi:10.1038/onc.2011.446.

Galdieri, L., and A. Vancura. 2012. Acetyl-CoA Carboxylase Regulates Global Histone Acetylation. *J. Biol. Chem.* 287:23865–23876. doi:10.1074/jbc.M112.380519.

Gefeng, Z., P.T. Spellman, T. Volpe, P.O. Brown, D. Botstein, T.N. Davis, and B. Futcher. 2000. Two yeast forkhead genes regulate the cell cycle and pseudohyphal growth. *Nature*. 406:90–94. doi:10.1038/35017581.

Ghavidel, A., K. Baxi, M. Prusinkiewicz, C. Swan, Z.R. Belak, C.H. Eskiw, C.E. Carvalho, and T.A. Harkness. 2018. Rapid nuclear exclusion of HCM1 in aging Saccharomyces cerevisiae leads to vacuolar alkalization and replicative senescence. *G3 Genes, Genomes, Genet.* 8:1579–1592. doi:10.1534/G3.118.200161/-/DC1/FIGURES5.PPTX.

Golam Mostofa, M., M.A. Rahman, N. Koike, A.M.S.T. Yeasmin, N. Islam, T.M. Waliullah, S. Hosoyamada, M. Shimobayashi, T. Kobayashi, M.N. Hall, and T. Ushimaru. 2018. CLIP and cohibin separate rDNA from nucleolar proteins destined for degradation by nucleophagy. *J. Cell Biol.* 217:2675–2690. doi:10.1083/JCB.201706164.

Golden, A., J. Liu, and O. Cohen-Fix. 2009. Inactivation of the C. elegans lipin homolog leads to ER disorganization and to defects in the breakdown and reassembly of the nuclear envelope. *J. Cell Sci.* 122:1970. doi:10.1242/JCS.044743.

Gotta, M., T. Laroche, A. Formenton, L. Maillet, H. Scherthan, and S.M. Gasser. 1996. The clustering of telomeres and colocalization with Rap1, Sir3, and Sir4 proteins in wild-type Saccharomyces cerevisiae. *J. Cell Biol.* 134:1349–63.

Gotta, M., S. Strahl-Bolsinger, H. Renauld, T. Laroche, B.K. Kennedy, M. Grunstein, and S.M. Gasser. 1997. Localization of Sir2p: the nucleolus as a compartment for silent information regulators. *EMBO J.* 16:3243–3255. doi:10.1093/emboj/16.11.3243.

Gottlieb, S., and R.E. Esposito. 1989. A new role for a yeast transcriptional silencer gene, SIR2, in regulation of recombination in ribosomal DNA. *Cell*. 56:771–776. doi:10.1016/0092-8674(89)90681-8.

Green, M.R., and J. Sambrook. 2021. Total RNA Extraction from Saccharomyces cerevisiae Using Hot Acid Phenol. *Cold Spring Harb. Protoc.* 2021:pdb.prot101691. doi:10.1101/PDB.PROT101691.

Grunstein, M., and S.M. Gasser. 2013. Epigenetics in Saccharomyces cerevisiae. *Cold Spring Harb. Perspect. Biol.* 5:a017491. doi:10.1101/cshperspect.a017491.

Guan, X.L., C.M. Souza, H. Pichler, G. Dewhurst, O. Schaad, K. Kajiwara, H. Wakabayashi, T. Ivanova, G.A. Castillon, M. Piccolis, F. Abe, R. Loewith, K. Funato, M.R. Wenk, and H. Riezman. 2009. Functional Interactions between Sphingolipids and Sterols in Biological Membranes Regulating Cell Physiology. *Mol. Biol. Cell*. 20:2083. doi:10.1091/MBC.E08-11-1126.

Guthrie, C., and G.R. Fink. 1991. Guide to yeast genetics and molecular biology. Academic Press. 933 pp.

Haider, A., Y.C. Wei, K. Lim, A.D. Barbosa, C.H. Liu, U. Weber, M. Mlodzik, K. Oras, S. Collier, M.M. Hussain, L. Dong, S. Patel, A. Alvarez-Guaita, V. Saudek, B.J. Jenkins, A. Koulman, M.K. Dymond, R.C. Hardie, S. Siniossoglou, and D.B. Savage. 2018. PCYT1A Regulates Phosphatidylcholine Homeostasis from the Inner Nuclear Membrane in Response to Membrane Stored Curvature Elastic Stress. *Dev. Cell*. 45:481-495.e8. doi:10.1016/J.DEVCEL.2018.04.012.

Hall, D.B., J.T. Wade, and K. Struhl. 2006. An HMG protein, Hmo1, associates with promoters of many ribosomal protein genes and throughout the rRNA gene locus in Saccharomyces cerevisiae. *Mol. Cell. Biol.* 26:3672–3679. doi:10.1128/MCB.26.9.3672-3679.2006.

Harbison, C.T., D.B. Gordon, T.I. Lee, N.J. Rinaldi, K.D. Macisaac, T.W. Danford, N.M. Hannett, J.B. Tagne, D.B. Reynolds, J. Yoo, E.G. Jennings, J. Zeitlinger, D.K. Pokholok, M. Kellis, P.A. Rolfe, K.T. Takusagawa, E.S. Lander, D.K. Gifford, E. Fraenkel, and R.A. Young. 2004. Transcriptional regulatory code of a eukaryotic genome. *Nature*. 431:99–104. doi:10.1038/NATURE02800.

Haugen, A.C., R. Kelley, J.B. Collins, C.J. Tucker, C. Deng, C.A. Afshari, J.M. Brown, T. Ideker, and B. Van Houten. 2004. Integrating phenotypic and expression profiles to map arsenic-response networks. *Genome Biol.* 5:1–18. doi:10.1186/GB-2004-5-12-R95.

Hediger, F., F.R. Neumann, G. Van Houwe, K. Dubrana, and S.M. Gasser. 2002. Live Imaging of Telomeres: yKu and Sir Proteins Define Redundant Telomere-Anchoring Pathways in Yeast. *Curr. Biol.* 12:2076–2089. doi:10.1016/S0960-9822(02)01338-6.

Holm, S. 1979. A Simple Sequentially Rejective Multiple Test Procedure on JSTOR. *Scand. J. Stat.* 6:65–70.

Hoppe, G.J., J.C. Tanny, A.D. Rudner, S.A. Gerber, S. Danaie, S.P. Gygi, and D. Moazed. 2002. Steps in assembly of silent chromatin in yeast: Sir3-independent binding of a Sir2/Sir4 complex to silencers and role for Sir2-dependent deacetylation. *Mol. Cell. Biol.* 22:4167–4180. doi:10.1128/MCB.22.12.4167-4180.2002.

Hoppe, T., K. Matuschewski, M. Rape, S. Schlenker, H.D. Ulrich, and S. Jentsch. 2000. Activation of a membrane-bound transcription factor by regulated ubiquitin/proteasome-dependent processing. *Cell*. 102:577–86. doi:10.1016/S0092-8674(00)00080-5.

Hozé, N., M. Ruault, C. Amoruso, A. Taddei, and D. Holcman. 2013. Spatial telomere organization and clustering in yeast Saccharomyces cerevisiae nucleus is generated by a random dynamics of aggregation-dissociation. *Mol. Biol. Cell*. 24:1791–1800. doi:10.1091/mbc.E13-01-0031.

Hughes, T.R., M.J. Marton, A.R. Jones, C.J. Roberts, R. Stoughton, C.D. Armour, H.A. Bennett, E. Coffey, H. Dai, Y.D. He, M.J. Kidd, A.M. King, M.R. Meyer, D. Slade, P.Y. Lum, S.B. Stepaniants, D.D. Shoemaker, D. Gachotte, K. Chakraburtty, J. Simon, M. Bard, and S.H. Friend. 2000.

Functional discovery via a compendium of expression profiles. *Cell*. 102:109–126. doi:10.1016/S0092-8674(00)00015-5.

Ikeda, A., T. Muneoka, S. Murakami, A. Hirota, Y. Yabuki, T. Karashima, K. Nakazono, M. Tsuruno, H. Pichler, K. Shirahige, Y. Kodama, T. Shimamoto, K. Mizuta, and K. Funato. 2015. Sphingolipids regulate telomere clustering by affecting the transcription of genes involved in telomere homeostasis. *J. Cell Sci.* 128:2454–67. doi:10.1242/jcs.164160.

Imai, S.I., C.M. Armstrong, M. Kaeberlein, and L. Guarente. 2000. Transcriptional silencing and longevity protein Sir2 is an NAD-dependent histone deacetylase. *Nat. 2000 4036771*. 403:795–800. doi:10.1038/35001622.

Jesch, S.A., X. Zhao, M.T. Wells, and S.A. Henry. 2005. Genome-wide analysis reveals inositol, not choline, as the major effector of Ino2p-Ino4p and unfolded protein response target gene expression in yeast. *J. Biol. Chem.* 280:9106–9118. doi:10.1074/jbc.M411770200.

Jin, Q.W., E. Trelles-Sticken, H. Scherthan, and J. Loidl. 1998. Yeast Nuclei Display Prominent Centromere Clustering That Is Reduced in Nondividing Cells and in Meiotic Prophase. *J. Cell Biol.* 141:29. doi:10.1083/JCB.141.1.21.

jmw86069. 2020. venndir: Venn diagrams with directionality (concordance), optional display of items inside the figure, text Venn diagrams. *GitHub*.

Karpichev, I. V., J.M. Durand-Heredia, Y. Luo, and G.M. Small. 2008. Binding Characteristics and Regulatory Mechanisms of the Transcription Factors Controlling Oleate-responsive Genes in Saccharomyces cerevisiae*. *J. Biol. Chem.* 283:10264–10275. doi:10.1074/JBC.M708215200.

Kasahara, K., K. Ohtsuki, S. Ki, K. Aoyama, H. Takahashi, T. Kobayashi, K. Shirahige, and T. Kokubo. 2007. Assembly of regulatory factors on rRNA and ribosomal protein genes in Saccharomyces cerevisiae. *Mol. Cell. Biol.* 27:6686–6705. doi:10.1128/MCB.00876-07.

Kennedy, B.K., M. Gotta, D.A. Sinclair, K. Mills, D.S. McNabb, M. Murthy, S.M. Pak, T. Laroche, S.M. Gasser, and L. Guarente. 1997. Redistribution of Silencing Proteins from Telomeres to the Nucleolus Is Associated with Extension of Life Span in S. cerevisiae. *Cell*. 89:381–391. doi:10.1016/S0092-8674(00)80219-6.

Knott, S.R.V., J.M. Peace, A.Z. Ostrow, Y. Gan, A.E. Rex, C.J. Viggiani, S. Tavaré, and O.M. Aparicio. 2012. Forkhead transcription factors establish origin timing and long-range clustering in S. cerevisiae. *Cell*. 148:99–111. doi:10.1016/J.CELL.2011.12.012.

Kny, G. 1969. Über Lysolecithin-Analoga - Synthese und biologische Eigenschaften. University of Feriburg.

Kurylowicz, A. 2016. In Search of New Therapeutic Targets in Obesity Treatment: Sirtuins. *Int. J. Mol. Sci.* 17. doi:10.3390/IJMS17040572.

Kyrion, G., K.A. Boakye, and A.J. Lustig12. 1992. C-terminal truncation of RAP1 results in the deregulation of telomere size, stability, and function in Saccharomyces cerevisiae. *Mol. Cell. Biol.* 12:5159–5173. doi:10.1128/MCB.12.11.5159-5173.1992.

Ladner, C.L., J. Yang, R.J. Turner, and R.A. Edwards. 2004. Visible fluorescent detection of proteins in polyacrylamide gels without staining. *Anal. Biochem.* 326:13–20. doi:10.1016/J.AB.2003.10.047.

Laroche, T., S.G. Martin, M. Gotta, H.C. Gorham, F.E. Pryde, E.J. Louis, and S.M. Gasser. 1998. Mutation of yeast Ku genes disrupts the subnuclear organization of telomeres. *Curr. Biol.* 8:653–6.

Lavoie, H., H. Hogues, J. Mallick, A. Sellam, A. Nantel, and M. Whiteway. 2010. Evolutionary Tinkering with Conserved Components of a Transcriptional Regulatory Network. *PLOS Biol.* 8:e1000329. doi:10.1371/JOURNAL.PBIO.1000329.

Lee, J.B., and A.J. Keung. 2018. Chromatin Immunoprecipitation in Human and Yeast Cells. *Methods Mol. Biol.* 1767:257–269. doi:10.1007/978-1-4939-7774-1_14.

Lee, T.I., N.J. Rinaldi, F. Robert, D.T. Odom, Z. Bar-Joseph, G.K. Gerber, N.M. Hannett, C.T. Harbison, C.M. Thompson, I. Simon, J. Zeitlinger, E.G. Jennings, H.L. Murray, D. Benjamin Gordon, B. Ren, J.J. Wyrick, J.B. Tagne, T.L. Volkert, E. Fraenkel, D.K. Gifford, and R.A. Young. 2002. Transcriptional regulatory networks in Saccharomyces cerevisiae. *Science (80-.).* 298:799–804. doi:10.1126/SCIENCE.1075090.

Lieb, J.D., X. Liu, D. Botstein, and P.O. Brown. 2001. Promoter-specific binding of Rap1 revealed by genome-wide maps of protein-DNA association. *Nat. Genet.* 28:327–334. doi:10.1038/NG569.

Linke, C., A. Chasapi, A. González-Novo, I. Al Sawad, S. Tognetti, E. Klipp, M. Loog, S. Krobitsch, F. Posas, I. Xenarios, and M. Barberis. 2017. A Clb/Cdk1-mediated regulation of Fkh2 synchronizes CLB expression in the budding yeast cell cycle. *NPJ Syst. Biol. Appl.* 3. doi:10.1038/S41540-017-0008-1.

Livak, K.J., and T.D. Schmittgen. 2001. Analysis of relative gene expression data using real-time quantitative PCR and the 2(-Delta Delta C(T)) Method. *Methods*. 25:402–408. doi:10.1006/METH.2001.1262.

Lockshon, D., L.E. Surface, E.O. Kerr, M. Kaeberlein, and B.K. Kennedy. 2007. The Sensitivity of Yeast Mutants to Oleic Acid Implicates the Peroxisome and Other Processes in Membrane Function. *Genetics*. 175:77. doi:10.1534/GENETICS.106.064428.

Loewen, C.J.R., M.L. Gazpar, S.A. Jesch, C. Delon, N.T. Ktistakis, S.A. Henry, and T.P. Levine. 2004. Phospholipid metabolism regulated by a transcription factor sensing phosphatidic acid. *Science (80-.).* 304:1644–1647. doi:10.1126/science.1096083.

Luo, K., M.A. Vega-Palas, and M. Grunstein. 2002. Rap1–Sir4 binding independent of other Sir, yKu, or histone interactions initiates the assembly of telomeric heterochromatin in yeast. *Genes Dev.* 16:1528. doi:10.1101/GAD.988802.

MacDonald, C., J.A. Payne, M. Aboian, W. Smith, D.J. Katzmann, and R.C. Piper. 2015. A Family of Tetraspans Organizes Cargo for Sorting into Multivesicular Bodies. *Dev. Cell*. 33:328. doi:10.1016/J.DEVCEL.2015.03.007.

Manford, A.G., C.J. Stefan, H.L. Yuan, J.A. MacGurn, and S.D. Emr. 2012. ER-to-Plasma Membrane Tethering Proteins Regulate Cell Signaling and ER Morphology. *Dev. Cell*. 23:1129–1140. doi:10.1016/j.devcel.2012.11.004.

Marr, N., J. Foglia, M. Terebiznik, K. Athenstaedt, and V. Zaremberg. 2012. Controlling lipid fluxes at glycerol-3-phosphate acyltransferase step in yeast: Unique contribution of Gat1p to oleic acid-induced lipid particle formation. *J. Biol. Chem.* 287:10251–10264. doi:10.1074/jbc.M111.314112.

Martin, C.E., C.S. Oh, and Y. Jiang. 2007. Regulation of long chain unsaturated fatty acid synthesis in yeast. *Biochim. Biophys. Acta - Mol. Cell Biol. Lipids*. 1771:271–285. doi:10.1016/J.BBALIP.2006.06.010.

Martin, S.G., T. Laroche, N. Suka, M. Grunstein, and S.M. Gasser. 1999. Relocalization of telomeric Ku and SIR proteins in response to DNA strand breaks in yeast. *Cell*. 97:621–633. doi:10.1016/S0092-8674(00)80773-4.

Matos-Perdomo, E., and F. Machín. 2019. Nucleolar and Ribosomal DNA Structure under Stress: Yeast Lessons for Aging and Cancer. *Cells*. 8:779. doi:10.3390/CELLS8080779.

Mazzola, D., C. Pimentel, S. Caetano, C. Amaral, R. Menezes, C.N. Santos, E. Eleutherio, and C. Rodrigues-Pousada. 2015. Inhibition of Yap2 activity by MAPKAP kinase Rck1 affects yeast tolerance to cadmium. *FEBS Lett.* 589:2841–2849. doi:10.1016/J.FEBSLET.2015.07.049.

McDonnell, E., S.B. Crown, D.B. Fox, B. Kitir, O.R. Ilkayeva, C.A. Olsen, P.A. Grimsrud, and M.D. Hirschey. 2016. Lipids Reprogram Metabolism to Become a Major Carbon Source for Histone Acetylation. *Cell Rep.* 17:1463–1472. doi:10.1016/j.celrep.2016.10.012.

Meister, P., L.R. Gehlen, E. Varela, V. Kalck, and S.M. Gasser. 2010. Visualizing yeast chromosomes and nuclear architecture. *Methods Enzymol.* 470:535–567. doi:10.1016/S0076-6879(10)70021-5.

Mekhail, K., J. Seebacher, S.P. Gygi, and D. Moazed. 2008. Role for perinuclear chromosome tethering in maintenance of genome stability. *Nature*. 456:667–670. doi:10.1038/NATURE07460.

Mills, K.D., D.A. Sinclair, and L. Guarente. 1999. MEC1-dependent redistribution of the Sir3 silencing protein from telomeres to DNA double-strand breaks. *Cell*. 97:609–620. doi:10.1016/S0092-8674(00)80772-2.

Miyoshi, K., T. Miyakawa, and K. Mizuta. 2001. Repression of rRNA synthesis due to a secretory defect requires the C-terminal silencing domain of Rap1p in Saccharomyces cerevisiae. *Nucleic Acids Res.* 29:3297–3303. doi:10.1093/NAR/29.16.3297.

Mizuta, K., R. Tsujii, J.R. Warner, and M. Nishiyama. 1998. The C-terminal silencing domain of Rap1p is essential for the repression of ribosomal protein genes in response to a defect in the secretory pathway. *Nucleic Acids Res.* 26:1063–9. doi:10.1093/nar/26.4.1063.

Mollinedo, F., C. Gajate, S. Martín-Santamaría, and F. Gago. 2004. ET-18-OCH 3 (Edelfosine): A Selective Antitumour Lipid Targeting Apoptosis Through Intracellular Activation of Fas/CD95 Death Receptor. 11. 3163 pp.

Monteiro, P.T., J. Oliveira, P. Pais, M. Antunes, M. Palma, M. Cavalheiro, M. Galocha, C.P. Godinho, L.C. Martins, N. Bourbon, M.N. Mota, R.A. Ribeiro, R. Viana, I. Sá-Correia, and M.C. Teixeira. 2020. YEASTRACT+: a portal for cross-species comparative genomics of transcription regulation in yeasts. *Nucleic Acids Res.* 48:D642–D649. doi:10.1093/NAR/GKZ859.

Moradi-Fard, S., J. Sarthi, M. Tittel-Elmer, M. Lalonde, E. Cusanelli, P. Chartrand, and J.A. Cobb. 2016. Smc5/6 Is a Telomere-Associated Complex that Regulates Sir4 Binding and TPE. *PLoS Genet.* 12:e1006268. doi:10.1371/journal.pgen.1006268.

Moretti, P., K. Freeman, L. Coodly, and D. Shore. 1994. Evidence that a complex of SIR proteins interacts with the silencer and telomere-binding protein RAP1. *Genes Dev.* 8:2257–2269. doi:10.1101/gad.8.19.2257.

Moretti, P., and D. Shore. 2001. Multiple Interactions in Sir Protein Recruitment by Rap1p at Silencers and Telomeres in Yeast. *Mol. Cell. Biol.* 21:8082. doi:10.1128/MCB.21.23.8082-8094.2001.

Morin, A., A.W. Moores, and M. Sacher. 2009. Dissection of Saccharomyces Cerevisiae Asci. *J. Vis. Exp.* 1146. doi:10.3791/1146.

Ni, L., C. Bruce, C. Hart, J. Leigh-Bell, D. Gelperin, L. Umansky, M.B. Gerstein, and M. Snyder. 2009. Dynamic and complex transcription factor binding during an inducible response in yeast. *Genes Dev.* 23:1351–1363. doi:10.1101/GAD.1781909.

Nikawa, J.I., and J. Kamiuto. 2004. The promoter of the yeast OPI1 regulatory gene. *J. Biosci. Bioeng.* 97:369–373. doi:10.1016/S1389-1723(04)70220-0.

Niu, W., Z. Li, W. Zhan, V.R. Iyer, and E.M. Marcotte. 2008. Mechanisms of cell cycle control revealed by a systematic and quantitative overexpression screen in S. cerevisiae. *PLoS Genet.* 4. doi:10.1371/JOURNAL.PGEN.1000120.

Nocedal, I., E. Mancera, and A.D. Johnson. 2017. Gene regulatory network plasticity predates a switch in function of a conserved transcription regulator. *Elife*. 6. doi:10.7554/ELIFE.23250.

Oakes, M., Y. Nogi, M.W. Clark, and M. Nomura. 1993. Structural alterations of the nucleolus in mutants of Saccharomyces cerevisiae defective in RNA polymerase I. *Mol. Cell. Biol.* 13:2441–2455. doi:10.1128/MCB.13.4.2441-2455.1993.

Oelkers, P., A. Tinkelenberg, N. Erdeniz, D. Cromley, J.T. Billheimer, and S.L. Sturley. 2000. A Lecithin Cholesterol Acyltransferase-like Gene Mediates Diacylglycerol Esterification in Yeast. *J. Biol. Chem.* 275:15609–15612. doi:10.1074/JBC.C000144200.

Ostrow, A.Z., T. Nellimoottil, S.R.V. Knott, C.A. Fox, S. Tavaré, and O.M. Aparicio. 2014. Fkh1 and Fkh2 Bind Multiple Chromosomal Elements in the S. cerevisiae Genome with Distinct Specificities and Cell Cycle Dynamics. *PLoS One*. 9:e87647. doi:10.1371/JOURNAL.PONE.0087647.

Palladino, F., T. Laroche, E. Gilson, A. Axelrod, L. Pillus, and S.M. Gasser. 1993. SIR3 and SIR4 proteins are required for the positioning and integrity of yeast telomeres. *Cell*. 75:543–555. doi:10.1016/0092-8674(93)90388-7.

Papagiannidis, D., P.W. Bircham, C. Lüchtenborg, O. Pajonk, G. Ruffini, B. Brügger, and S. Schuck. 2021. Ice2 promotes ER membrane biogenesis in yeast by inhibiting the conserved lipin phosphatase complex. *EMBO J.* 40. doi:10.15252/EMBJ.2021107958.

Papsdorf, K., and A. Brunet. 2019. Linking Lipid Metabolism to Chromatin Regulation in Aging. *Trends Cell Biol.* 29:97–116. doi:10.1016/j.tcb.2018.09.004.

Park, S., E.E. Patterson, J. Cobb, A. Audhya, M.R. Gartenberg, and C.A. Fox. 2011. Palmitoylation controls the dynamics of budding-yeast heterochromatin via the telomere-binding protein Rif1. *Proc. Natl. Acad. Sci. U. S. A.* 108:14572–14577. doi:10.1073/PNAS.1105262108/-/DCSUPPLEMENTAL/PNAS.201105262SI.PDF.

Perrod, S., M.M. Cockell, T. Laroche, H. Renauld, A.L. Ducrest, C. Bonnard, and S.M. Gasser. 2001. A cytosolic NAD-dependent deacetylase, Hst2p, can modulate nucleolar and telomeric silencing in yeast. *EMBO J.* 20:197. doi:10.1093/EMBOJ/20.1.197.

Pillus, L., and J. Rine. 1989. Epigenetic inheritance of transcriptional states in S. cerevisiae. *Cell*. 59:637–647. doi:10.1016/0092-8674(89)90009-3.

Pondugula, S., D.W. Neef, W.P. Voth, R.P. Darst, A. Dhasarathy, M.M. Reynolds, S. Takahata, D.J. Stillman, and M.P. Kladde. 2009. Coupling phosphate homeostasis to cell cycle-specific transcription: mitotic activation of Saccharomyces cerevisiae PHO5 by Mcm1 and Forkhead proteins. *Mol. Cell. Biol.* 29:4891–4905. doi:10.1128/MCB.00222-09.

R Core Team. 2021. R: A Language and Environment for Statistical Computing.

Radman-Livaja, M., G. Ruben, A. Weiner, N. Friedman, R. Kamakaka, and O.J. Rando. 2011. Dynamics of Sir3 spreading in budding yeast: secondary recruitment sites and euchromatic localization. *EMBO J.* 30:1012. doi:10.1038/EMBOJ.2011.30.

Reimand, J., J.M. Vaquerizas, A.E. Todd, J. Vilo, and N.M. Luscombe. 2010. Comprehensive reanalysis of transcription factor knockout expression data in Saccharomyces cerevisiae reveals many new targets. *Nucleic Acids Res.* 38:4768–4777. doi:10.1093/NAR/GKQ232.

Reja, R., V. Vinayachandran, S. Ghosh, and B.F. Pugh. 2015. Molecular mechanisms of ribosomal protein gene coregulation. *Genes Dev.* 29:1942–1954. doi:10.1101/GAD.268896.115.

Renis, M., V. Cardile, M. Palumbo, and A. Russo. 2000. ET-18-OCH3-induced cytotoxicity and DNA damage in rat astrocytes. *Int. J. Dev. Neurosci.* 18:545–555. doi:10.1016/S0736-5748(00)00020-4.

Robyr, D., Y. Suka, I. Xenarios, S.K. Kurdistani, A. Wang, N. Suka, and M. Grunstein. 2002. Microarray deacetylation maps determine genome-wide functions for yeast histone deacetylases. *Cell*. 109:437–446. doi:10.1016/S0092-8674(02)00746-8.

Romanauska, A., and A. Köhler. 2018. The Inner Nuclear Membrane Is a Metabolically Active Territory that Generates Nuclear Lipid Droplets. *Cell*. 174:700-715.e18. doi:10.1016/j.cell.2018.05.047.

Romanauska, A., and A. Köhler. 2021. Reprogrammed lipid metabolism protects inner nuclear membrane against unsaturated fat. *Dev. Cell*. 56:2562-2578.e3. doi:10.1016/J.DEVCEL.2021.07.018.

Romero, A.M., T. Jordá, N. Rozès, M.T. Martínez-Pastor, and S. Puig. 2018. Regulation of yeast fatty acid desaturase in response to iron deficiency. *Biochim. Biophys. Acta - Mol. Cell Biol. Lipids*. 1863:657–668. doi:10.1016/J.BBALIP.2018.03.008.

Ruault, M., A. De Meyer, I. Loïodice, and A. Taddei. 2011. Clustering heterochromatin: Sir3 promotes telomere clustering independently of silencing in yeast. *J. Cell Biol.* 192:417–431. doi:10.1083/jcb.201008007.

Ruault, M., V.F. Scolari, L. Lazar-Stefanita, A. Hocher, I. Loiödice, R. Koszul, and A. Taddei. 2021. Sir3 mediates long-range chromosome interactions in budding yeast. *Genome Res.* 31:411–425. doi:10.1101/GR.267872.120/-/DC1.

Rudra, D., J. Mallick, Y. Zhao, and J.R. Warner. 2007. Potential Interface between Ribosomal Protein Production and Pre-rRNA Processing. *Mol. Cell. Biol.* 27:4815–4824. doi:10.1128/MCB.02062-06.

Rudra, D., Y. Zhao, and J.R. Warner. 2005. Central role of Ifh1p-Fhl1p interaction in the synthesis of yeast ribosomal proteins. *EMBO J.* 24:533–542. doi:10.1038/SJ.EMBOJ.7600553.

Rundlett, S.E., A.A. Carmen, R. Kobayashi, S. Bavykin, B.M. Turner, and M. Grunstein. 1996. HDA1 and RPD3 are members of distinct yeast histone deacetylase complexes that regulate silencing and transcription. *Proc. Natl. Acad. Sci. U. S. A.* 93:14503–14508. doi:10.1073/PNAS.93.25.14503.

De Sanctis, V., S. La Terra, A. Bianchi, D. Shore, L. Burderi, E. Di Mauro, and R. Negri. 2002. In vivo topography of Rap1p-DNA complex at Saccharomyces cerevisiae TEF2 UAS(RPG) during transcriptional regulation. *J. Mol. Biol.* 318:333–349. doi:10.1016/S0022-2836(02)00110-9.

Santos-Rosa, H., J. Leung, N. Grimsey, S. Peak-Chew, and S. Siniossoglou. 2005. The yeast lipin Smp2 couples phospholipid biosynthesis to nuclear membrane growth. *EMBO J.* 24:1931–41. doi:10.1038/sj.emboj.7600672.

Schawalder, S.B., M. Kabani, I. Howald, U. Choudhury, M. Werner, and D. Shore. 2004. Growth-regulated recruitment of the essential yeast ribosomal protein gene activator Ifh1. *Nature*. 432:1058–1061. doi:10.1038/NATURE03200.

Schindelin, J., I. Arganda-Carreras, E. Frise, V. Kaynig, M. Longair, T. Pietzsch, S. Preibisch, C. Rueden, S. Saalfeld, B. Schmid, J.Y. Tinevez, D.J. White, V. Hartenstein, K. Eliceiri, P. Tomancak, and A.

Cardona. 2012. Fiji: an open-source platform for biological-image analysis. *Nat. Methods 2012 97*. 9:676–682. doi:10.1038/nmeth.2019.

Schober, H., V. Kalck, M.A. Vega-Palas, G. Van Houwe, D. Sage, M. Unser, M.R. Gartenberg, and S.M. Gasser. 2008. Controlled exchange of chromosomal arms reveals principles driving telomere interactions in yeast. *Genome Res.* 18:261–271. doi:10.1101/gr.6687808.

Schreiner, S.M., P.K. Koo, Y. Zhao, S.G.J. Mochrie, and M.C. King. 2015. The tethering of chromatin to the nuclear envelope supports nuclear mechanics. *Nat. Commun.* 6:7159. doi:10.1038/ncomms8159.

Shannon, P., A. Markiel, O. Ozier, N.S. Baliga, J.T. Wang, D. Ramage, N. Amin, B. Schwikowski, and T. Ideker. 2003. Cytoscape: a software environment for integrated models of biomolecular interaction networks. *Genome Res.* 13:2498–2504. doi:10.1101/GR.1239303.

Shapira, M., E. Segal, and D. Botstein. 2004. Disruption of yeast forkhead-associated cell cycle transcription by oxidative stress. *Mol. Biol. Cell*. 15:5659–5669. doi:10.1091/MBC.E04-04-0340.

Sidak, Z. 1967. Rectangular Confidence Regions for the Means of Multivariate Normal Distributions. *J. Am. Stat. Assoc.* 62:633. doi:10.2307/2283989.

Simon, I., J. Barnett, N. Hannett, C.T. Harbison, N.J. Rinaldi, T.L. Volkert, J.J. Wyrick, J. Zeitlinger, D.K. Gifford, T.S. Jaakkola, and R.A. Young. 2001. Serial regulation of transcriptional regulators in the yeast cell cycle. *Cell*. 106:697–708. doi:10.1016/S0092-8674(01)00494-9.

Siniossoglou, S., H. Santos-Rosa, J. Rappsilber, M. Mann, and E. Hurt. 1998. A novel complex of membrane proteins required for formation of a spherical nucleus. *EMBO J.* 17:6449. doi:10.1093/EMBOJ/17.22.6449.

Smith, E.R., Y. Meng, R. Moore, J.D. Tse, A.G. Xu, and X.X. Xu. 2017. Nuclear envelope structural proteins facilitate nuclear shape changes accompanying embryonic differentiation and fidelity of gene expression. *BMC Cell Biol.* 18:1–14. doi:10.1186/s12860-017-0125-0.

Smith, J.S., and J.D. Boeke. 1997. An unusual form of transcriptional silencing in yeast ribosomal DNA. *Genes Dev.* 11:241–254. doi:10.1101/GAD.11.2.241.

Sołtysik, K., Y. Ohsaki, T. Tatematsu, J. Cheng, and T. Fujimoto. 2019. Nuclear lipid droplets derive from a lipoprotein precursor and regulate phosphatidylcholine synthesis. *Nat. Commun. 2019 101*. 10:1–12. doi:10.1038/s41467-019-08411-x.

Sussel, L., and D. Shore. 1991. Separation of transcriptional activation and silencing functions of the RAP1-encoded repressor/activator protein 1: Isolation of viable mutants affecting both silencing and telomere length. *Proc. Natl. Acad. Sci. U. S. A.* 88:7749–7753. doi:10.1073/pnas.88.17.7749.

Szaflarski, W., M. Leśniczak-Staszak, M. Sowiński, S. Ojha, A. Aulas, D. Dave, S. Malla, P. Anderson, P. Ivanov, and S.M. Lyons. 2022. Early rRNA processing is a stress-dependent regulatory event whose inhibition maintains nucleolar integrity. *Nucleic Acids Res.* 50:1033–1051. doi:10.1093/NAR/GKAB1231.

Szymanski, K.M., D. Binns, R. Bartz, N. V. Grishin, W.P. Li, A.K. Agarwal, A. Garg, R.G.W. Anderson, and J.M. Goodman. 2007. The lipodystrophy protein seipin is found at endoplasmic reticulum lipid droplet junctions and is important for droplet morphology. *Proc. Natl. Acad. Sci. U. S. A.* 104:20890–20895. doi:10.1073/PNAS.0704154104.

Taddei, A., and S.M. Gasser. 2012. Structure and Function in the Budding Yeast Nucleus. *Genetics*. 192:107–129. doi:10.1534/GENETICS.112.140608.

Taddei, A., G. Van Houwe, S. Nagai, I. Erb, E. van Nimwegen, and S.M. Gasser. 2009. The functional importance of telomere clustering: global changes in gene expression result from SIR factor dispersion. *Genome Res.* 19:611–25. doi:10.1101/gr.083881.108.

Tai, A., Y. Kamei, and Y. Mukai. 2017. The forkhead-like transcription factor (Fhl1p) maintains yeast replicative lifespan by regulating ribonucleotide reductase 1 (RNR1) gene transcription. *Biochem. Biophys. Res. Commun.* 488:218–223. doi:10.1016/J.BBRC.2017.05.038.

Tambellini, N.P., V. Zaremberg, S. Krishnaiah, R.J. Turner, and A.M. Weljie. 2017. Primary Metabolism and Medium-Chain Fatty Acid Alterations Precede Long-Chain Fatty Acid Changes Impacting Neutral Lipid Metabolism in Response to an Anticancer Lysophosphatidylcholine Analogue in Yeast. *J. Proteome Res.* 16:3741–3752. doi:10.1021/ACS.JPROTEOME.7B00430.

Taneva, S.G., J.M.C. Lee, and R.B. Cornell. 2012. The amphipathic helix of an enzyme that regulates phosphatidylcholine synthesis remodels membranes into highly curved nanotubules. *Biochim. Biophys. Acta - Biomembr.* 1818:1173–1186. doi:10.1016/J.BBAMEM.2012.01.006.

Teixeira, M.T., B. Dujon, and E. Fabre. 2002. Genome-wide nuclear morphology screen identifies novel genes involved in nuclear architecture and gene-silencing in Saccharomyces cerevisiae. *J. Mol. Biol.* 321:551–561. doi:10.1016/S0022-2836(02)00652-6.

Tinkelenberg, A.H., Y. Liu, F. Alcantara, S. Khan, Z. Guo, M. Bard, and S.L. Sturley. 2000. Mutations in yeast ARV1 alter intracellular sterol distribution and are complemented by human ARV1. *J. Biol. Chem.* 275:40667–40670. doi:10.1074/JBC.C000710200.

Vanni, S., H. Hirose, H. Barelli, B. Antonny, and R. Gautier. 2014. A sub-nanometre view of how membrane curvature and composition modulate lipid packing and protein recruitment. *Nat. Commun.* 5:4916. doi:10.1038/ncomms5916.

Venters, B.J., and B.F. Pugh. 2009. A canonical promoter organization of the transcription machinery and its regulators in the Saccharomyces genome. *Genome Res.* 19:360–371. doi:10.1101/GR.084970.108.

Vogler, W.R., and W.E. Berdel. 2009. Autologous Bone Marrow Transplantation with Alkyl-Lysophospholipid-Purged Marrow. *J. Hematother.* 2:93–102. doi:10.1089/SCD.1.1993.2.93.

Wade, J.T., D.B. Hall, and K. Strahl. 2004. The transcription factor Ifh1 is a key regulator of yeast ribosomal protein genes. *Nat. 2004 4327020*. 432:1054–1058. doi:10.1038/nature03175.

Wang, Y., C. Xu, Y. Liang, and P.M. Vanhoutte. 2012. SIRT1 in metabolic syndrome: where to target matters. *Pharmacol. Ther.* 136:305–318. doi:10.1016/J.PHARMTHERA.2012.08.009.

Welch, B.L. 1947. The Generalization of ‘Student’s’ Problem when Several Different Population Variances are Involved. *Biometrika*. 34:28–35. doi:10.1093/BIOMET/34.1-2.28.

Wickham, H. 2016. ggplot2: Elegant Graphics for Data Analysis. Springer-Verlag New York.

Winnik, S., J. Auwerx, D.A. Sinclair, and C.M. Matter. 2015. Protective effects of sirtuins in cardiovascular diseases: from bench to bedside. *Eur. Heart J.* 36:3404–3412. doi:10.1093/EURHEARTJ/EHV290.

Witkin, K.L., Y. Chong, S. Shao, M.T. Webster, S. Lahiri, A.D. Walters, B. Lee, J.L.Y. Koh, W.A. Prinz, B.J. Andrews, and O. Cohen-Fix. 2012. The budding yeast nuclear envelope adjacent to the nucleolus serves as a membrane sink during mitotic delay. *Curr. Biol.* 22:1128–33. doi:10.1016/j.cub.2012.04.022.

Wolinski, H., H.F. Hofbauer, K. Hellauer, A. Cristobal-Sarramian, D. Kolb, M. Radulovic, O.L. Knittelfelder, G.N. Rechberger, and S.D. Kohlwein. 2015. Seipin is involved in the regulation of phosphatidic acid metabolism at a subdomain of the nuclear envelope in yeast. *Biochim. Biophys. Acta - Mol. Cell Biol. Lipids*. 1851:1450–1464. doi:10.1016/J.BBALIP.2015.08.003.

Workman, C.T., H.C. Mak, S. McCuine, J.B. Tagne, M. Agarwal, O. Ozier, T.J. Begley, L.D. Samson, and T. Ideker. 2006. A systems approach to mapping DNA damage response pathways. *Science (80-.).* 312:1054–1059. doi:10.1126/SCIENCE.1122088.

Wotton, D., and D. Shore. 1997. A novel Rap1p-interacting factor, Rif2p, cooperates with Rif1p to regulate telomere length in Saccharomyces cerevisiae. *Genes Dev.* 11:748–760. doi:10.1101/gad.11.6.748.

Yang, C.H., E.J. Lambie, J. Hardin, J. Craft, and M. Snyder. 1989. Higher order structure is present in the yeast nucleus: autoantibody probes demonstrate that the nucleolus lies opposite the spindle pole body. *Chromosoma*. 98:123–128. doi:10.1007/BF00291048.

Yarragudi, A., L.W. Parfrey, and R.H. Morse. 2007. Genome-wide analysis of transcriptional dependence and probable target sites for Abf1 and Rap1 in Saccharomyces cerevisiae. *Nucleic Acids Res.* 35:193–202. doi:10.1093/NAR/GKL1059.

Young, B.P., J.J.H. Shin, R. Orij, J.T. Chao, S.C. Li, X.L. Guan, A. Khong, E. Jan, M.R. Wenk, W.A. Prinz, G.J. Smits, and C.J.R. Loewen. 2010. Phosphatidic acid is a pH biosensor that links membrane biogenesis to metabolism. *Science (80-.).* 329:1085–1088. doi:10.1126/SCIENCE.1191026.

Zaremberg, V., C. Gajate, L.M. Cacharro, F. Mollinedo, and C.R. McMaster. 2005. Cytotoxicity of an anti-cancer lysophospholipid through selective modification of lipid raft composition. *J. Biol. Chem.* 280:38047–58. doi:10.1074/jbc.M502849200.

Zaremberg, V., and C.R. McMaster. 2002. Differential partitioning of lipids metabolized by separate yeast glycerol-3-phosphate acyltransferases reveals that phospholipase D generation of phosphatidic acid mediates sensitivity to choline-containing lysolipids and drugs. *J. Biol. Chem.* 277:39035–39044. doi:10.1074/JBC.M207753200.

Zhang, H., C. Gajate, L.-P. Yu, Y.-X. Fang, and F. Mollinedo. 2007. Mitochondrial-derived ROS in edelfosine-induced apoptosis in yeasts and tumor cells 1. *Acta Pharmacol Sin*. 28:888–894. doi:10.1111/j.1745-7254.2007.00568.x.

Zhang, S., T.J. Burkett, I. Yamashita, and D.J. Garfinkel. 1997. Genetic redundancy between SPT23 and MGA2: regulators of Ty-induced mutations and Ty1 transcription in Saccharomyces cerevisiae. *Mol. Cell. Biol.* 17:4718–4729. doi:10.1128/MCB.17.8.4718.

Zhang, S., Y. Skalsky, and D.J. Garfinkel. 1999. MGA2 or SPT23 is required for transcription of the delta9 fatty acid desaturase gene, OLE1, and nuclear membrane integrity in Saccharomyces cerevisiae. *Genetics*. 151:473–483. doi:10.1093/GENETICS/151.2.473.

Zhou, J., B.O. Zhou, B.A. Lenzmeier, and J.Q. Zhou. 2009. Histone deacetylase Rpd3 antagonizes Sir2-dependent silent chromatin propagation. *Nucleic Acids Res.* 37:3699. doi:10.1093/NAR/GKP233.

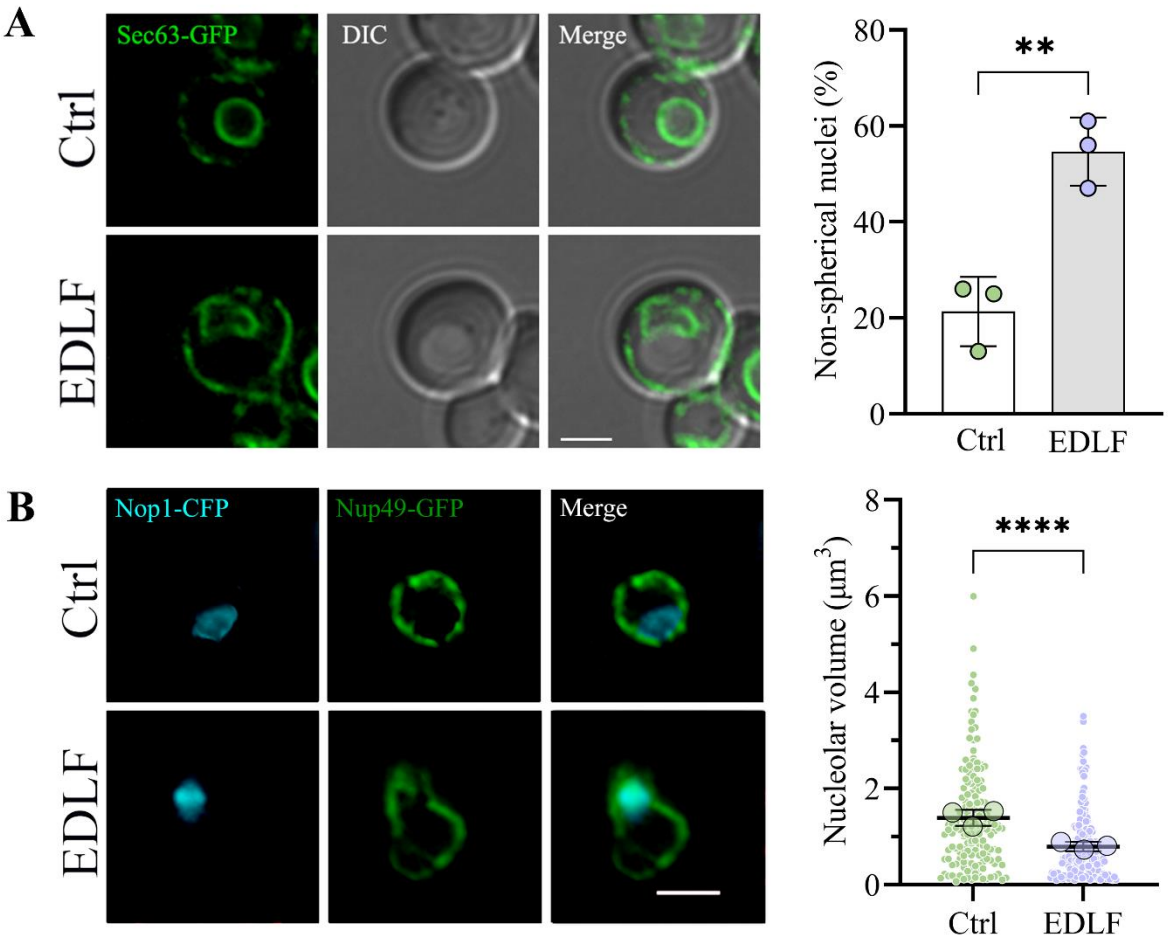
A
Sec63-GFP
DIC
Merge
Ctrl
EDLF
Non-spherical nuclei (%)
80
60
40
20
0
**
Ctrl
EDLF
B
Nop1-CFP
Nup49-GFP
Merge
Ctrl
EDLF
Nucleolar volume (μm3)
8
6
4
2
0
****
Ctrl
EDLF

1586

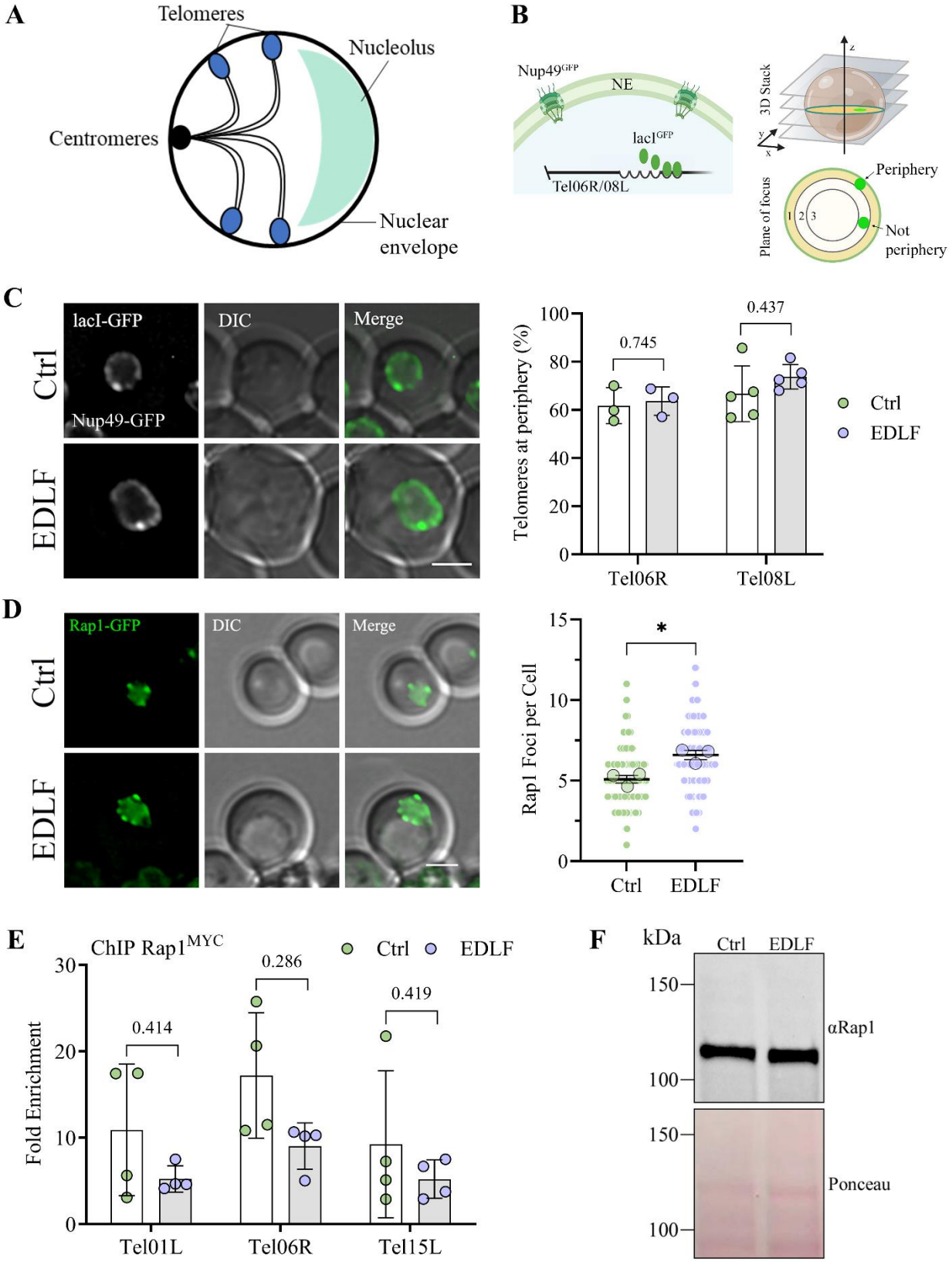
A
Telomeres
Nucleolus
Centromeres
Nuclear envelope
B
Nup49GFP
NE
lacIGFP
Tel06R/08L
3D Stack
Plane of focus
Periphery
Not periphery
C
lacI-GFP
DIC
Merge
Nup49-GFP
Ctrl
EDLF
Telomeres at periphery (%)
0.745
0.437
Tel06R
Tel08L
D
Rap1-GFP
Rap1 Foci per Cell
*
E
ChIP Rap1MYC
Fold Enrichment
0.414
0.286
0.419
Tel01L
Tel06R
Tel15L
F
kDa
αRap1
Ponceau

1587

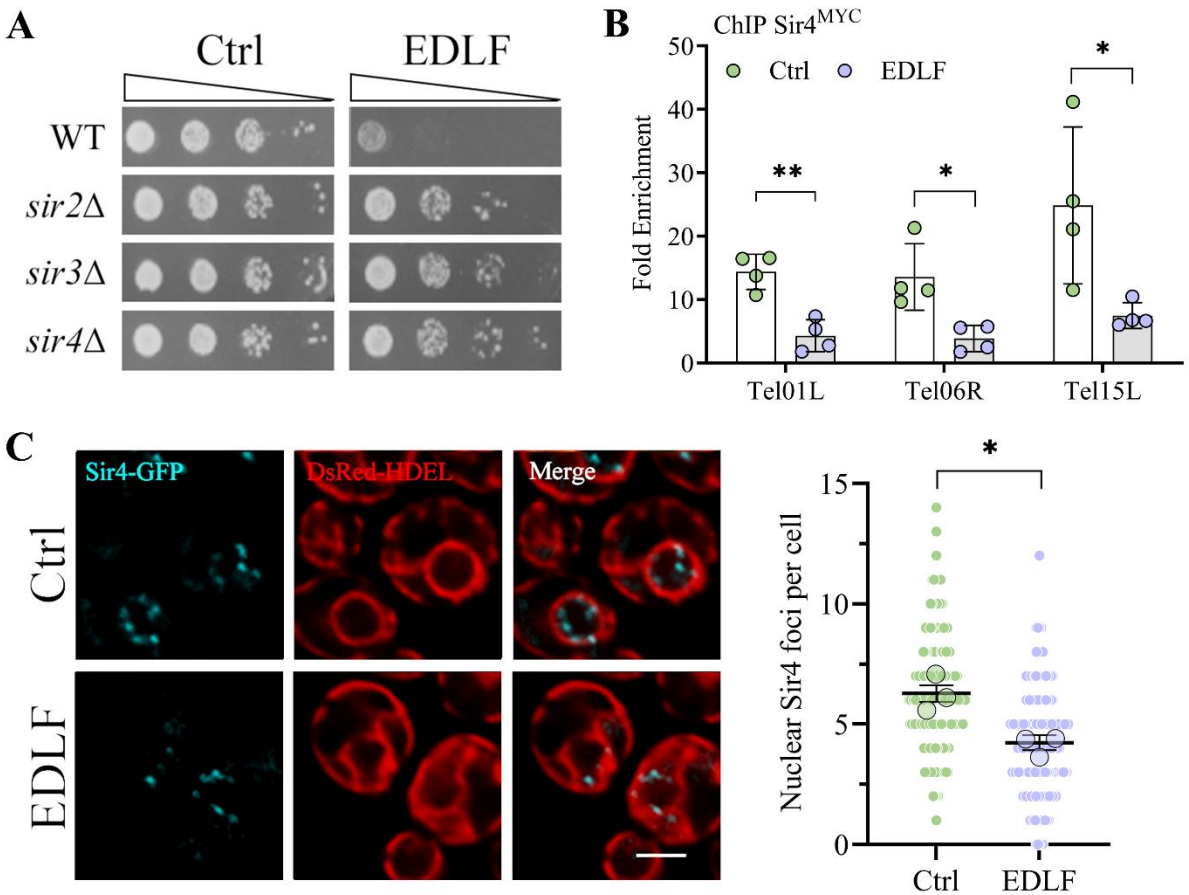

1588

1589

1590

1591

1592

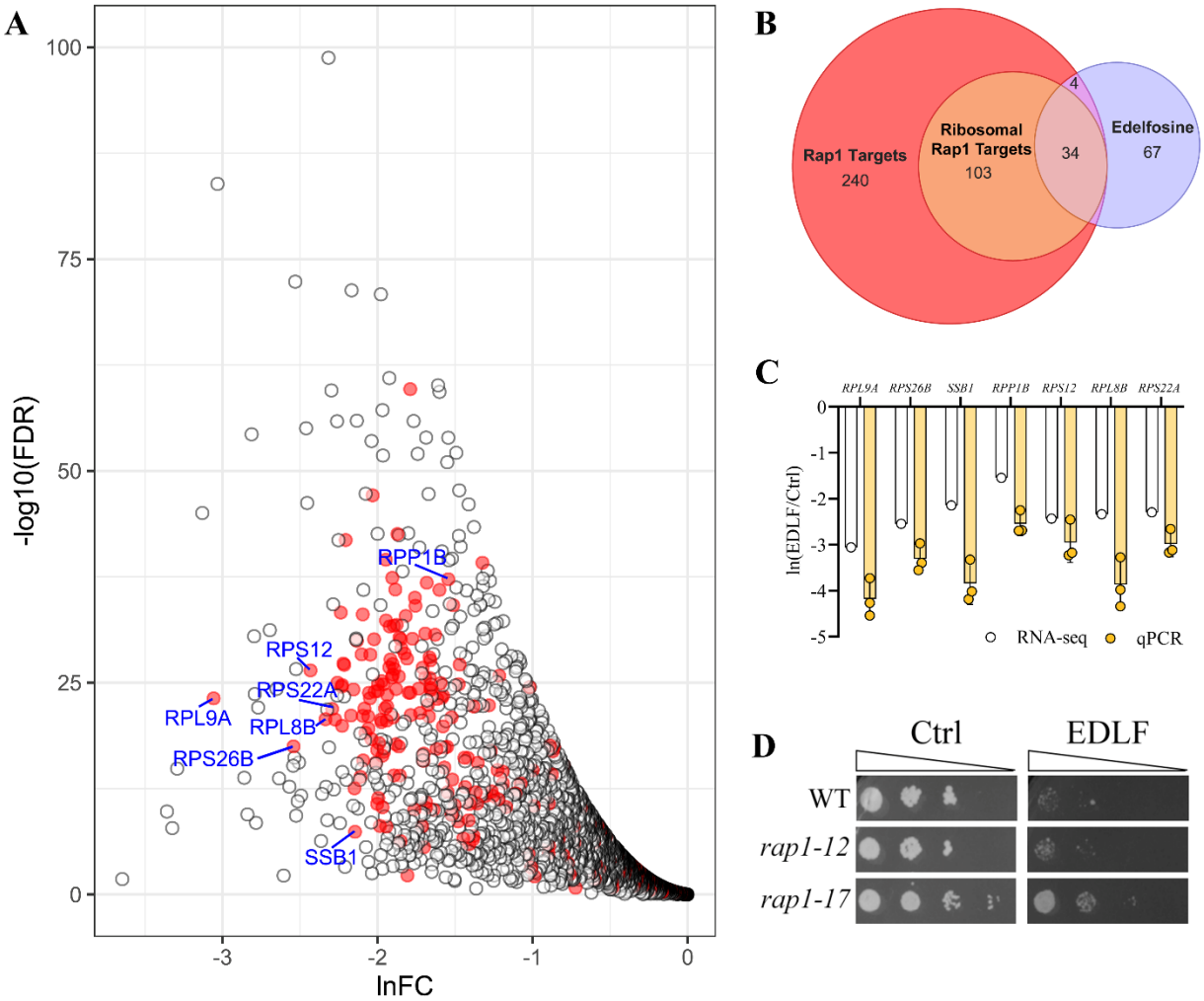

1593

1594

1595

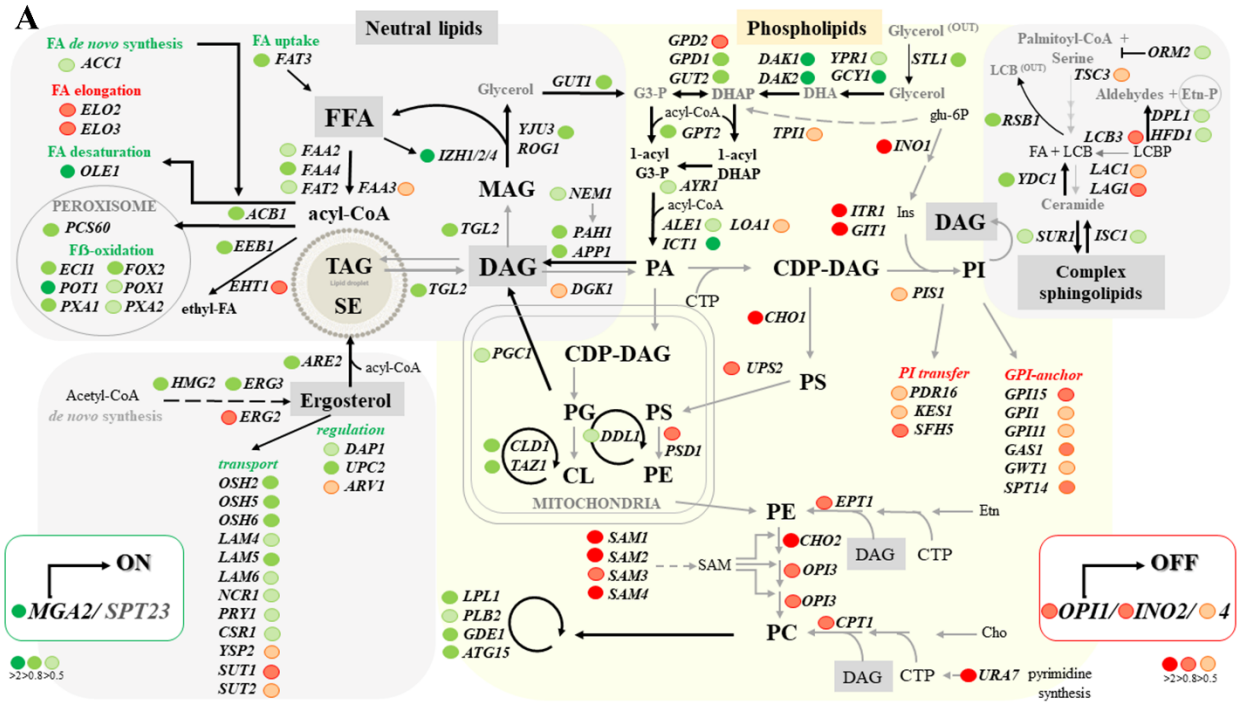
A
Neutral lipids
Phospholipids
FA de novo synthesis
ACC1
FA uptake
FAT3
FA elongation
ELO2
ELO3
FA desaturation
OLE1
FFA
Glycerol
GUT1
YJU3
ROG1
IZH1/2/4
FAA2
FAA4
FAT2
FAA3
MAG
NEM1
PEROXISOME
PCS60
Fß-oxidation
ECI1
FOX2
POT1
POX1
PXA1
PXA2
ACB1
acyl-CoA
EEB1
EHT1
ethyl-FA
TAG
SE
TGL2
DAG
PAH1
APP1
DGK1
PA
CTP
CDP-DAG
PGC1
PG
PS
DDL1
PSD1
CLD1
TAZ1
CL
PE
MITOCHONDRIA
ARE2
acyl-CoA
Acetyl-CoA
de novo synthesis
HMG2
ERG3
ERG2
Ergosterol
regulation
DAP1
UPC2
ARV1
transport
OSH2
OSH5
OSH6
LAM4
LAM5
LAM6
NCR1
PRY1
CSR1
YSP2
SUT1
SUT2
ON
MGA2/ SPT23
>2>0.8>0.5
GPD2
GPD1
GUT2
G3-P
DHAP
DAK1
DAK2
YPR1
GCY1
DHA
Glycerol
STL1
Glycerol (OUT)
glu-6P
acyl-CoA
GPT2
TPI1
1-acyl G3-P
1-acyl DHAP
AYR1
acyl-CoA
ALE1
ICT1
LOA1
INO1
ITR1
GIT1
Ins
DAG
PI
PIS1
CHO1
UPS2
PS
PI transfer
PDR16
KES1
SFH5
GPI-anchor
GPI15
GPI1
GPI11
GAS1
GWT1
SPT14
Palmitoyl-CoA + Serine
ORM2
TSC3
LCB (OUT)
Aldehydes + Etn-P
RSB1
DPL1
HFD1
LCB3
FA + LCB
LCBP
YDC1
LAC1
LAG1
Ceramide
SUR1
ISC1
Complex sphingolipids
PE
EPT1
Etn
SAM1
SAM2
SAM3
SAM4
SAM
CHO2
OPI3
OPI3
DAG
CTP
PC
CPT1
Cho
DAG
CTP
URA7
pyrimidine synthesis
LPL1
PLB2
GDE1
ATG15
OFF
OPI1/ INO2/ 4
>2>0.8>0.5

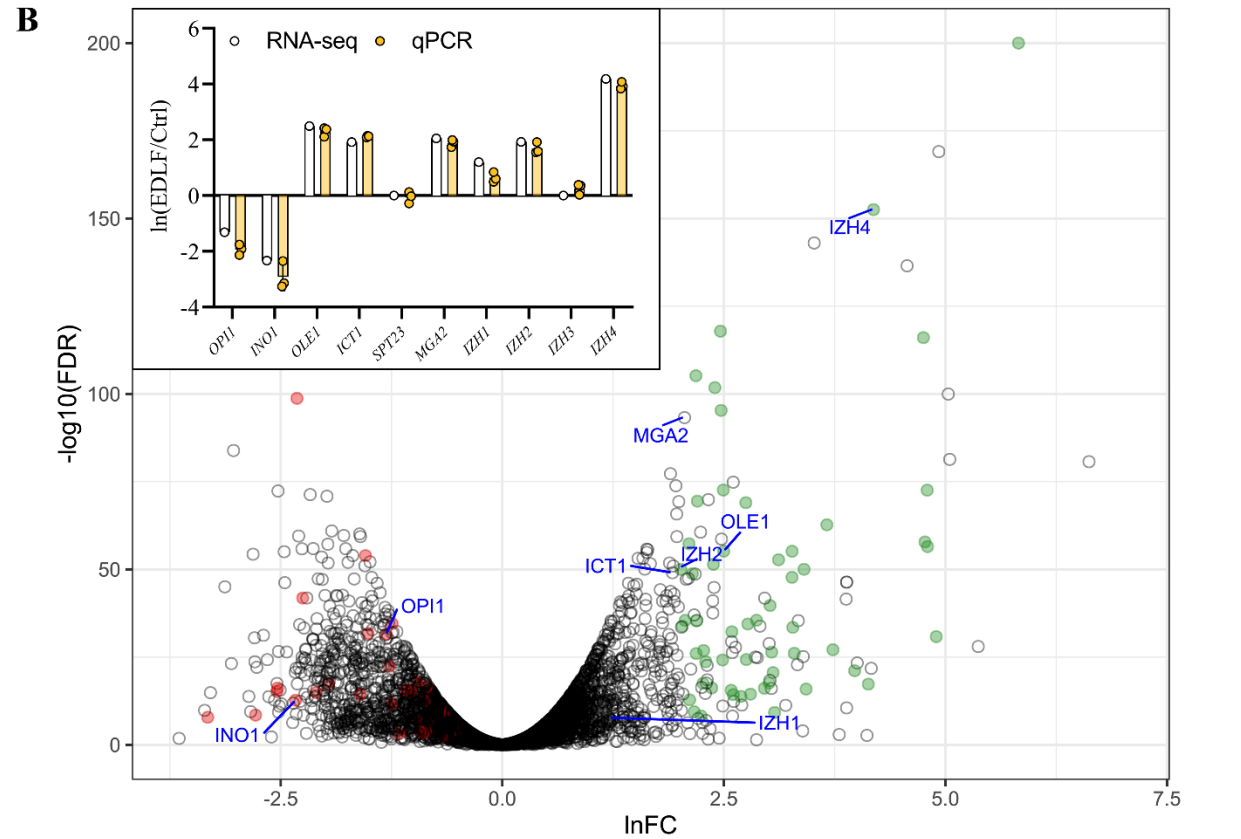
B
RNA-seq
qPCR
ln(EDLF/Ctrl)
OPI1
INO1
OLE1
ICT1
SPT23
MGA2
IZH1
IZH2
IZH3
IZH4
-log10(FDR)
lnFC
IZH4
MGA2
OLE1
IZH2
ICT1
OPI1
INO1
IZH1

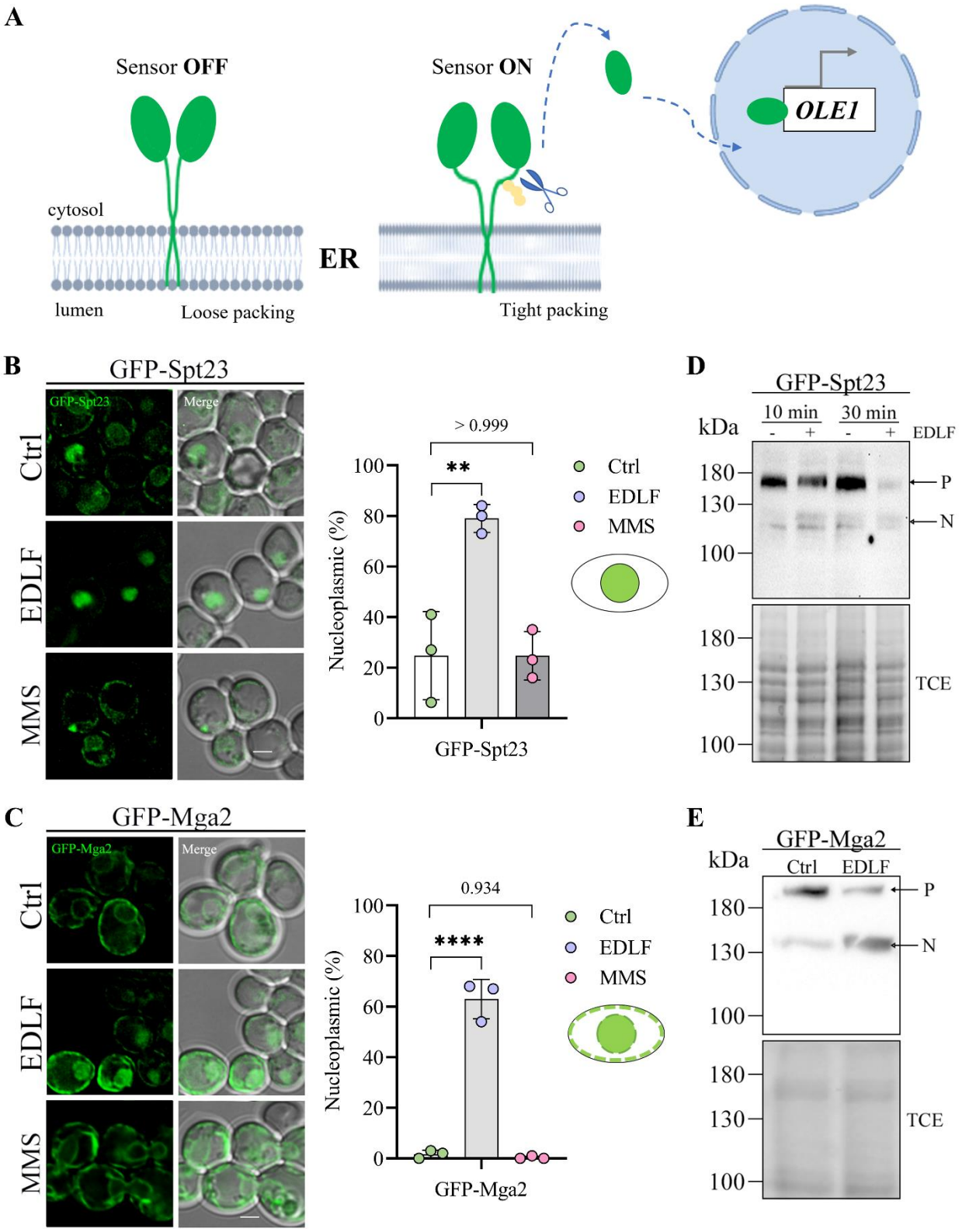
A
Sensor OFF
Sensor ON
OLE1
cytosol
ER
lumen
Loose packing
Tight packing
B
GFP-Spt23
GFP-Spt23
Merge
Ctrl
EDLF
MMS
> 0.999
**
Nucleoplasmic (%)
100
80
60
40
20
0
GFP-Spt23
Ctrl
EDLF
MMS
D
GFP-Spt23
10 min
30 min
kDa
- + - +
EDLF
180
130
100
P
N
TCE
C
GFP-Mga2
GFP-Mga2
Merge
Ctrl
EDLF
MMS
0.934
****
Nucleoplasmic (%)
GFP-Mga2
E
GFP-Mga2
kDa
Ctrl
EDLF
P
N
TCE

1597

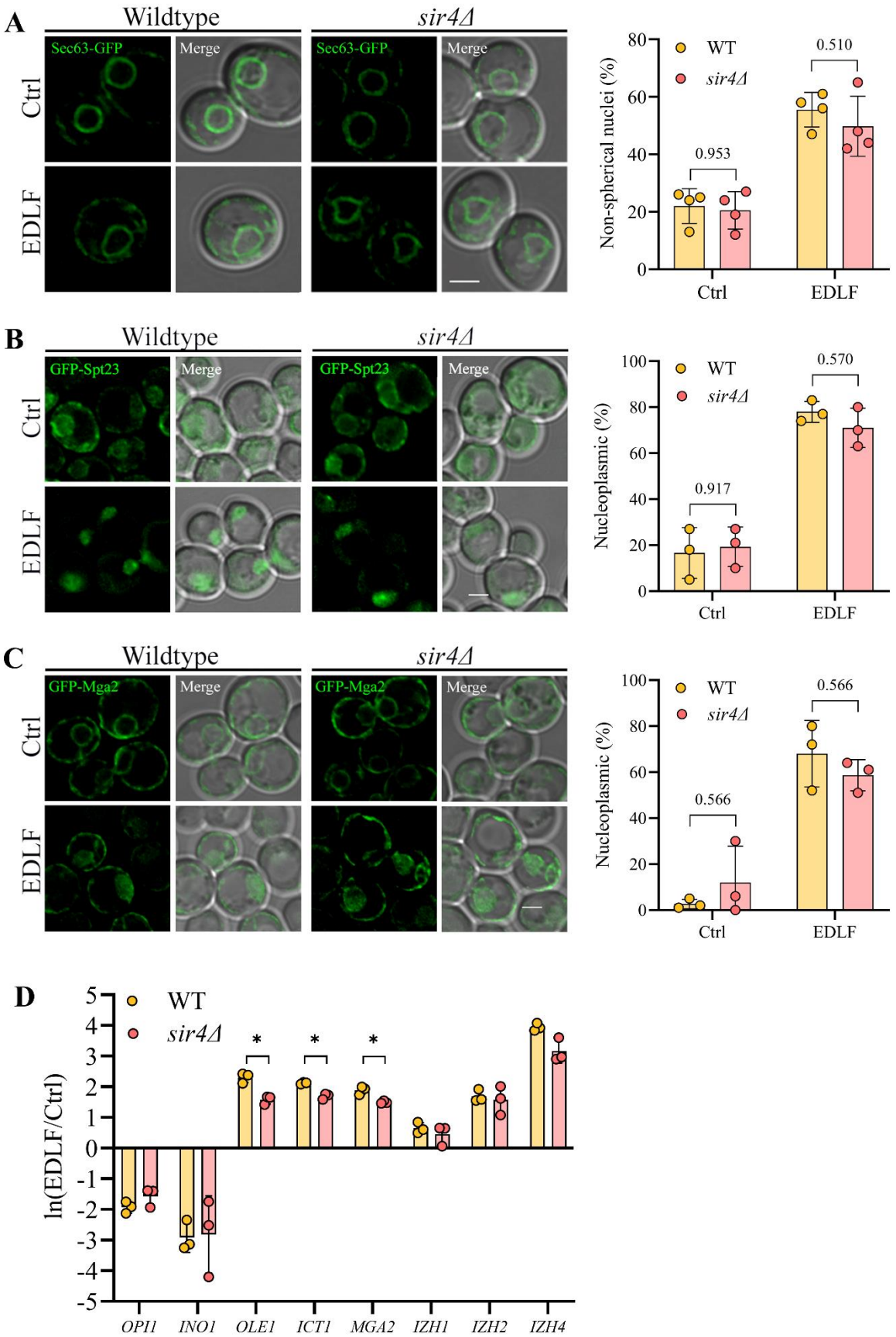
A
Wildtype
sir4Δ
Sec63-GFP
Merge
Ctrl
EDLF
Non-spherical nuclei (%)
WT
0.953
0.510
Ctrl
EDLF
B
GFP-Spt23
Nucleoplasmic (%)
0.917
0.570
C
GFP-Mga2
0.566
0.566
D
ln(EDLF/Ctrl)
OPI1
INO1
OLE1
ICT1
MGA2
IZH1
IZH2
IZH4

1598

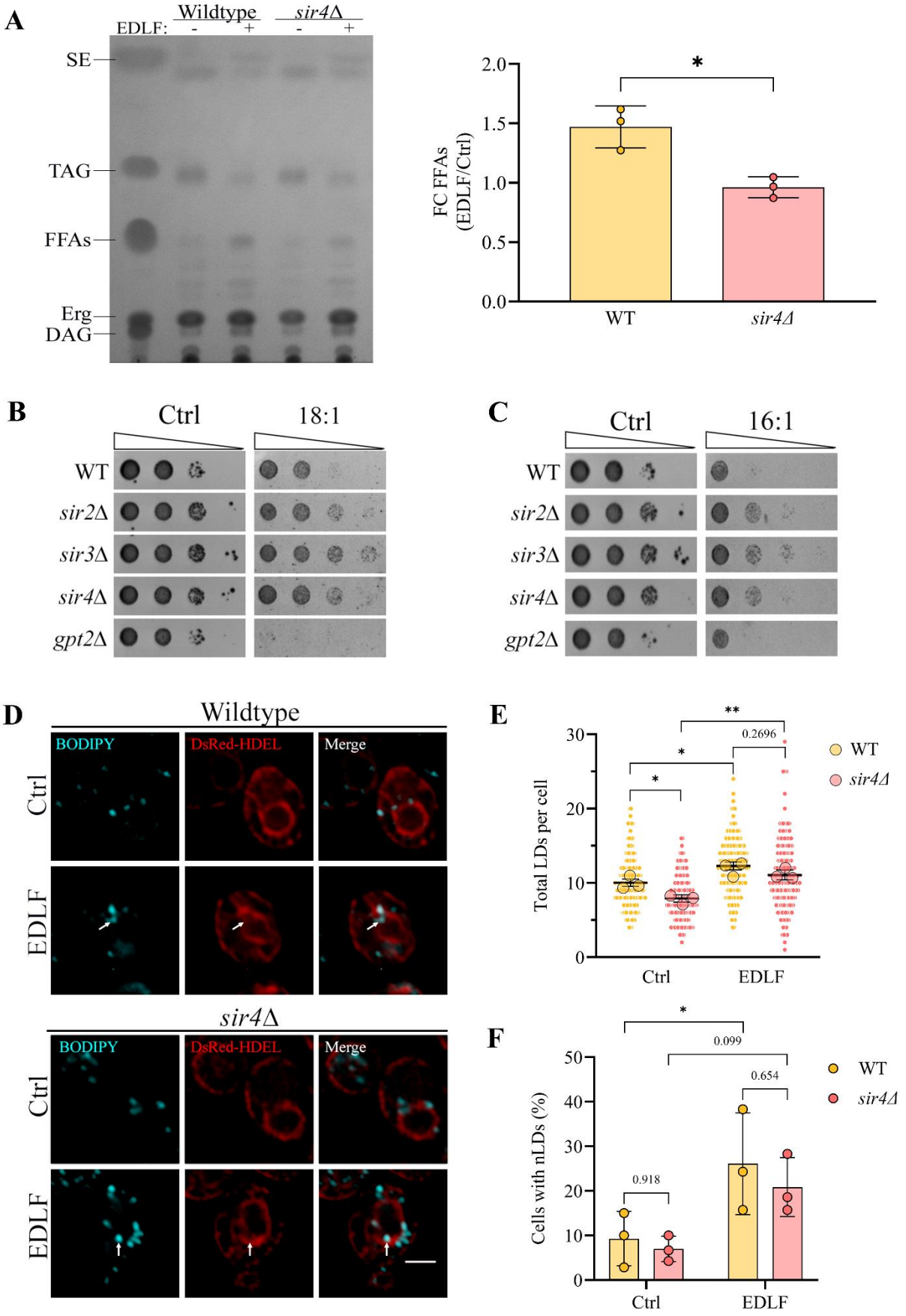
A
Wildtype
sir4Δ
EDLF:
-
+
-
+
SE
TAG
FFAs
Erg
DAG
FC FFAs (EDLF/Ctrl)
2.0
1.5
1.0
0.5
0.0
*
WT
sir4Δ
B
Ctrl
18:1
WT
sir2Δ
sir3Δ
sir4Δ
gpt2Δ
C
Ctrl
16:1
WT
sir2Δ
sir3Δ
sir4Δ
gpt2Δ
D
Wildtype
BODIPY
DsRed-HDEL
Merge
Ctrl
EDLF
sir4Δ
BODIPY
DsRed-HDEL
Merge
Ctrl
EDLF
E
Total LDs per cell
30
20
10
0
**
*
*
0.2696
WT
sir4Δ
Ctrl
EDLF
F
Cells with nLDs (%)
50
40
30
20
10
0
*
0.099
0.654
0.918
WT
sir4Δ
Ctrl
EDLF

1599

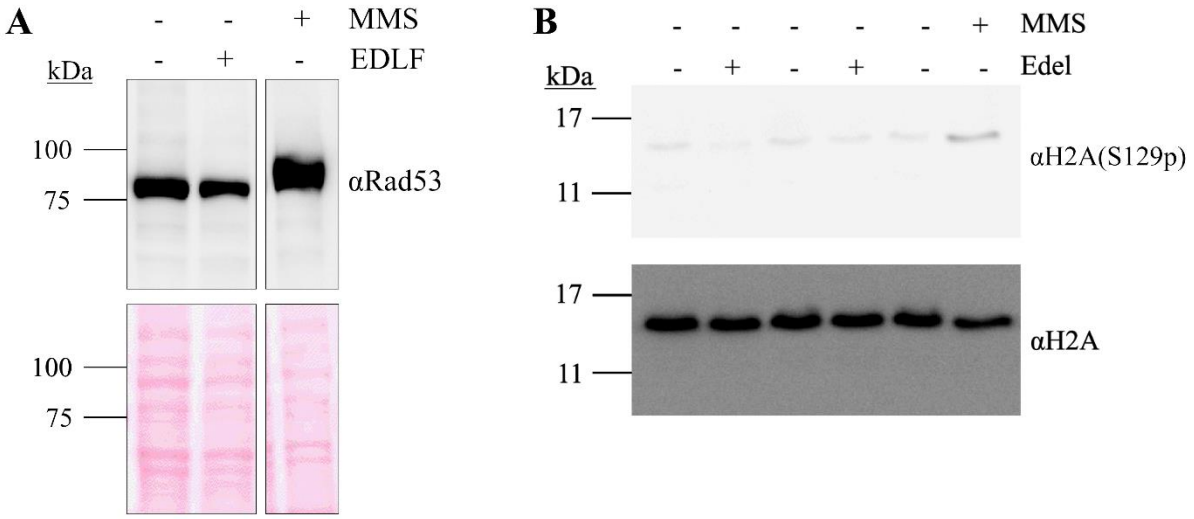

1600

1601

1602

1603

1604

1605

1606

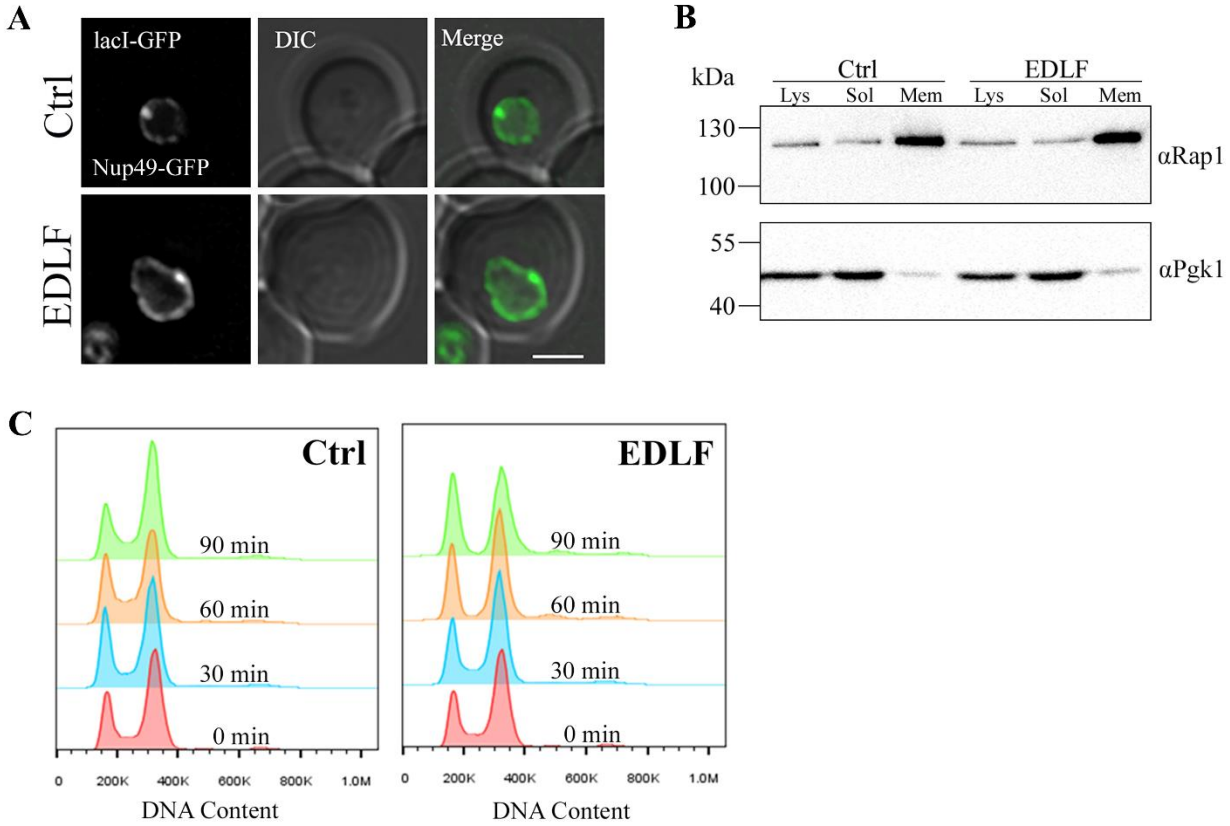
A
lacI-GFP
DIC
Merge
Ctrl
Nup49-GFP
EDLF
B
kDa
Ctrl
EDLF
Lys
Sol
Mem
Lys
Sol
Mem
130
100
αRap1
55
40
αPgk1
C
Ctrl
EDLF
90 min
60 min
30 min
0 min
0
200K
400K
600K
800K
1.0M
DNA Content

1607

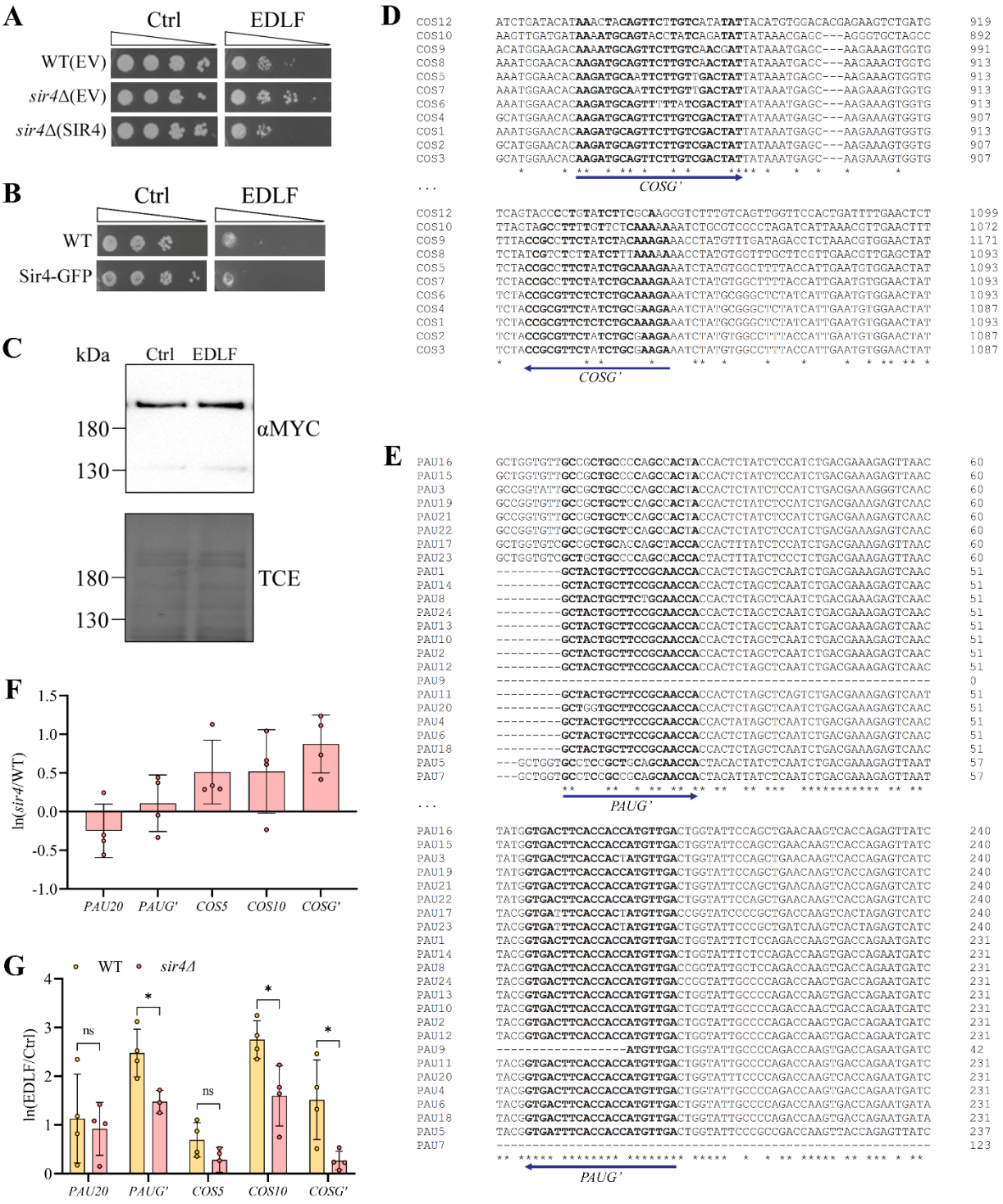
A
Ctrl
EDLF
WT(EV)
sir4Δ(EV)
sir4Δ(SIR4)
B
Ctrl
EDLF
WT
Sir4-GFP
C
kDa
Ctrl
EDLF
180
130
αMYC
180
130
TCE
D
COS12
COS10
COS9
COS8
COS5
COS7
COS6
COS4
COS1
COS2
COS3
COSG'
E
PAU16
PAU15
PAU3
PAU19
PAU21
PAU22
PAU17
PAU23
PAU1
PAU14
PAU8
PAU24
PAU13
PAU10
PAU2
PAU12
PAU9
PAU11
PAU20
PAU4
PAU6
PAU18
PAU5
PAU7
PAUG'
F
ln(sir4/WT)
1.5
1.0
0.5
0.0
-0.5
-1.0
PAU20
PAUG'
COS5
COS10
COSG'
G
WT
sir4Δ
ln(EDLF/Ctrl)
4
3
2
1
0
ns
*
ns
*
*
PAU20
PAUG'
COS5
COS10
COSG'

1608

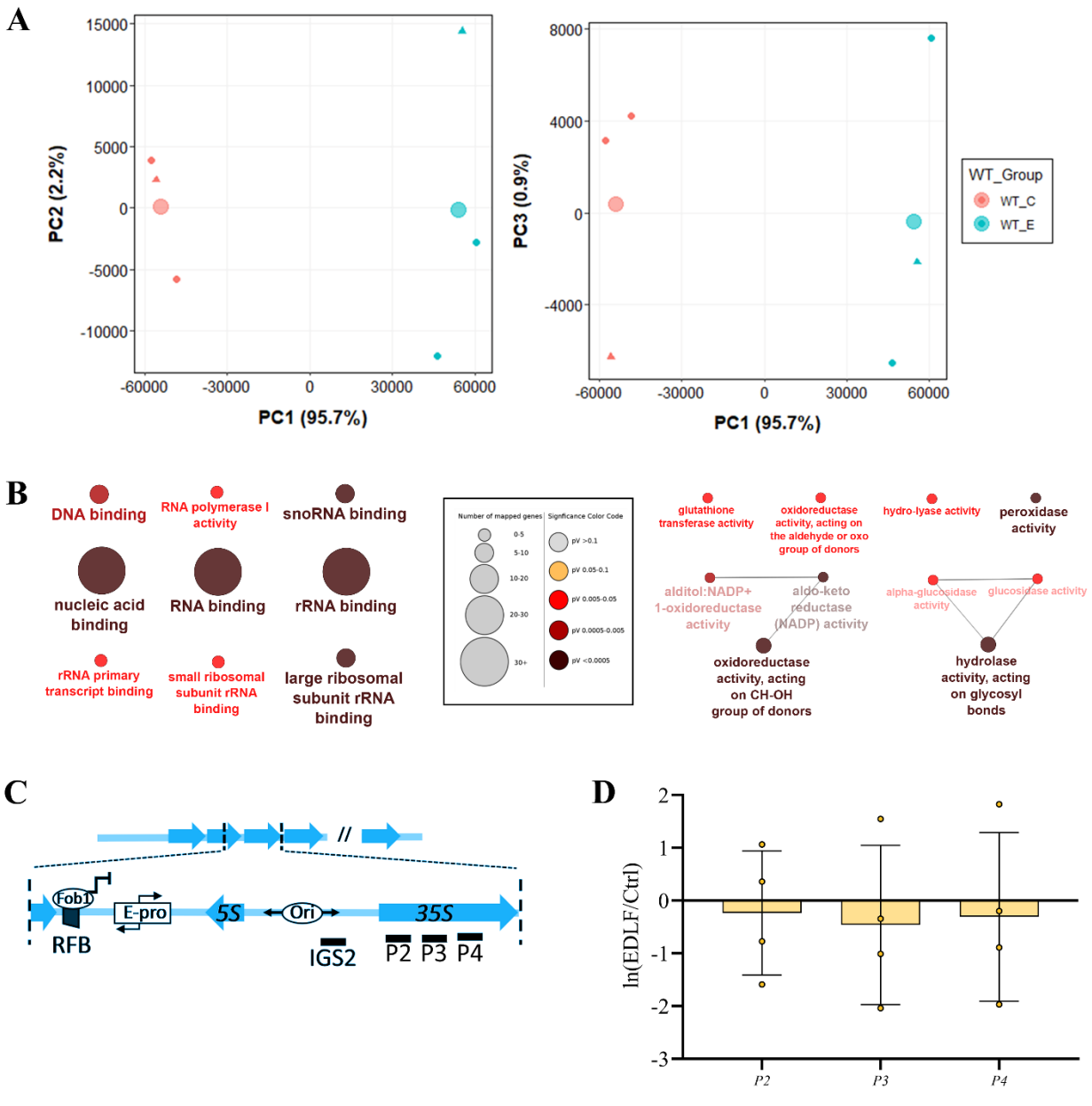
A
PC2 (2.2%)
PC1 (95.7%)
PC3 (0.9%)
WT_Group
WT_C
WT_E
B
DNA binding
RNA polymerase I activity
snoRNA binding
nucleic acid binding
RNA binding
rRNA binding
rRNA primary transcript binding
small ribosomal subunit rRNA binding
large ribosomal subunit rRNA binding
Number of mapped genes
Signficance Color Code
glutathione transferase activity
oxidoreductase activity, acting on the aldehyde or oxo group of donors
hydro-lyase activity
peroxidase activity
alditol:NADP+ 1-oxidoreductase activity
aldo-keto reductase (NADP) activity
alpha-glucosidase activity
glucosidase activity
oxidoreductase activity, acting on CH-OH group of donors
hydrolase activity, acting on glycosyl bonds
C
Fob1
E-pro
5S
Ori
35S
RFB
IGS2
P2
P3
P4
D
ln(EDLF/Ctrl)
P2
P3
P4

1609

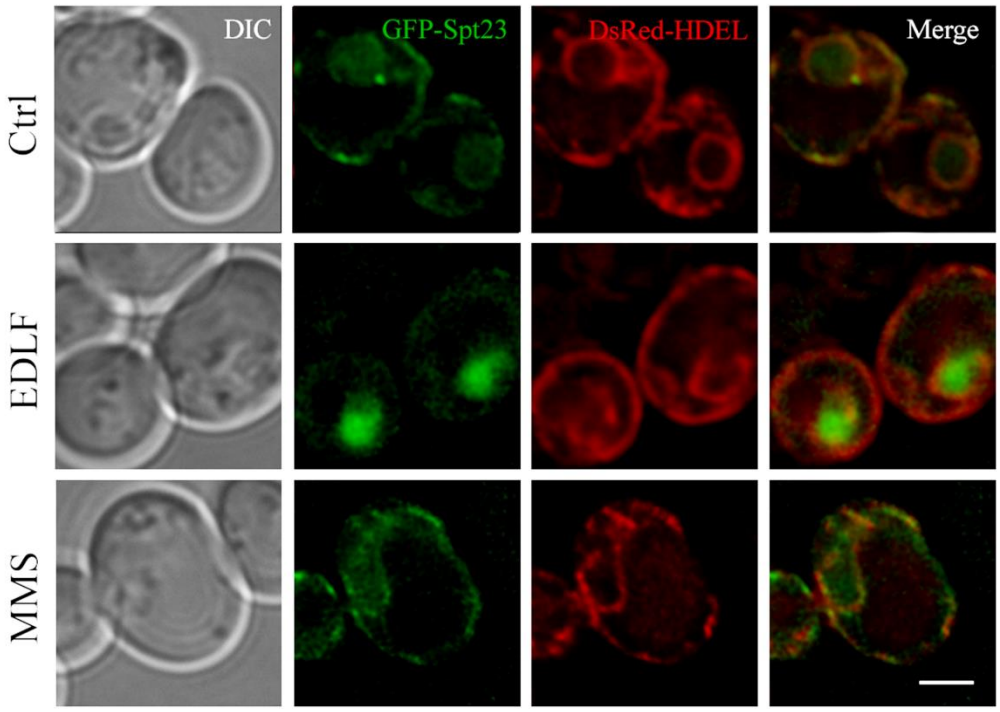

1610